AN ABSTRACT OF THE THESIS OF

Yousef M. Alanazi for the degree of Master of Science in Chemical Engineering presented on June 12, 2014.

Title: Oxidation of Hydrocarbon in a Carbon Nanotube Supported Corona Discharge in Micoreactor: Oxidation of Ethylene

Abstract approved:

_____

Goran N. Jovanovic Alexander F. Yokochi

Population growth driven sustainability issues, including the food resource issue, are pressing problems in need of attention. The goal of the present thesis is to examine the ability of an electric non-thermal plasma based microreactor to destroy ethylene, a known plant hormone responsible for losses in the range of 20% to 50% of fruits and vegetables in cold storage.

The research hypotheses investigated were that an electric glow discharge (non-thermal plasma) will efficiently destroy ethylene present at the ppm level in ethylene/air mixtures, and that a carbon nanotube based emitter electrode will enable lower voltage ignition of the glow discharge.

For the purpose, a microreactor device was constructed and equipped with a carbon nanotube based emitter electrode to produce a positive corona discharge in which the corona discharge is created between the surface of the carbon nanotube supported emitter electrode and a stainless steel grounded electrode. The performance of the system towards the oxidation of ethylene in air was investigated by a preliminary screening experiment, followed by systematic parameter sweeps of the identified important factors. Measurements of the reactor performance were based on gas chromatograms employing an on-line instrument equipped with both Thermal Conductivity and Helium Ionization detectors, and used conversion, defined as $X\%=([\text{ethylene}]_{in}-[\text{ethylene}]_{out})/[\text{ethylene}]_{in}*100\%$, as the measured variable for reactor performance.

Early experiments with the CNT based reactor indicated that while the CNTs may enable instantaneous spark discharges within the reactor at lower voltages, the CNT electrodes seemed to be destroyed in the process. For this reason work employed reactors from which the CNT structures had been removed.

The screening experiments showed that the most important factors in the destruction of ethylene in the gas mixtures was the thickness of the reactor, with a thicker reactor resulting in higher conversion, the initial concentration of ethylene, with lower concentrations of ethylene resulting in a higher fraction of the ethylene present destroyed, and the residence time of the gas flow within the reactor, with longer residence times (i.e., lower flowrates) resulting in a larger fraction of the ethylene being destroyed. Surprisingly, different applied reactor voltage was of little effect, nor was the interaction between residence time and reactor thickness.

The systematic examination of the microreactor performance focused on the conversion of ethylene as the residence time increases for inlet concentrations of ethylene between 200 ppm and 600 ppm, reactor thickness of 250 μm and 750 μm, and applied reactor current of 5 mA and 6.5 mA. Results showed ethylene conversion between X=35% and X=75%, again with very significant dependence on the reactor thickness, residence time, and inlet ethylene concentration. It should be noted that while higher conversion was observed for lower inlet concentrations of ethylene, that the absolute number of molecules of ethylene destroyed is higher for higher concentrations of ethylene, and this is reflected in the energetic efficiency of the system, with about $3x10^{-10}$ moles ethylene destroyed per Joule of electric power ($3x10^{-10}$ mol /J) applied to the reactor at low inlet concentrations, growing to about ($16x10^{-10}$ mol/J)at high inlet concentrations of ethylene.

The observed conversion of ethylene showed a sigmoid shaped dependence on residence time where the data could be fitted using a logistic function. This is possibly due to a localized corona discharge within the reactor that grows laterally within the reactor to fill the available reactor volume, even as the reacting volume is advocated by the moving fluid. This model results in little growth of the reaction volume at low residence times (high flow rates) and yielding low conversion, and maximal growth of the reacting volume at high residence times resulting in higher ethylene conversion. Confirming this model requires further work in future.

.

Oxidation of Hydrocarbon in a Carbon Nanotube Supported Corona Discharge in Micoreactor: Oxidation of Ethylene

by

Yousef M. Alanazi

A THESIS

submitted to

Oregon State University

in partial fulfillment of
the requirements for the
degree of

Master of Science

Presented June 12, 2014
Commencement June 2015

Master of Science thesis of Yousef M. Alanazi presented on June 12, 2014

APPROVED:

Co-Major Professor, representing Chemical Engineering

Co-Major Professor, representing Chemical Engineering

Head of the School of Chemical, Biological, and Environmental Engineering

Dean of the Graduate School

I understand that my thesis will become part of the permanent collection of Oregon State University libraries. My signature below authorizes release of my thesis to any reader upon request.

Yousef M. Alanazi, Author

ACKNOWLEDGEMENTS

First and foremost, my thanks go to my parents, brothers and sisters for being a constant support and encouragement.

I would like to express my sincere appreciation and thanks to my advisors, Dr. Goran Jovanovic and Dr. Alexander Yokochi, to whom I owe very much in many respects.

Their guidance, professional support that helped me enormously in the development, implementing and finishing of this degree.

I would like to thank colleges Peter Kreider and Justin Pommerenck for their collaboration in understanding the phenomena of corona discharge in both discussion, the sharing of great ideas, and for sharing the joy and frustrations with me through this journey.

I would also like to thank Frederick Atadana, Malachi Bunn, Miao Yu, Omar Mohamed and the rest of my fellow grad student in Dr. Goran Jovanovic and Dr. Alexander Yokochi's groups for helping me during this work.

Also, I would like to thank King Abdullah for the Foreign Scholarship Program and the Ministry of Higher Education of Sadie Arabia and the Royal Embassy of Saudi Arabia-Cultural for the success of the program, and the financial support during my study at Oregon State University.

TABLE OF CONTENTS

Page

TABLE OF CONTENTS (Continued)

Page

TABLE OF CONTENTS (Continued)

Page

TABLE OF CONTENTS (Continued)

Page

LIST OF FIGURES

Figure Page

LIST OF FIGURES (Continued)

Figure Page

LIST OF FIGURES (Continued)

Figure Page

LIST OF FIGURES (Continued)

Figure Page

LIST OF FIGURES (Continued)

Figure Page

LIST OF TABLES

Table Page

LIST OF APPENDIX

Appendix Page

LIST OF APPENDIX FIGURES

Figure Page

LIST OF APPENDIX TABLES

Table Page

Oxidation of Hydrocarbon in a Carbon Nanotube Supported Corona Discharge in Micoreactor: Oxidation of Ethylene

Chapter 1: Introduction

1.1. The impact of population on food sector

The rising growth in global population is worrying and experts project that the demand for food will rise considerably by over 70%, unless the impending food crisis is addressed. The rising demand for agricultural yields that is expected to grow will deprive the growing population of a sufficient food supply [1]. There has been a significant rise in population for the last 5 decades, which continues to create pressure on the efforts to sustain the global food basket. *Figure 1.* illustrates the effect that an increasing human population has on the food and energy demand. The trend is expected to increase if no long-term actions are put in place. Growth of urban settlements will put enormous pressure on land which will compete with agriculture for necessary factors of production [3]

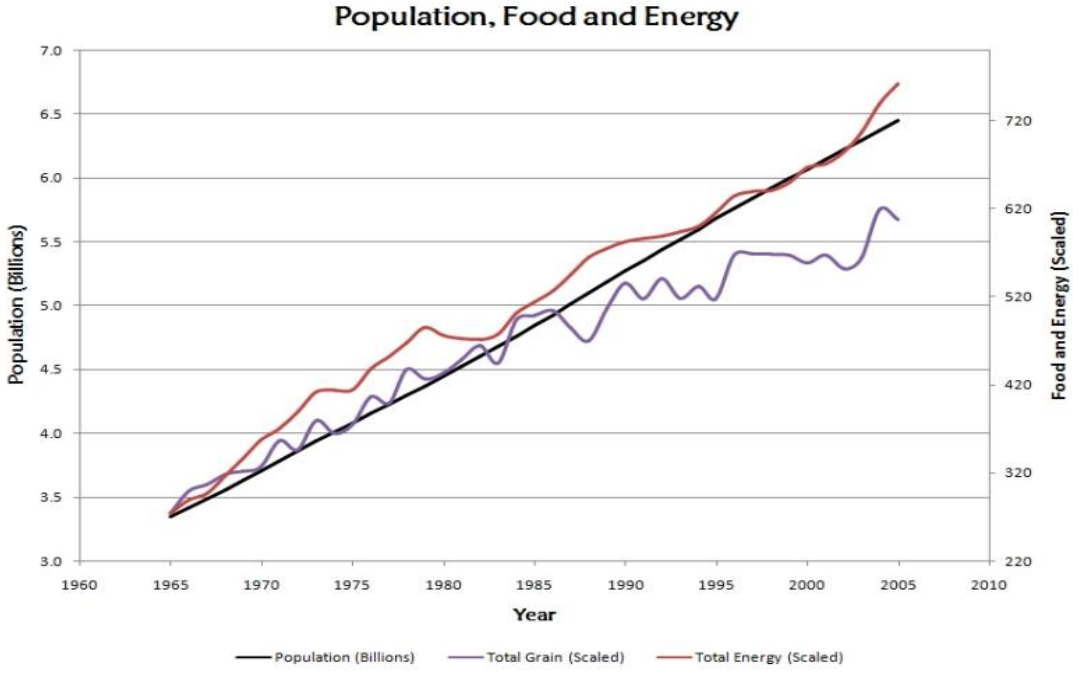

Figure 1.The effects of population on the food and energy demand [3]

Although urbanization is set to rise less than in rural areas, new population in rural agricultural-based areas will shift rapidly into non-agricultural employment and most of this rural population will depend on an even smaller agricultural population segment for food. The world food supply system faces major challenges such as climate change (reducing the harvests) and the expense of energy. Due to certain climate changes and global warming, it is safe to assume that the increase in the utilization of energy has correlated to an increase in CO_2 which has contributed to global warming. Each region of the world has been affected differently by global warming, certain areas face droughts such as California and other places face more devastating storm systems all of which affect crops and their harvest [2].

1.2. Air purification

One of the major sources of air pollution that impacts climate change is volatile organic compounds (VOCs). These VOCs are released into the atmosphere from a variety of sources such as are found in the chemical industries, producing petroleum refineries, paints, detergents and industrial waste [4]. VOCs have also been found to be harmful compounds when they are released into the air and can cause serious health effects such as difficulties in breathing and interference with the central nervous system [5].

Figure 2.Fruit and vegetable a warehouse

Presently, research is underway to establish the health effects that arise from organic VOCs. Evidence, though scant, shows that even in smaller concentrations, VOCs found in organics may have mild health effects. Following these revelations, it is now clear that VOCs will have a significant impact on the global food basket, especially if no technology is adopted to handle the VOCs in warehouse as showing in *Figure 2.* Research should be undertaken to increase agricultural productivity by extending the lifetime of fruits whose aging is controlled by the production and off-gasing of VOCs [1].

As a result, various methods for VOC removal, such as liquid absorption, condensation, biodegradation, catalytic combustion and photocatalytic have been studied. The breakdown of these VOCs through photocatalytic mechanisms at extremely low concentrations have been found to be an effective and cost-effective way of managing this dangerous gas. Using the ultra violet light that comes from direct sunlight or light that is induced artificially can be used to activate nanoparticulate titanium dioxide that is known to breakdown VOCs into non-toxic compounds.

1.3. Food ripping

Although the effects of ethylene were discovered many centuries ago, its significance in agriculture was discovered barely five decades ago. A research that set off to examine the effect of ethylene in Europe found that crops around leaky pipes carrying ethylene exhibited strange growth signs such as hastened growth and falling of leaves prematurely. This study aroused many researchers to want to know more about the role of ethylene in food production [6].

While researchers have found many compounds that can impact food production, ethylene still stands out as the most known compound that impacts ripening of plants and fruits [6]. Studies that have been conducted show that if the synthesis of ethylene, a hormone, is inhibited within plants and fruits, the ripening of fruits is slowed. When manipulated in a well-controlled process, ethylene can be an incredible factor in shaping the future of the food industry in a great way [7]

Ethylene is arguably beneficial, but can be harmful, especially when it comes to storage and packaging of horticultural products. Practical applications of ethylene in agriculture and research

to slow its negative effects on food production have been remained subject to food sustainability debates for many years [6]. The effects of ethylene ripening process are showing in *Figure 3*.

Figure 3.Photograph of the process of ripen Bananas with time

Researchers agree that proper modulation of ethylene activity in the farming, storage and packaging of fruits and other plants can shape the food industry in the right way. For instance, altering and using response mechanisms to influence growth and aging of plants has been found to be an effective way of turning negative effects of ethylene into benefits that could see the world's food stock increase dramatically.

Studies to identify the functioning of ethylene and its synthesis has been instrumental in informing experts to develop favorable storage and packaging conditions that would minimize the negative effects of ethylene and increase post-harvest yields [8]. Commercial production of fruits and other plants that need to be ripened can be extremely challenging.

Since its discovery, ethylene has caused the food industry to devise the best ventilation and temperatures that can spur ripening while reducing food spoil. Therefore, artificial plant hormones can help to both maximize storage life and improve the quality of the fruits with a careful study of ethylene concentrations in storage spaces [7].

While evidence abound that ethylene is an invaluable component in facilitating fruit ripening, it has been found to be extremely harmful to most fruits and vegetables, especially if the compound

occurs in high concentrations that can cause ageing and decline in the quality of the produce. The level of damage caused by ethylene is dependent on the room temperatures and concentration levels of ethylene [8]

Since fruit maturation, shelf life and quality depends on ethylene, clearly, this hormonal compound has a significant role to play in the food industry. When left unmanaged, excess concentration of ethylene in storage rooms can lower shelf life since prolonged exposure to high amounts of ethylene accelerates the growth and causes ageing in food products. In plants that are supposed to maintain their green leaves such as cucumbers and vegetables, excess concentration of synthetic or natural ethylene can cause loss of chlorophyll and this can lead to rotting. To help eliminate wastage that occur in farms and stores due to the effects of ethylene, postharvest physiologists should continuously devise mechanisms that can help strengthen the existing technologies for the sake of turning around the food sector amidst food insecurity crisis that continue to rock the entire globe [7].

Therefore, farmers and experts in the horticulture sector must devise ways of minimizing the effects of ethylene while ensuring that farms and storage facilities are equipped with the necessary equipment to check and regulate ethylene levels for better product quality and increased shelf life going forward [8].

Ethylene that is produced through biological means affects the development and ripening of many climacteric fruits. Food production can be affected when the amount of the released ethylene changes. When high amounts of ethylene are released during the early stages, fruits and vegetables suffer poor tissue development, which can reduce farm yields dramatically [7]. Ethylene has the ability to cause plant death if it is generated in extremely large concentrations. Examples of damages that can be caused by ethylene include poor tissue development, abscission in plants, shortening of the stems and reduced levels of chlorophyll in leafy vegetables. These effects can be exasperated, especially when these plants are subjected to abiotic stress. Similarly, the production of ethylene can increase if the farm produce is stored in rooms that have unfavorable conditions [7].

1.4. Microtechnology

Microtechnology defined as microreactors or microstructures or microchannel reactor system and it is the study, development and application of devices that operate on channel thickness on the scale of 1-1000 microns, the length and the width of that channel could exceed to centimeters. The microreactors lowering chemical reaction systems dimension and that change the physical and the chemical characteristics of a system to be sufficient benefit. Miniaturized reaction system offer many exceptional technical advantages for a large number of applications. This will break down much faster the barrier that still exists for the big scale application. The Micro-reactor channel is showing in *Figure 4*.

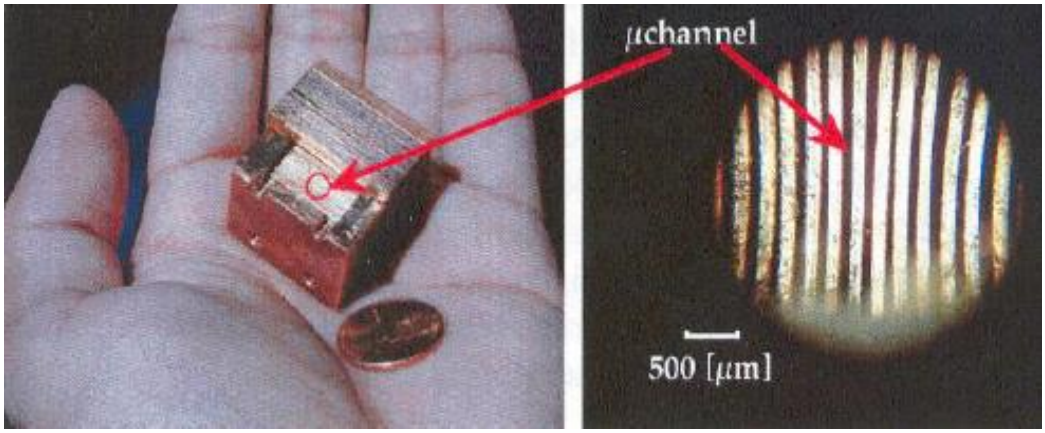

Figure 4. Photograph of a Micro-reactor channel

1.4.1. Advantage of Microtechnology

Advantage in fundamental phenomena

Miniaturizing the dimension of a system introduce a thin layer fluid thickness that incorporate (resemble) to large surface to volume ratios. Some production systems have a ratio of 100/1000 m^2/m^3 and in microreactor capable to deliver a ratio exceed 10,000 m^2/m^3. Shrinking the characteristic dimension of a microreactor down to the micro scale played an important role in the intensification of mass transfer by shorting the diffusion time and heat transfer. Also this will enhance the promoted catalytic reactions through mixing caused by large gradients in concentration and temperature.

Advantage in Safety and Security

Due to the small diameter channel and the large surface to volume ratio, extreme exothermic reactions and their operation are made safer. Such experiments and operations having small volume are inherently less hazardous, safer and more secure.

Advantage in Commercial Applications

Due to the small size reactors, it is easy to integrate a microreactor distribution unit within an assembly line of other processes. This will allow for the implementation and distribution of microreactor units in remote area.

Advantage in Parallel Architecture

Microreactor shows flexibility in production by numbering up units by series and parallel systems to achieve the same production of big scale processes.

1.5. Thesis Goal and Objectives

1.5.1. Research goals

The primary goal of this Thesis is to develop a microscale-based system (device) equipped with a carbon nanotube based emitter electrode that has the capability to provide the complete destruction of hydrocarbon- such as the destruction of ethylene- in atmospheric oxygen through positive polarity corona discharge. The expected degradation products of ethylene are expected to be nontoxic, carbon dioxide and water.

1.5.2. Objectives

- Design and construct a well-defined reactor in a microscale-based technology that will deliver a controlled corona discharge to oxidize ethylene in atmospheric oxygen.
- Develop a carbon nanotube based emitter electrode, grown using thermal CVD, to provide low voltage corona discharge initiation.
- Collect data to characterize the system performance.
- Fitting the gathered data of the oxidation of ethylene into a model such as logistic function model.

Chapter 2: Background

2.1. Plasma discharge

Plasma is a chemically active media consisting of highly ionized gases that are the results of reorganize the electronic structure of a gas by applying energy to the gas molecules and atoms [9]. Plasma is the fourth state of matter, which occupies 99% of the universe and consists of particles known as ions, electrons, and neutrals, which exist in a gaseous excited state [10].

Plasma discharge is defined as an excited state of a gas, which when acted on by an electric field breaks down gaseous atoms and molecules into an avalanche of charged ions .The breakdown is caused by electrons, which when accelerated acquire sufficient energy collide and knock off electrons from the gaseous atoms and molecules, leaving behind ionized gaseous particles to create an avalanche of free electrons [11, 12]. *Figure 5.* Illustrate the breakdown to initiation of a plasma discharge between a point and a plate electrode.

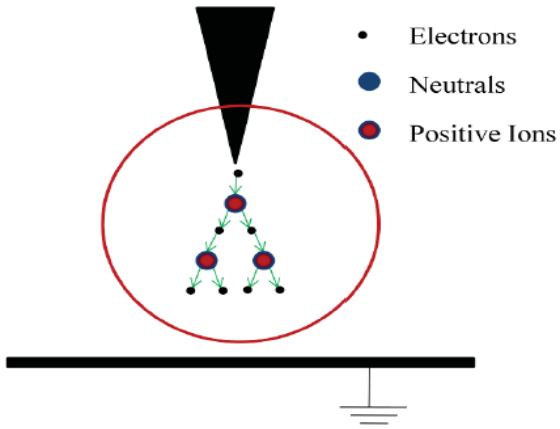

Figure 5. A schematic description of the initiation of a plasma discharge between a point and a plate electrode [13]

Due to electrons exist as quantized particles, which have different forms of internal energy. The quantized structure consists of particles in translation, rotation, vibration and excitation states. The kinetic forms of energy possessed by the gaseous atoms are associated with a critical temperature in the range of 10000k or 1.0 eV [10]

Plasma has different properties and each type of plasma depends on the amount of energy supplied to the neutral species. The energy, which is supplied to the neutral species, is in the form of temperature changes or electronic density. classifying plasma discharge to a thermal and non-thermal (cold plasma) plasma discharge are identify by the temperature changes, which influence the behavior of the gaseous atoms, molecules, and electrons by making them exist in excited states for a very short time [10]. *Figure 6.* Shows the classification of plasma electrons temperature vs. electron density [14**]**

$$T_{trans} = T_{rot} = T_{vib} = T_{elex} = T_e$$

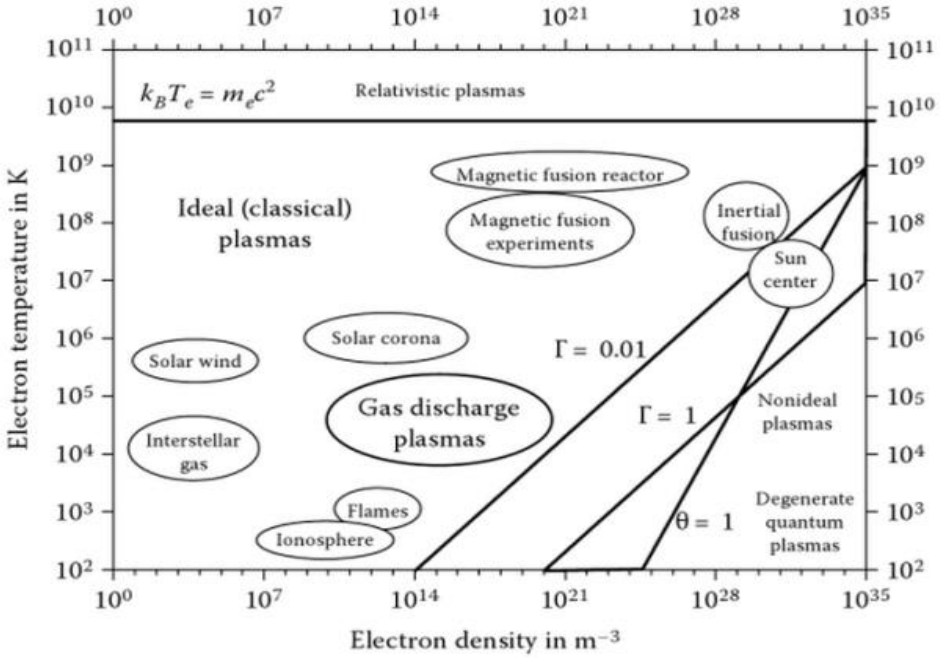

Figure 6. A schematic description of classification of plasma (electrons temperature vs. electron density) [14]

2.1.1. Thermal vs. Non-Thermal plasma discharge

Thermal plasma is governed by the fast movement of electrons, which knock heavy static particles to create ions and behavior of the moving electrons is manage by collisions. Thermal plasma can be characterized by electron temperature (T_e) and it must be low enough to allow particle to reach equilibrium. Also, in a Thermal plasma heavy particle temperature (T_h) is close to electron temperature. Also Thermal plasma can be characterized by high electron density

when it fall between 10^{21} to 10^{26} m^{-3} .Thermal plasma is can be produce by atmospheric arcs, sparks and flames.

$$T_e=T_h\sim 10{,}000\ K$$

Non-thermal plasma (cold plasma) is characterized by inelastic collisions, which occur when heavy particles collide -which are caused by the steep gradient of the plasma- with electrons to create reactive gaseous species in non-equilibrium media. Non-thermal plasma can be describe by the huge temperature difference of electron temperature (T_e=10000-100000 K) and heavy particle temperature T_h=300-1000 K) Also, Non-thermal plasma characterized by low electron density between $<10^{19}$ m^{-3}. Non-thermal plasma includes the Earth's ionosphere and flow discharge in a fluorescent tube [10, 14].

$$T_e>>T_h$$

2.2. Corona Discharge

Corona discharge is a process, which is characterized by the flow of current from an electrode at a high potential into a gas at a low potential [15]. When current flows from an electrode in a fluid, it ionizes the particles of the fluid in its path to form plasma around the electrode. The result is a corona discharge, which occurs in different forms depending on the geometrical configuration of the electrode and the polarity of the electrical field [16]. corona discharge process include high voltage current for creating free electric charges, space charges, which allow an avalanche of electrons to build up, new charge carriers for the photons in the avalanche outside the free space area, and a new avalanche effect around the cathode [17].

Corona discharge generated at low temperatures and it's classified as a non-LTE (Local thermodynamic (or thermal) equilibrium plasma discharge in strong non-uniform electric fields. The discharge can either be positive or negative corona depending on the applied voltage at the end of the cathode. Corona discharge processes develop either the ions produced or the energetic electrons to produce the plasma.

Corona discharges occur on sharp points, thin wires, and edges where the electric field has enough potential to cause the discharge. Corona discharge is defined as "a weak luminous discharge that usually takes place at or near atmospheric pressure" [18]. *Figure 7.* Illustrates a direct current (DC) positive corona in wire-cylinder geometry. A positive voltage is applied to the wire and the cylinder is grounded. When the potential difference is high enough between two conductive electrodes (wire and cylinder), the emission of ion and electron is happen the corona discharge is created.

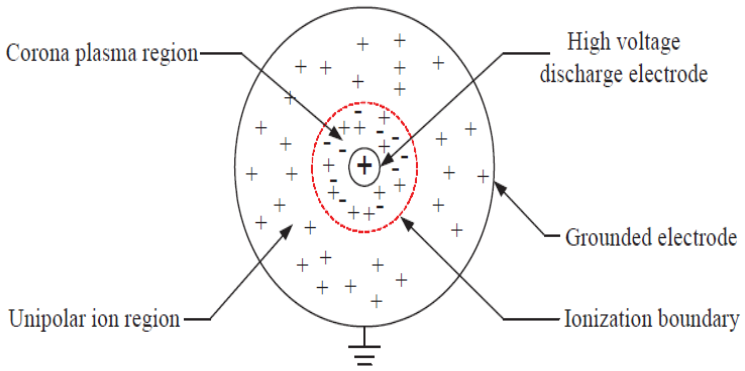

Figure 7. Illustration of the positive corona discharge in a wire and cylinder geometry [4]

2.2.1. Physics of Corona:

The mechanism for generating electrons for negative corona is shown below. Corona plasma is found in a small area of the electrode spacing known as the corona plasma region and has a weak ability to sustain ionization at the outer boundary of the corona system [19]. During the ionization process, pulses occur which cause discharges to occur for a very short time. The short duration cannot allow the discharge to be conducted by the gaseous particles to make a transition to a spark. At the beginning of the discharge, the capacity to ionize the gas depends on the area or surface condition of the gas, the field strength of the gas, the mean free path of the electrons, and the conditions of the high voltage electrode [10]. *Figure 8.* Illustrates a direct current (DC) consists of cathode pin and anode plane geometry.

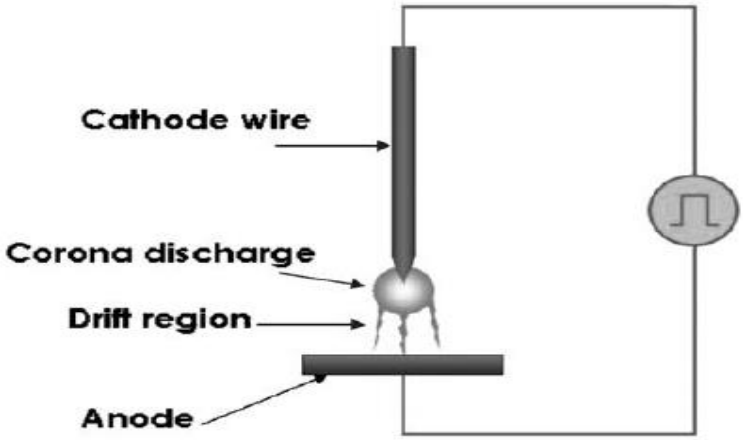

Figure 8. Illustrates a direct current (DC) consists of cathode pin and anode plane geometry.

Positive or anode corona

Generated by the removal electron from a molecule by the high electric field gradient potential that will create other cationic species and electron that can move fast to knock off molecules to emitted an electron from other molecules species. Positive corona is responsible for producing secondary electrons to sustain the ionization process [20, 24].

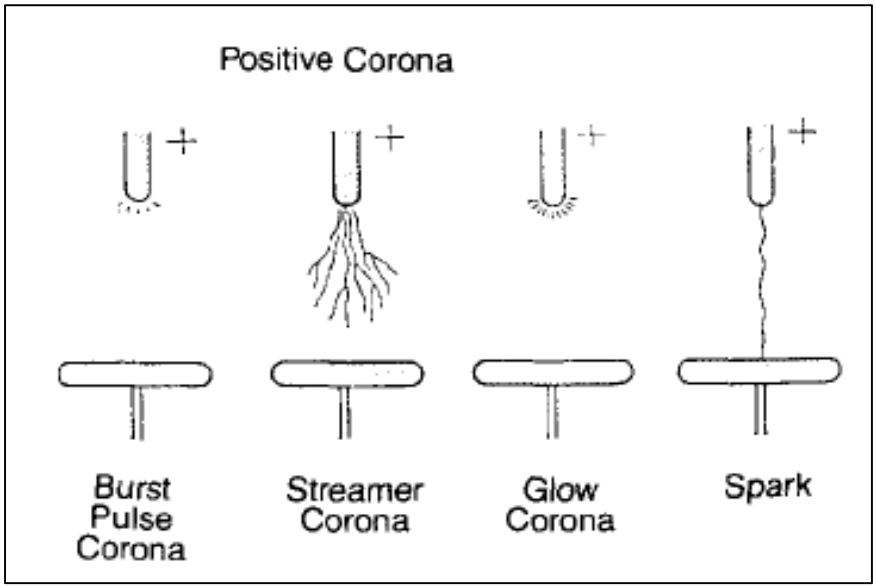

Figure 9. A schematic description of the stage of initiation of positive Corona discharge

The region of high potential gradient leads to the formation of positive ions. The positive ions around the electrodes are repelled and move away while the electrons, which are created when collisions occur, move towards the positive electrode causing an avalanche of secondary

electrons. The electrons are directly caused by the photons of light, which are found at the boundary of the regions that have been ionized. The process involves the photons striking the neutral gas molecules, which are then used to strike and create more electrons to sustain the avalanche effect [19, 21, and 22] (see *Figure 9.*).

Burst pulse corona: a small sharp streamer no self-sustained discharge in the discharge gap and to accumulate it requires a very fast rise in current and slow increase in voltage. Also, it generate weak electron avalanches

Streamer corona: when an increase in the voltage that results in generation of series of long electron avalanches. That will cause molecules and atoms to excite and generate a few photoionization events which cause increase the length of the streamer.

Glow corona or breakdown streamers: when the electric field strength beyond the streamer corona, the discharge becomes self-sustained and the glow steady discharge will happen. This glow will give continuous increase in the voltage but slightly in the current.

Spark: when the electrical field gradient potential across the gap reaches a certain gradient lead to breakdown the gap between the two electrodes and spark will happen.

Negative or cathode corona

Generated by the emitted of a high energy electron from the discharge electrode, which move out fast to knock off molecules to create other anionic species. Negative corona exists in electronegative gases only [19, 21, and 22] (see *Figure 10.*).

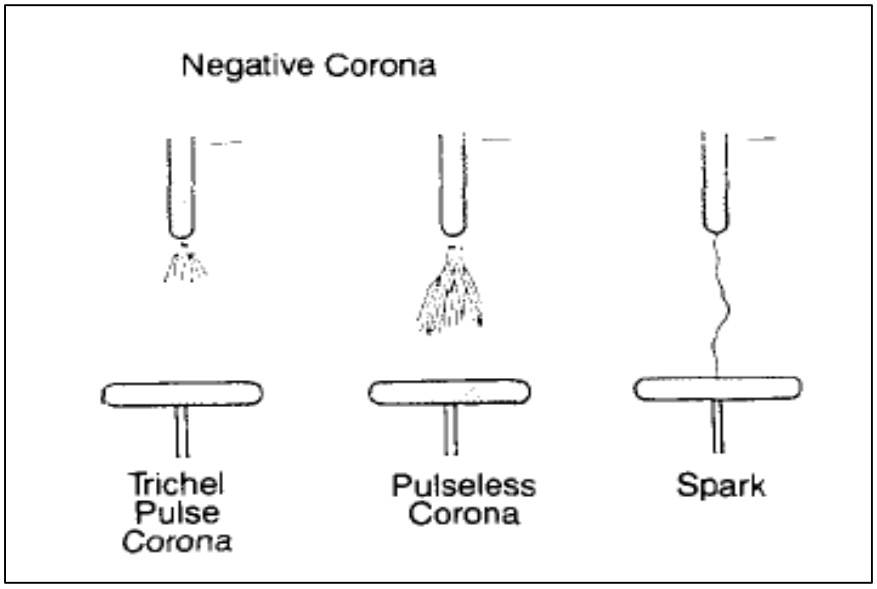

Figure 10. A schematic description of the initiation of negative Corona discharge

Trichel pulse: No corona is self-sustained which occurs for less than a few nanoseconds. Trichel pulses are caused by the occurrence of pulses, which are caused by one or more electrons in the high field region move very fast as they ionize the gas in the region where they have migrated to.

Pulseless corona or negative glow: when the electric field strength beyond the Trichel pulse, the electron avalanches becomes more efficient to develop s glow discharge. This glow will increase in the voltage but slightly in the current.

Spark or negative streamers: when the electrical field gradient potential across the gap reaches a certain gradient, this leads to breakdown in the gap between the two electrodes and a spark may happen if the discharge propagates rapidly enough to reach the opposite electrode during the voltage pulse.

2.2.2. Applications of Corona

Corona discharge has many applications and it has grown in a variety of technologies. In Surface treatment, corona discharge is used as an oil film remover from metallic foils and for antifogging treatment of plastic sheets. In chemical synthesis, corona discharge is used to generate ozone. In gas treatment, corona can be used for the destruction of VOCs.

2.3. Breakdown of Gases:

The breakdown of a gas is defined as the process of forming ions in the discharge gap, which are caused by an avalanche multiplication of electrons. It implies that electrons, which are excited/accelerated by the applied electric field gain sufficient energy to ionize neutral atoms or molecules to form new, free electrons as part of the ionization process. The breakdown process is a prerequisite to the formation of all types of plasma. Breakdown voltage must exist between the electrodes, which depend on the value of the field strength between the two electrodes. The field strength is the factor, which determines the occurrence of the glow discharge. Different gases have different breakdown values [10, 14].

The breakdown mechanism in the gaseous phase shows *Figure 11*. That the flow of elections between the two electrodes can cause a partial or complete breakdown of the gases. For a breakdown to occur, an electrode gap has to be present and if the gap increase that required more voltage. The flow of electrons occurs because of the drift of the positive ions, which is caused by the movement of ions towards the positive electrode. The ions move away from the other electrode to achieve a peak value where further voltage increases does not cause any further flow of current in the gas. The flow of current is sustained by an ionizing mechanism that is external to the system being used [11].

If the gap voltage is slightly increased to maybe a few tens of volts, a very small amount of current will flow. This is because the free electrons will drift in the air towards the anode before they can recombine. Further voltage increase will produce no more current.

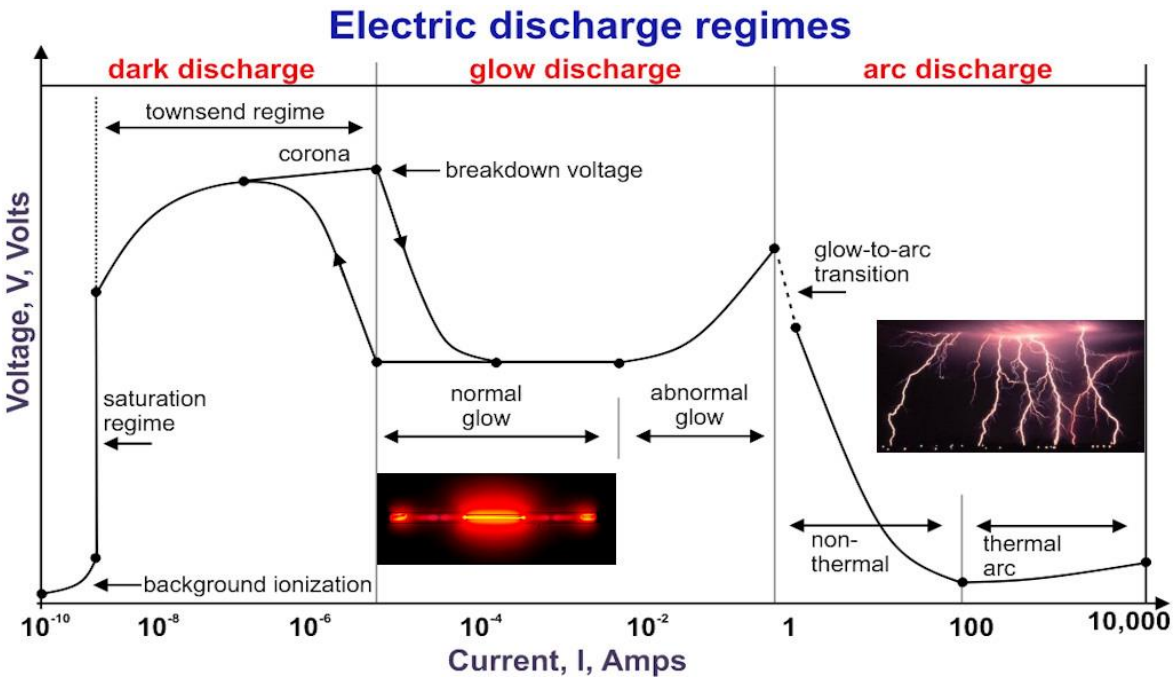

Figure 11. A schemata of Voltage-current relationship for gaseous discharge [23]

When current is increased above the saturation level, increasing the current causes a corona discharge. The discharges can either be the glow discharge or the corona discharge and depends on the voltage and the breakdown phase, which has been reached. Corona region, which allows for a breakdown to occur because of further increases in voltage. When the discharge occurs, the sign of a drastic drop in the potential difference is seen, which leads to a drastic increase in the current flowing between the electrodes.

The application of strong electric fields breakdown creates non-thermal plasma, which makes active particles to exist in the environment. Typically, the free radicals include OH, H, O, $^{1}O_2$, HO_2, O_2, H_2O_2, O_3, species, which depend on the existing environment and the resulting substances, which are caused by electronic reactions in that environment [14,24].

2.4. Nickel Electroplating:

Nickel electroplating is used for electroforming, functional and decorative purposes. Nickel plating is divided into two categories, electroless plating and electrolytic plating Nickel.

Electroplating involves covering metallic surfaces using electricity sources. It required passing of direct current between two electrodes that are submerge in a conductive aqueous solution of nickel salts. The flow of the current will force the anode (electrode) to dissolve and the cathode (electrode) to cover with nickel. At the cathode (electrode) not only nickel ions will react with it but also, the discharge of hydrogen ion from the water will affect the nickel deposition and form bubbles of hydrogen gas at the cathode surface. At the anode (electrode) no hydroxyl ions are formed from water but if the pH of the solution is too high, hydroxyl ion may be discharge in the solution and a termination of nickel and oxygen will be evolved causing a passive layer to form on the anode that will stop the dissolution of nickel. During the electrolytic plating process, the amount of nickel deposited at the cathode and the dissolve at the anode are determines by Faraday's Law [25].

$$Ni^{+2}_{(aq)} + 2e^{-} \rightarrow Ni_{(s)} \qquad E^{0} = +0.23V$$

Electroless plating (EN) involves covering of metallic surfaces with nickel alloys without the application of external electricity sources. (EN) plating has several industrial and commercial applications due to the nature of electroless nickel deposits. The physical and chemical properties of the electroless nickel coatings depend on their composition. Often, the electroless nickel bath solution contains reducing agents, stabilizers, energy, source of nickel ions and complexing agents [26].

2.4.1. Watts's solution

The Watts solution is an electrolyte containing a mixture of nickel chloride ($NiCl_2.6H_2O$), boric acid ($B(OH)_3$) and nickel sulfate ($NiSO_4.6H_2O$), and is the most commonly used nickel plating bath. The Watts solution is used in decorative plating solutions and protection against corrosion. Nickel sulfate in the solution is used to provide the needed concentration of nickel ions, while boric acid is used to maintain the pH of the solution by acting as a weak buffer. Nickel chloride is used to increase conductivity and improve anode corrosion. The Watts solution results in bright nickel used in decorations and semi-bright nickel used for engineering purposes. Composition of the Watts bath varies depending on the purpose of the nickel electroplating. The main advantages of the Watts bath include its simplicity and availability in high purity grade. Watts's bath is also relatively cheap and deposits electroplated from the Watts bath solutions

show little internal stress and are less brittle. Watts's bath solution is also less corrosive to equipment as compared to nickel chloride solutions. [24]

2.4.2. Applications and benefits:

Nickel Electroplating has a lot of application and benefit such as increased resistance to corrosion and improved hardness. It can produce lustrous metallic finishes such as are required on the ramp and bumper in the automotive industry.

2.5. Carbon nanotube

Although carbon nanotubes were accidentally discovered in 1991, they have generated great interest due to their many applications in industry and for scientific equipment. Some of the applications of carbon nanotubes include its use in reinforced materials, semiconductor devices, catalysts and sensors. Carbon nanotubes grow on negative electrodes in reaction chambers and it develops by rolling a sheet of graphene into hollow tubes. Carbon nanotubes have high mechanical strengths and good electrical properties, which makes them useful in many applications. *Figure 12.* Shows three major carbon nanotubes structures include the chiral, armchair and zigzag structures.

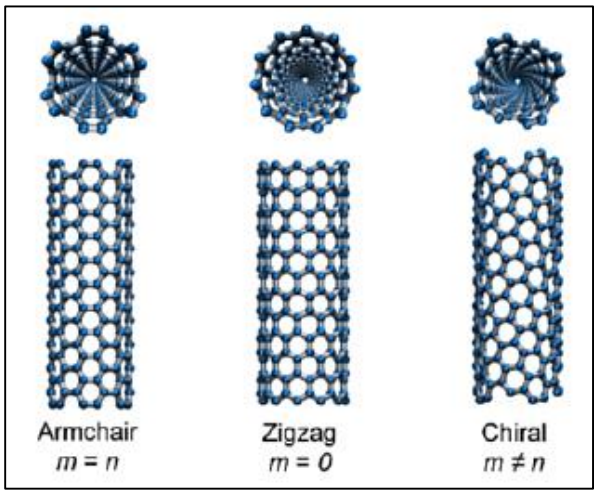

Figure 12. A schematic illustration of the structures of armchair, zigzag, and chiral CNT.

Carbon nanotubes are part of the Fullerenes family and are of two main types: single-walled carbon nanotubes (SWCNTs) and multi-walled carbon nanotubes (MWCNTs). The single-walled carbon nanotubes exist as single cylinders while the multi-walled carbon nanotubes exist as concentric cylindrical tubes. Carbon nanotubes are produced using laser ablation, arc discharge,

plasma enhanced chemical vapor deposition, and carbon vapor deposition as well as through electrolytic methods. However, the electrolytic methods are rarely used. Properties of carbon nanotubes vary depending on the method used to produce them. This is because different methods used in synthesizing carbon nanotubes result in different carbon nanotube structures, and different levels of byproducts and defects. The four major deformities which arise during synthesis of carbon nanotubes include topological, rehybridization, incomplete bonding and doping defects [28].

2.5.1. Methods of Preparation

Regardless of the method used in the synthesis of carbon nanotubes, the production methods are relatively similar. Carbon nanotubes are usually produced using four methods: laser ablation, arc-discharge, plasma-enhanced chemical vapor deposition (PECVD) and thermochemical vapor deposition (CVD) methods. All these synthesis methods involve heat, metal catalysts and carbon feedstock, except the carbon arc discharge method does not require metal catalysts during the synthesis of multi-walled carbon nanotubes [27, 28]

In the laser ablation method, an intense laser pulse is used to ablate a carbon target in the presence of catalysts and an inert gas within a furnace. A constant supply of gas (either helium or argon) is allowed to flow through the tube, and this helps in transferring formed soot out of the reaction chamber. Formation of the carbon nanotubes occurs on cold substrates. The laser ablation method is mainly used in the synthesis of single-walled carbon nanotubes. However, the laser ablation method requires high growth temperature to release carbon atoms from the carbon targets also, it cannot be used in high-volume processing.

The carbon arc-discharge method, occurs in vacuum chambers containing an inert gas and two carbon electrodes. The inert gas increases the rate of carbon deposition while the carbon electrodes act as the source of carbon atoms a high direct current (DC) voltage applied across the two electrodes results in generation of plasma from the inert gas. This evaporates carbon atoms which deposit on cathode as carbon nanotubes while the anode is expended. The hard inner layer of the cathode contains a mixture of amorphous carbon, polyhedral particles and multi-walled carbon nanotubes. When a mixture of metal catalysts is put into the anode, single-walled carbon

nanotubes may also be produced. The structure of the multi-walled carbon nanotubes depends on the gas used during the synthesis.

The PECVD method combines electrical energy and heating to produce the carbon nanotubes. The electricity is supplied to the substrates through powdered electrodes. Combining electricity and heat helps in dissociating more carbon atoms. This method has the advantage of producing carbon nanotubes at low temperatures .The method also makes it possible to produce vertically aligned carbon nanotubes.

In the thermochemical vapor deposition (CVD) system, a hydrocarbon source mainly, ethylene, acetylene, or methane, is broken down into different reactive species in the reaction chamber. The hydrocarbon is subjected to temperatures ranging between 550^0C and 1000^0C. When the right operating temperature is achieved, the gas source is closed and the carbon source valve is opened. The presence of catalysts on substrates and high temperatures in the reaction chamber helps in the formation of the carbon nanotubes. The main catalysts used in the carbon vapor deposition method are the transition metals, such as nickel, iron and cobalt. Carbon nanotubes can be produced at low temperatures through CVD. The method is also the most efficient in production of single-walled carbon nanotubes (SWCNTs) and multi-walled carbon nanotubes (MWCNTs). Single-walled carbon nanotubes are usually produced at higher temperatures while production of the multi-walled carbon nanotubes occurs at lower temperatures.

During the production of carbon nanotubes using the CVD method, metallic and carbonaceous impurities are produced. Metallic impurities arise from residual catalysts, such as nickel, while carbonaceous impurities are by-products which arise from the reaction. The carbonaceous impurities are removed through oxidation. This is achieved using gas phase and liquid phase purification. Gas phase purification uses high temperatures to eliminate the carbonaceous impurities, whereas the liquid phase purification involves use of acidic solutions to wash the carbon nanotubes. Metallic impurities are removed by evaporation. The thermochemical vapor deposition (CVD) method has several advantages, such as producing hollow and uniform carbon nanotubes, forming highly aligned ensembles and lack of macroscopic defects.

Electrolysis is the least commonly used methods in the synthesis of carbon nanotubes. In this method, two graphite electrodes are immersed in molten ionic salts and current is passed through. After completion of the electrolysis process, the remaining carbonaceous material is dissolved in distilled water. This dissolves the ionic salt, and the dispersion is separated by filtration. The residues contain a mixture of carbon filaments, amorphous carbon, remnants of the salt ions, which cove some of the carbon, and multi-walled carbon nanotubes. However, the electrolysis method cannot be used to in the production of single-walled carbon nanotubes.

2.5.2. Behavior in Electrical discharge

Carbon nanotubes have unique electrical properties, and they are either semiconducting or metallic. These properties depend on the chirality and tube diameter of the carbon nanotubes. The chirality of carbon nanotubes is represented by the integer pair (n and m). Carbon nanotubes with $n - m = 3j$ (where j is a nonzero integer) are metallic. All the other carbon nanotubes are semiconducting. Carbon nanotubes are highly anisotropic in their dielectric properties, and this arises from their uni-dimensional structures. This increases the efficiency of carrying high current electricity in carbon nanotubes with minimum loss in terms of heating. Current density in most metallic conductors is limited by electromigration. Conducting carbon nanotubes have high current densities due to their small cross-sectional areas. Semiconducting SWCNTs have the advantage of operating at high frequencies and are used in integrated circuits to increase their number densities and speeds. SWCNTs have low electron scattering, which makes them useful for building transistors. Carbon nanotubes are also used in for high voltage application, such as providing reduced initiation voltage required for corona discharges [29, 30]

2.5.3. Application

The characteristic of carbon nanotube made it useable by wide verity of applications that integrated of different application such as membrane for filtering toxic chemical, and contamination from water. Also, it used to strengthen materials such as building materials and vehicles and body armor. Moreover carbon nanotube electrodes provide more current and better electrical and mechanical stability.

2.5.4. Carbon Nanotubes Defects

Four major categories of carbon nanotubes exist and include topological, rehybridization, incomplete bonding and doping defects. Topological defects are localized and do not change the lengths of the carbon nanotubes, but only affect electronic structures on sidewalls in some locations along the nanotube. Graphite is mostly affected by the incomplete bonding defect where dislocations and vacancies arise. Incomplete bonding and doping defects have the ability to increase the chemical reactivity and electrical conductivity of carbon nanotubes [27].

2.6. Oxidation of Hydrocarbon: Oxidation processes of Ethylene

Hydrocarbons combustion responsible to drive our high-tech world. Combustion of fossil fuels such as petroleum and natural gas deliver 75% of world energy. Hydrocarbons molecules released into the environment are termed Volatile Organic Compounds (VOC). They are released into the earth's atmosphere continually from industry-wide workshops causing hazards to the environment and humans. As a result, various oxidative process used to break down complex VOC compounds, such as absorption, condensation, adsorption, biodegradation, catalytic combustion and thermal oxidation have been studied [31, 32].

Thermal oxidation is the process of increasing the temperature of the contaminant air until it pass the auto ignition temperature, it vary from 650^0C to 1100^0C depend in the feed stream composition. Feed stream the conversing to carbon dioxide and water.

Catalytic combustion processes are similar to the thermal oxidation process, except for the existence of catalysts in the process to increase the reaction kinetics to allow the reaction occur at lower the temperature around 250^0C and under lower residence times in the reactor [33]

Biodegradation is the process that involves microbe to transfer of the VOC to carbon dioxide, water, nitrogen oxides, and salts. Also, each VOC has different microbe to convert to nontoxic material. This process requires extensive control of the microbial population health and growth rates.

Absorption process is passing the contaminated air through a solvent to remove the VOC and it depends on diffusion between gas-liquid interfaces. The basic system of this process relies on a column and packing material to increase the surface contact and that will improve the overall mass transfer of the absorbent gas to the solvent.

Adsorption process is passing the contaminated air through a solid porous absorbent bed for the removal of the VOC. This process is used in-line to another process such as a distillation column or regenerative thermal oxidizer for final removal. It requires regeneration of the bed when it is saturated. This is done by changing them or passing hot inert gas through the absorbent beds.

Condensation processes can be approached by fixing the temperature and increasing the pressure (compression condensation) or by fixing the pressure and lowering the temperature (refrigeration condensation). This condensation process is limited to VOCs with boiling points above 38^0C and at concentrations above 5000 ppm [34].

2.7. Screening design

Statgraphics centurion a statistical package is used to perform a screening design. Screening designs a popular designs for industrial experimentation and it is typically initial stages of experiment because it examine a list of many factors to identify those that have significant main effects of the response factor. In screening design, each factor contain two level which is high and low. It requires experimental runs to establish a basic understanding of interdependencies within complex processes.

In the screening design we will generate a standardized Pareto chart and main effects plot using Statgraphics centurion: the standardized Pareto chart It contain bars of effects for all factors and it sorts from the most significant to the least significant. The main effects plot is used to study the differences between two levels, such as means in each factors high and low levels. When different level of factors affect the response differently, it will show as a connected line with

some slope in the main effects plot. The slope of a line, indicates how strong the effects of the factor is correlating to the response.

2.8. Logistic function:

The logistic function was invented in the 19th century to describe the growth behavior between discrete variable and predictor in many cases: the growth in population, autocatalytic chemical reactions, chain reactions and market penetration of new products and technology. The logistic function is useful as a normal fit for data that has growth behavior. The logistic regression model is a nonlinear model with a sigmoidal shape [35]. In general, the logistic function can be used to describe the dynamics of something subject to an exponential growth combined with saturation effect [37, 38].

The corresponding equation is called logistic ordinary differential equation [36].

$$\frac{dX}{dt} = rX\left(1-\frac{X}{K}\right) \quad (1)$$

Dr. Carallini [36], used this logistic ordinary differential equation in fitting his data. The separation of variables technique is used to solve the logistic differential equation. *Appendix L* show the solution of logistic ordinary differential equation using separation of variable.

$$X(t) = \frac{K}{1+Ce^{-r\,t}}$$

$$t \to \infty, \quad X(t) \to K \qquad (2)$$
$$t \to 0, \quad X(t) \to K/(1+C)$$

Where

X = X (t): the conversion of ethylene gas (%)

t : the resident time (sec)

r : the growth rate (sec^{-1})

K: saturation level (%)

C : is an integration constant

Chapter 3: Experimental Set-Up

3.1.Apparatus

The gas microscale-based corona discharge reaction system in this study consists of the following parts: power supply, Air gas tank, mass flow controller, ethylene syringe pump, microreactor, oscilloscope, resistor, gas chromatography (GC), and computer to send commands to the mass flow controller and to collect the data, and a ventilation system for the waste. *Figure 13.* Shows the schematic of micro scale-based corona discharge reaction system.

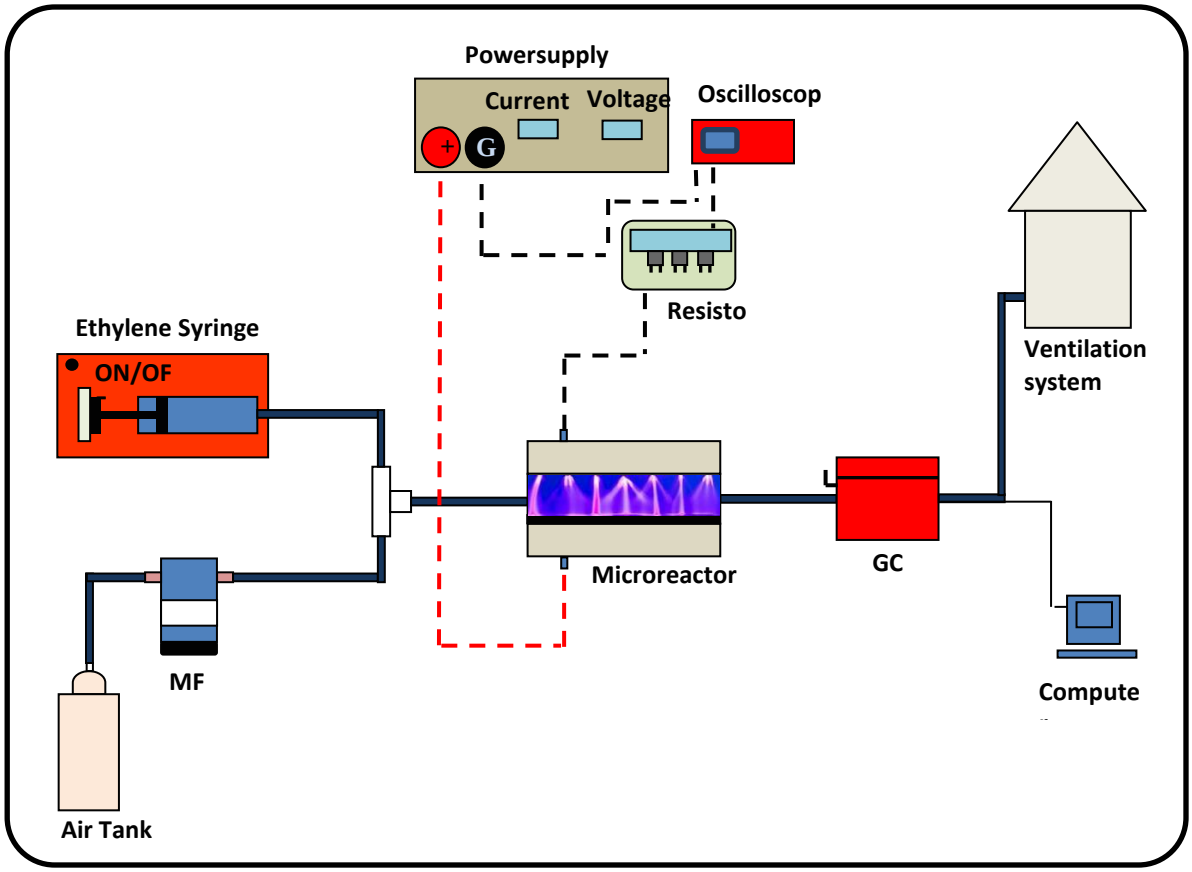

Figure 13.Schematic of micro scale-based corona discharge reaction system

3.1.1. Syringe Pump and Syringe

A NE-1000 Mulit-Phaser™ Programmable Syringe pump from New Era Pump Systems Inc, shown in *Figure 14 (a),* is used to supply the ethylene to the microreactor. It is a single syringe pump and it is capable of infusion or withdrawal of a dispensed volume. This pump has a built-in programmable phases allowing complex pumping rates, the pumping rates variety from µL/hr to 2120mL/hr. also, it has two modes of RS-232 control, basic and safe. The safe mode is important because it provides communication error defection, loss of communication detection and automatic transmitting of alarm condition. A removable luer lock syringe from SGE Analytical Science, shown in *Figure 14 (b),* is used because it is a gas tight syringe and that will not allowed any leak of the ethylene gas to the surrounding.

(a) **(b)**

Figure 14. (a) Photograph of NE-1000 Mulit-Phaser™Programmable Syringe pump (b) Photograph of a removable luer lock syringe from SGE Analytical Science.

3.1.2. Mass Flow Controller

A 4800 Series thermal mass flow controller from Brook's Instrument, shown in *Figure 15(a),* is used to supply the air to the microreactor. This devise has a micro electro mechanical system (MEMS) based thermal sensor. It measures a change in temperature across the MEMS sensor to determine mass flow rate and presents an ultra-fast responding time. It offers great control of a variety of gasses and it has a wide flow range. *Appendix C* shows the calibration curves of air.

A USB-6009 data acquisition from National Instruments (NI) *Figure 15 (b)*, is used to link the mass flow control to the computer, to control and send command from the computer to the mass flow controller using a program called LabView. LabView program is called virtual instrument (VI), because it able to operate another instrument such as an oscilloscope. Also it is able to analyze display and store data. The most important window is the front panel and the block diagram window.

The front panel window is where the user interface for the VI is displayed and from where you command to disperse certain amount of flow rate of air to the system. *Appendix C* shows the front panel window. The block diagram window is where you put the functions, constants, structures to transfer data between other block diagrams. The block diagram window contains the graphical source code. *Appendix C* shows the block diagram window.

(a) **(b)**

Figure 15. (a) Photograph 4800 Series thermal mass flow controllers from Brooks Instrument (b) Photograph of USB-6009 data acquisition from National Instruments (NI)

3.1.3. Power Supply

A EQ Series 1200 W regulated High Voltage DC power Supplies from Glassman High Voltage Inc. ,as illustrated in *Figure 16,* is used to supply the high electric field to the microreactor. This device has a range of 1 to 60 kV, single-phase power, air insulated, fast response and low current and noise.

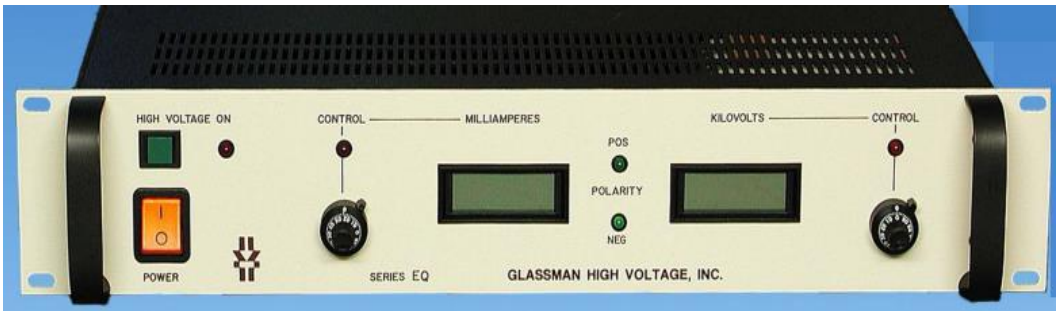

Figure 16. Photograph of EQ Series 1200 W regulated high voltage DC power supply from Glassman High Voltage Inc.

3.1.4. Ballast Resistors

A MP 925 power film resistor with exposed ceramic heat dissipating mounting surface from Kool-Pak, as illustrated in *Figure 17 (a) and (b),* is used to impede or limits the flow of the electrical current in the reactor to prevent the reactor from shorting. In the circuit, two 100kΩ resistor and a single 10kΩ are all connected in series with the microreactor. The resistors are mounted on a flat heat sink and the entire ceramic back is in thermal contact with the heat sink. A100kΩ resistor allows a maximum of 500V to be applied and more than this will destroy the resistor. The system has a total of 210kΩ that allow around a maximum voltage of 1050 V to be applied across the ballast resistor without damaging the circuit.

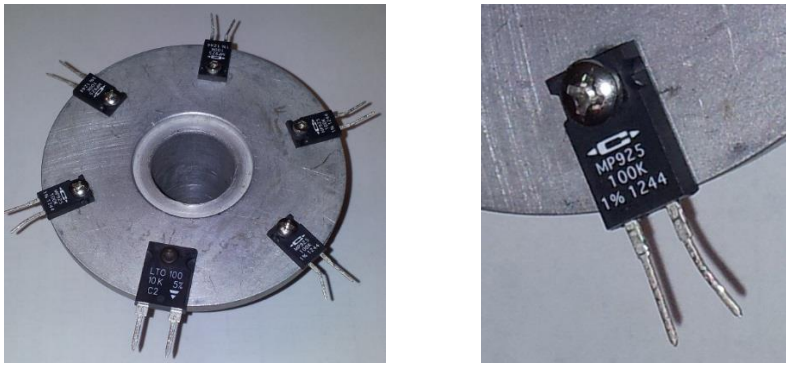

(a) **(b)**

Figure 17.(a) Photograph of A MP 925 power resistor with exposed ceramic heat dissipating mounting surface from Kool-Pak. (b) is a zoom in picture of the Resistor

3.1.5. Nickel Electroplating Setup

The electroplating setup, as illustrated in *Figure 18,* consists of the object to be plated which is attached to the negative post of a power source, causing the object to attract positive metal ions from the electrolytic solution. The nickel-iron alloy sheet acts as the anode, constantly supplying nickel ions into the electrolyte bath via an oxidation reaction. The stainless steel plate acts as the cathode, attracting the nickel ions to itself, where they are reduced to nickel-iron alloy on its surface. The electrolyte bath is the Watt's solution and it consists of nickel sulfate, nickel chloride and boric acid. *Appendix E* shows the diagram of a typical electroplating set-up

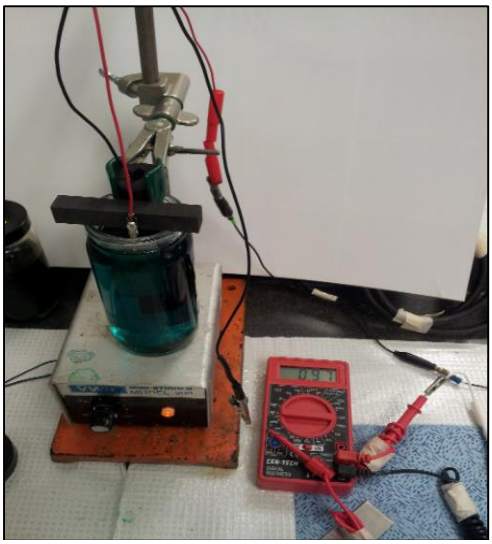

Figure 18. Photograph electroplating experiment with current measurement.

3.1.6. Chemical Vapor Deposition (CVD) Set-up

An OTF 1200X-S split tube furnace with 2" O.D quartz tube from MTI Corporation, as illustrated in *Figure 19*, is used to grow carbon nanotubes. This device can ramp in temperature as fast as 1200°C / hr. It has a built-in temperature controller that is programmable and can give up to 30 steps of heating and cooling with +/- 1°C accuracy and offers thermocouple failure protection. *Appendix F* shows the temperature ramp in *Table F-1* that used to grow carbon nanotube.

Figure 19.Photograph OTF 1200X-S split tube furnace with 2" O.D quartz tube CVD from MTI Corporation experiment

3.2.Operation Procedure

3.2.1. Experimental Variables

1- Screening design

In this study, a screening design is imperative in determining the factors that are most important for the system. So the screening design was essential in our work to quickly build a framework for a useful design of experiments. Four experimental variables were examined: Reaction spacer, flow rate, power supply voltage, and inlet ethylene concentration. *Table 1.* List the different experiments performed.

Flow rate (mL/min)	**Spacer (µm)**	**Concentration(ppm)**	**Voltage (kV)**
50	750	200	2
50	750	200	1.4
50	750	600	1.4
50	750	600	2
100	750	200	1.4
100	750	200	2
100	750	600	1.4
100	750	600	2
50	250	200	1.4
50	250	200	2
50	250	600	1.4
50	250	600	2
100	250	200	1.4
100	250	200	2
100	250	600	1.4
100	250	600	2

Table 1.Screening design experimental variables

2- Experiment variables at small spacer (250μm)

Spacer (μm)	RT(1/s)	Concentration(ppm)	Current (mA)
250	0.008	200	5
250	0.016	200	5
250	0.023	200	5
250	0.029	200	5
250	0.039	200	5
250	0.047	200	5
250	0.058	200	5
250	0.008	600	5
250	0.016	600	5
250	0.023	600	5
250	0.029	600	5
250	0.039	600	5
250	0.047	600	5
250	0.058	600	5
250	0.008	200	6.5
250	0.016	200	6.5
250	0.023	200	6.5
250	0.029	200	6.5
250	0.039	200	6.5
250	0.047	200	6.5
250	0.058	200	6.5
250	0.008	600	6.5
250	0.016	600	6.5
250	0.023	600	6.5
250	0.029	600	6.5
250	0.039	600	6.5
250	0.047	600	6.5
250	0.058	600	6.5

Table 2.Experiment variables at small spacer (250μm)

3- Experiment variables at bigger spacer (750µm)

Spacer (µm)	RT(1/s)	Concentration(ppm)	Current (mA)
750	0.016	200	5
750	0.023	200	5
750	0.029	200	5
750	0.039	200	5
750	0.047	200	5
750	0.058	200	5
750	0.016	600	5
750	0.023	600	5
750	0.029	600	5
750	0.039	600	5
750	0.047	600	5
750	0.058	600	5
750	0.016	200	6.5
750	0.023	600	6.5
750	0.029	200	6.5
750	0.039	200	6.5
750	0.047	200	6.5
750	0.058	200	6.5
750	0.016	200	6.5
750	0.023	200	6.5
750	0.029	200	6.5
750	0.039	600	6.5
750	0.047	600	6.5
750	0.058	600	6.5

Table 3.Experiment variables at bigger spacer (750µm)

Chapter 4: Method, Material and Measurement

4.1. Analytical Method

4.1.1. Gas Chromatography

A 8610C model of gas chromatography from SRI Instruments, showing in *Figure 20*, is used in this study. The GC has a helium ionization detector (HID) and a 2m length of 2mm ID Porapak QS column that used to analyzing the outlet concentrations of ethylene and carbon dioxide by measuring the peak area of those species.

The operation condition of the measurement are: injection of 1 mL of gas mixture by the automated sampler into the column. Column temperature starts at 40^0C and is held for 3min then ramped up by 8^0C/min until 50^0C is reached and then ramped up 16^0C/min until the column is 100^0C. The sweep gas (helium) pressure is set at 15psi. The calibration curves of ethylene and carbon dioxide are operated at these conditions. *Appendix C* shows the calibration curves of ethylene and carbon dioxide.

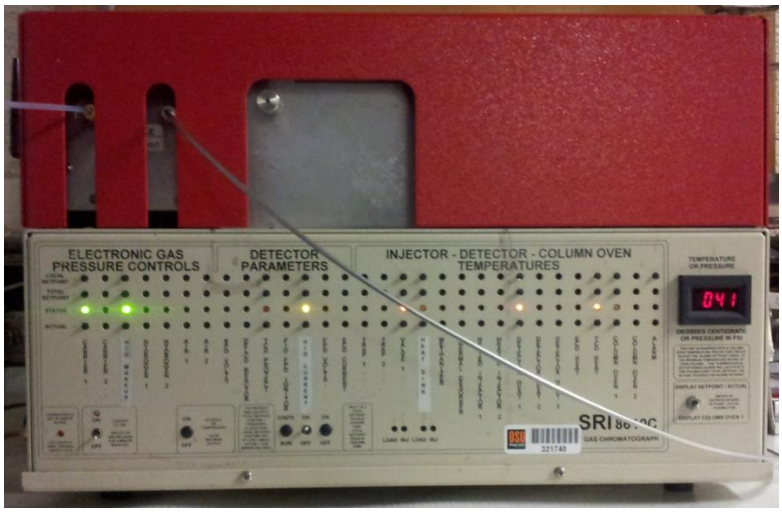

Figure 20.Photograph of an 8610C model of gas chromatography from SRI Instruments.

4.1.2. Oscilloscope

A 54542A 500MHz/2GSs four channel oscilloscope manufactured by Agilent-Hewlett Packard, shown in *Figure 21*, is used in this study to measure the current. The current is measured by capturing the voltage drop across a known resistance and because the voltage drop across a resistor is proportional to the current through that resistor the current will be translated into a voltage drop.

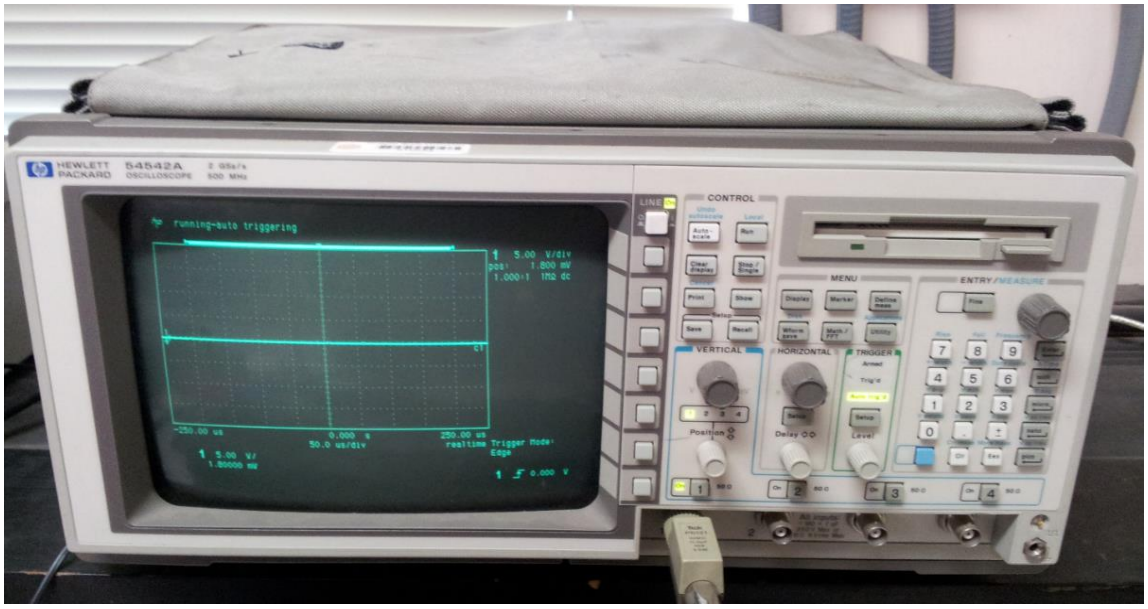

Figure 21.Photograph of A 54542A 500MHz/2GSs four channel oscilloscope manufactured by Agilent-Hewlett Packard

4.2. Reactor Materials

The micro reactors, illustrated in *Figure 22,* consist of Teflon PTFE spacers, two stainless steel electrodes, two clear polycarbonate sheets, two Delran nuts and 14 stainless steel screws.

(a)

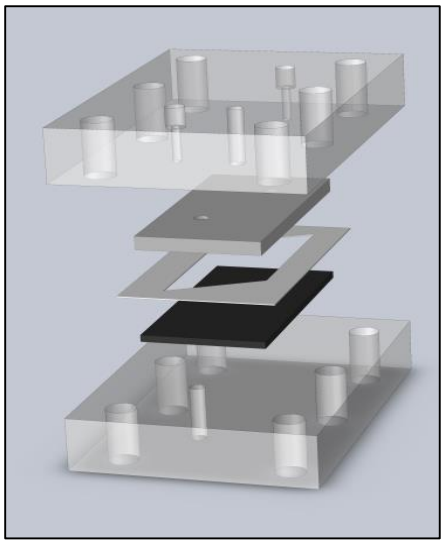

(b)

(c)

Figure 22.Photograph of corona micro reactor (a) components of the reactor (b) Assembly (Exploded View) (c) side view of the reactor.

4.2.1. Spacer:

A Teflon PTFE spacer with a length of 30 mm and 5.17mm width and thickness of 750µm and 250 µm is used to create the micro-channel where the chemically active corona discharge will occur. *Figure 23*, shows the design of the spacer.

Figure 23.Photograph of corona microreactor channel geometry

4.2.2. Counter Electrode

A corrosion-resistant 316 stainless steel plate, mirror-like finish, 0.120" Thick, 1" x 2" is used with two one sixteenth inch diameter holes drilled in on the corner for the inlet and outlet gas to enter and exit the microchannel. Designing the holes is critical. If the edge of the hole is sharp, this will allow the discharge to happen at the edge. So countersinking is performed at each hole to prevent the sharp edges or chamfering *Figure 24*, shows the finished electrode.

Figure 24.Photograph of corona micro reactor counter electrode

4.2.3. Emitter Electrode

A corrosion-resistant 316 stainless steel plate, mirror-like finish, 0.120" Thick, 1" x 2" is used. This plate goes through several processes: first, is the nickel electroplating process and the second, is the carbon nanotube growth cycle .the nanotube have diameters of the average of 50 nanometer and the length of hundreds of nanometers. *Figure 25*, shows the corona micro reactor emitter electrode processes (1) Electrode after the electroplating process (2) Electrode after the carbon nanotube process.

(1) **(2)**

Figure 25.Photograph of corona micro reactor emitter electrode processes (1) Electrode after the electroplating process (2) Electrode after the carbon nanotube process

4.3.Reactor Validation Measurements

4.3.1. Current-Voltage Test

The current-voltage (I-V) test is conducted to determine the behavior of the reactor before and after the turn-on voltage that is required to sustain the corona discharge. *Figure 26*, shows the performance of the current-voltage of the air Also, The current-voltage test for a mixture of ethylene/air (0.1/60) mL/min performed and it looks like the air I-V test and that is due to the low hydrocarbon concentration

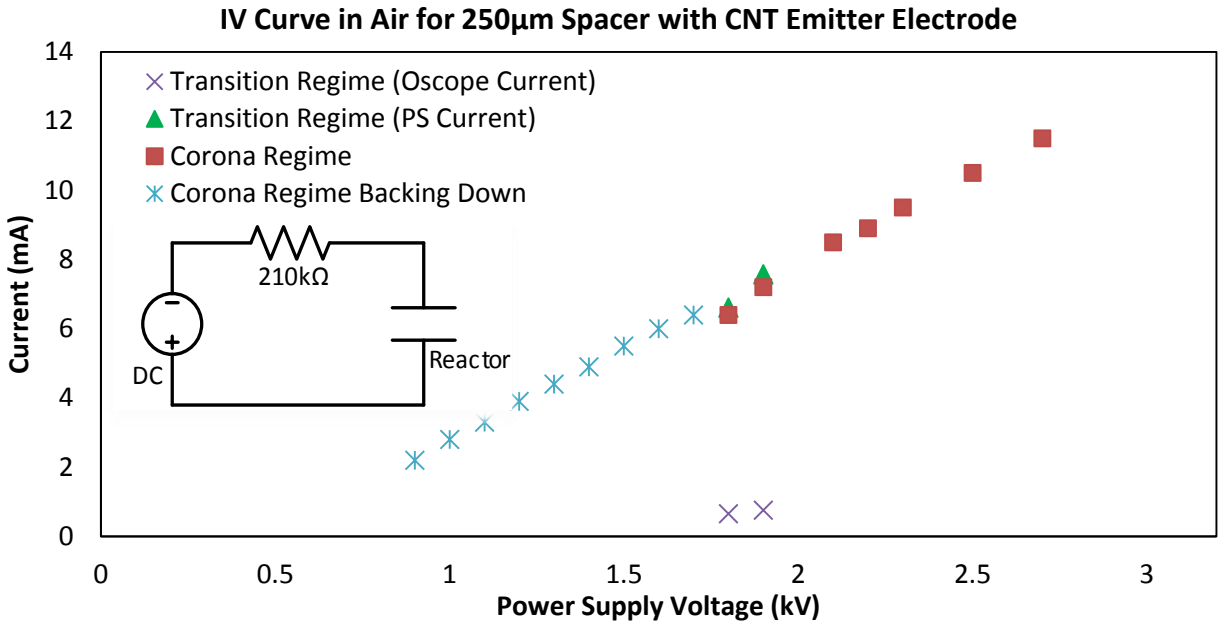

Figure 26.Plot the behavior of current (mA) vs. power supply voltage (kV)in the present of airat atmospheric pressure

4.3.2. Early Analysis by Gas Chromatography

Early experiments are conducted by supplying 1.8kv to the reactor and analyzing the result of a mixture of ethylene/air (0.1/60) mL/min performance to see if the reactor performed for the oxidation of low concentrations of hydrocarbon in atmospheric air *Figure 27*, shows the result of the gas chromatography

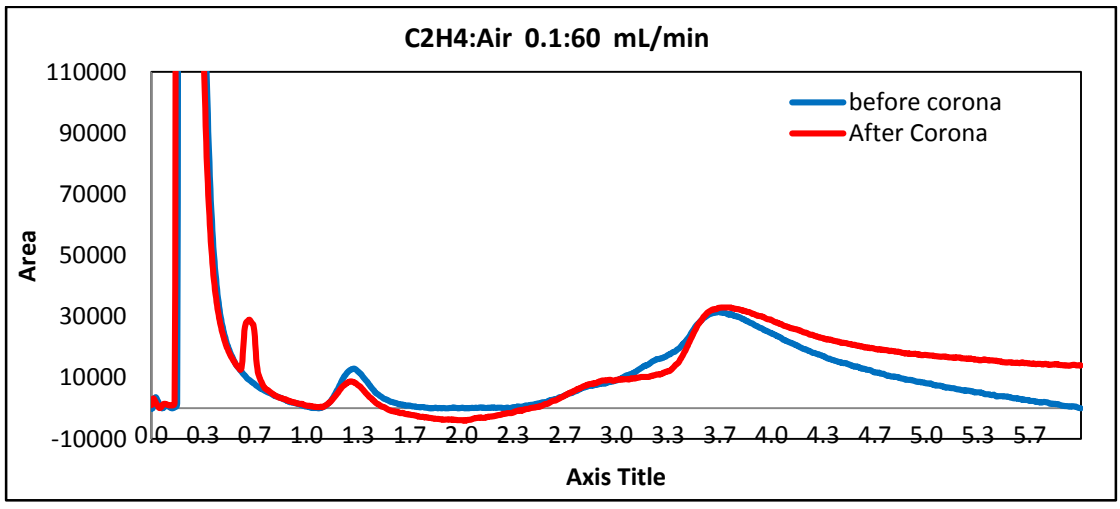

Figure 27.Plot of validation measurementsof ethylene and air mixture before and after corona discharge using the gas chromatography

4.3.3. Mass Spectrometry Results

For the same early experiment, a mixture gas collected using a sample bags before supplying the microreactor with 1.8kv and after to analyze the reactant and the products using quadruple mass spectrometry. *Figure 28 (a)*, shows the result of the gas mixture before supplying the reactor any voltage and *Figure 28 (b)*, shows the result of the gas mixture after supplying the reactor with 1.8kv.

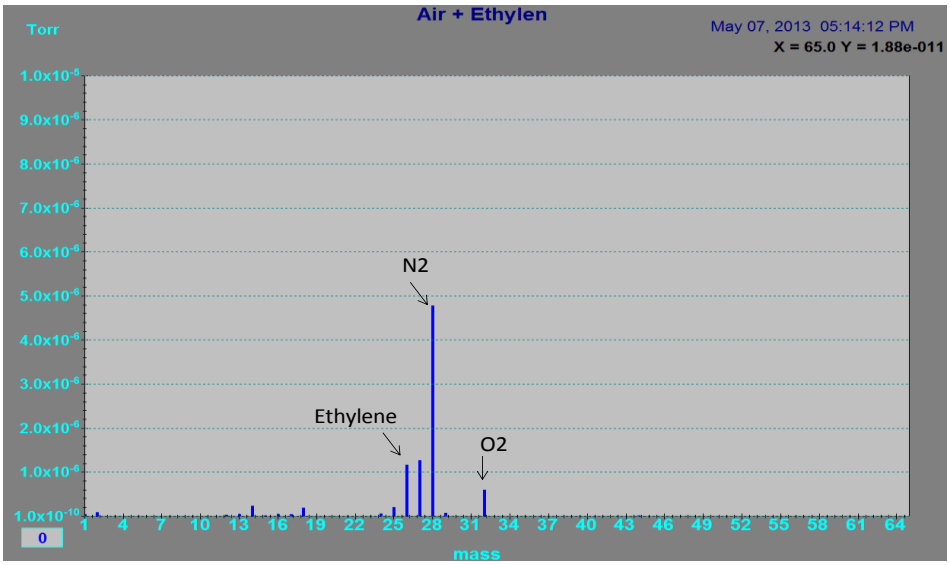

(a)

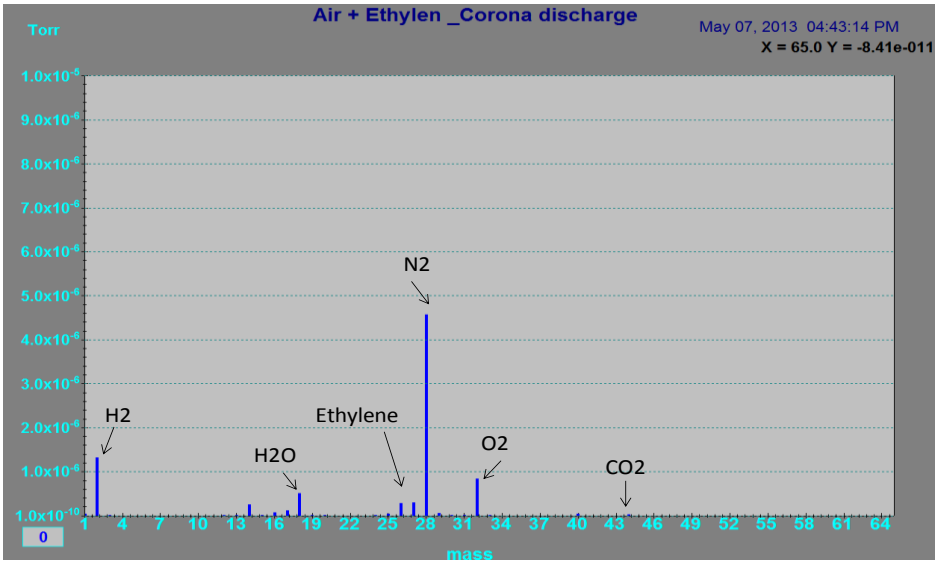

(b)

Figure 28.Plot of validation measurements of Ethylene and air mixture (a) before and (b) after corona discharge using quadruple mass spectrometry

Chapter 5: Experimental Data

5.1. Oscilloscope and IV test

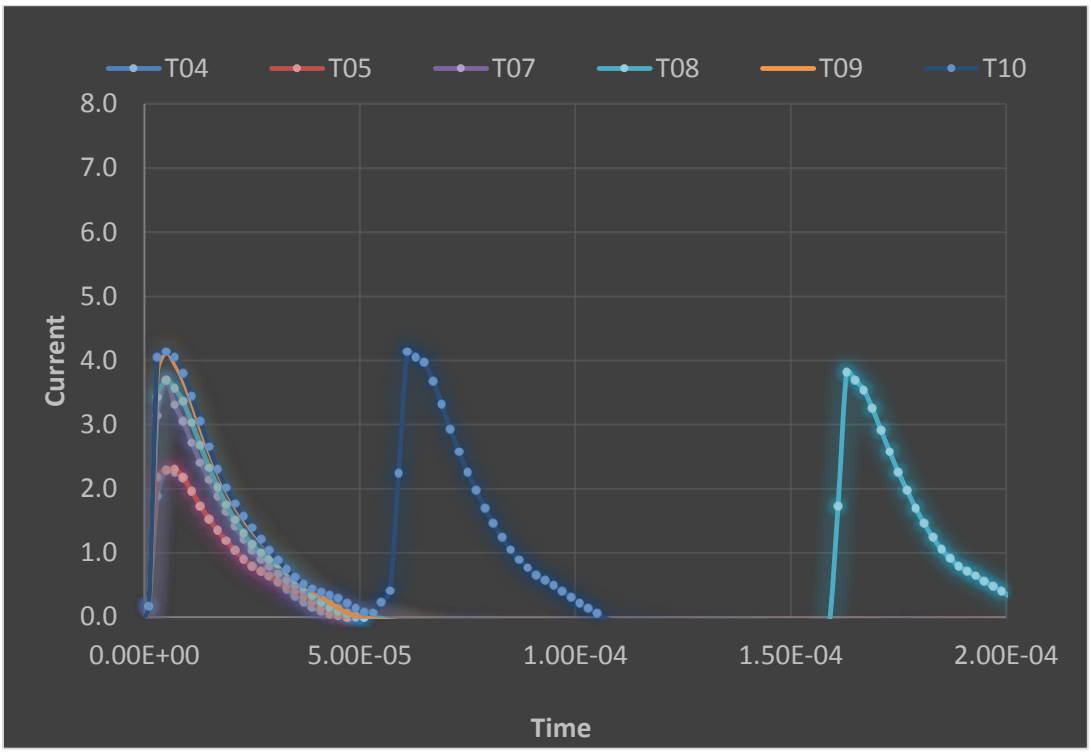

(a)

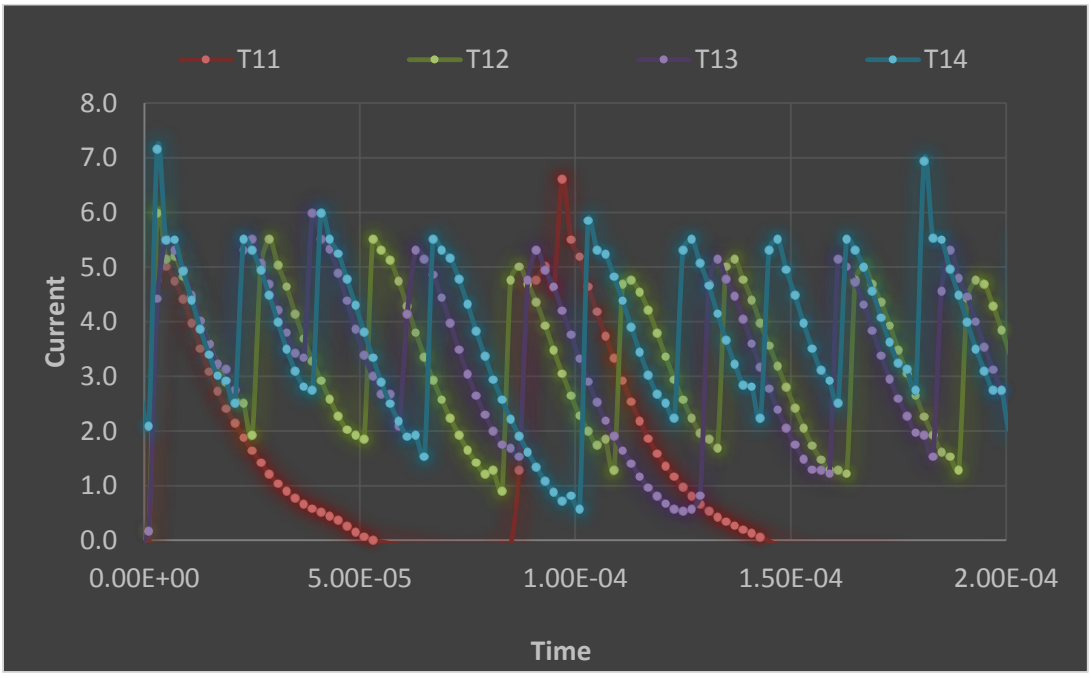

(b)

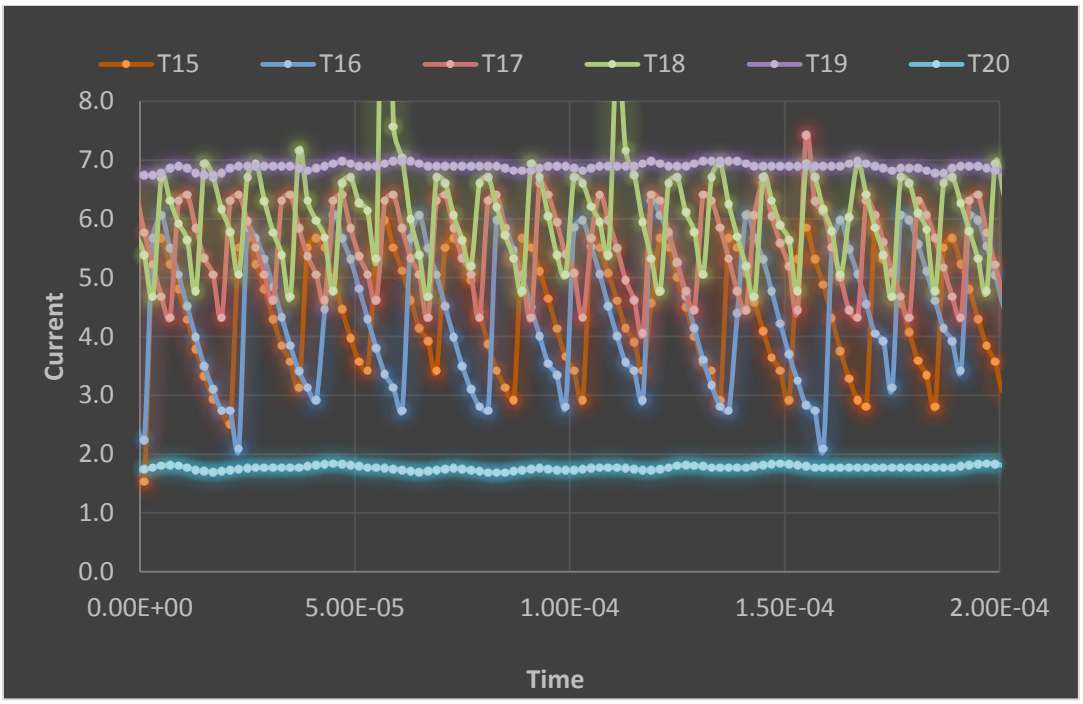

(c)

Figure 29.Plot of oscilloscope measurements of ethylene and air mixture (a) the initiation of onset streamer (b) the increase of streamer but not self-sustained (c) the transition between self-sustained streamers to corona discharge

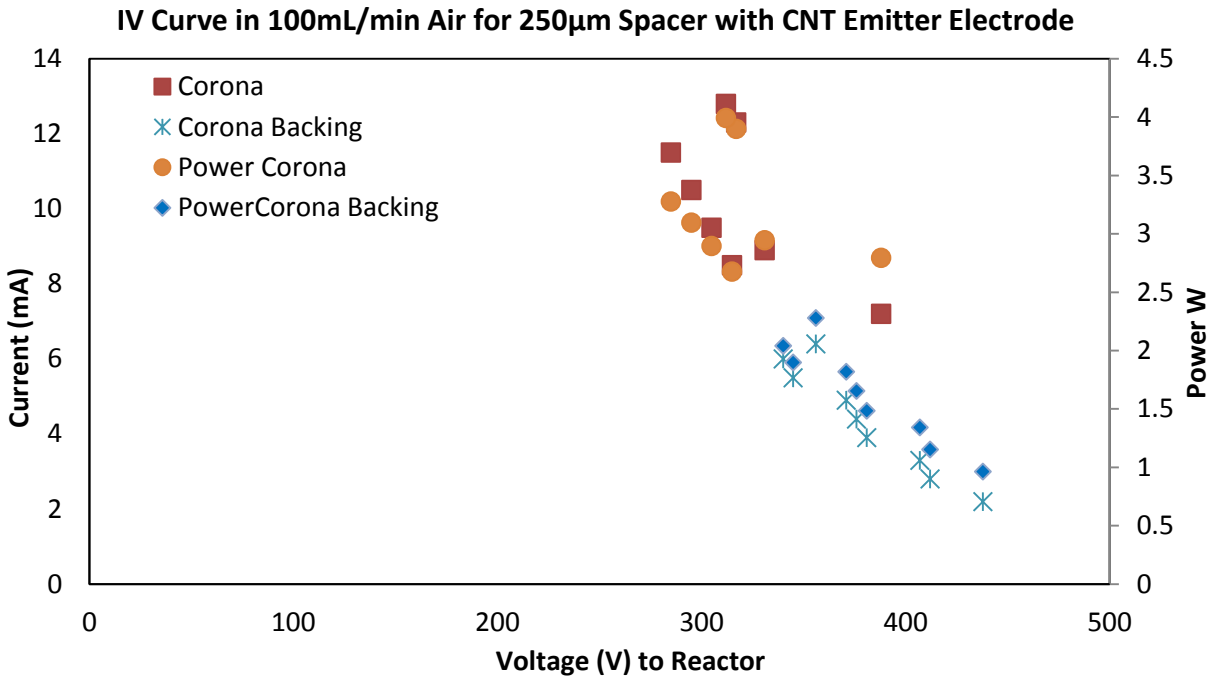

Figure 30.Plot the behavior of current (mA) vs. applied voltage to reactor (V) and the power (W) vs. applied voltage to reactor (V) the in the present of air at atmospheric pressure

5.2. Effects of Current on Conversion of Ethylene

The data collected is to see the effects of current on the Ethylene on (%) conversion of through a seven residence time (sec) in the small spacer (250 µm) (0.008, 0.016, 0.023, 0.029, 0.039, 0.047, and 0.058). and six residence time (sec) in the big spacer (750 µm) (0.016, 0.023, 0.029, 0.039, 0.047, and 0.058).also, each point represents an average of three run experiment.

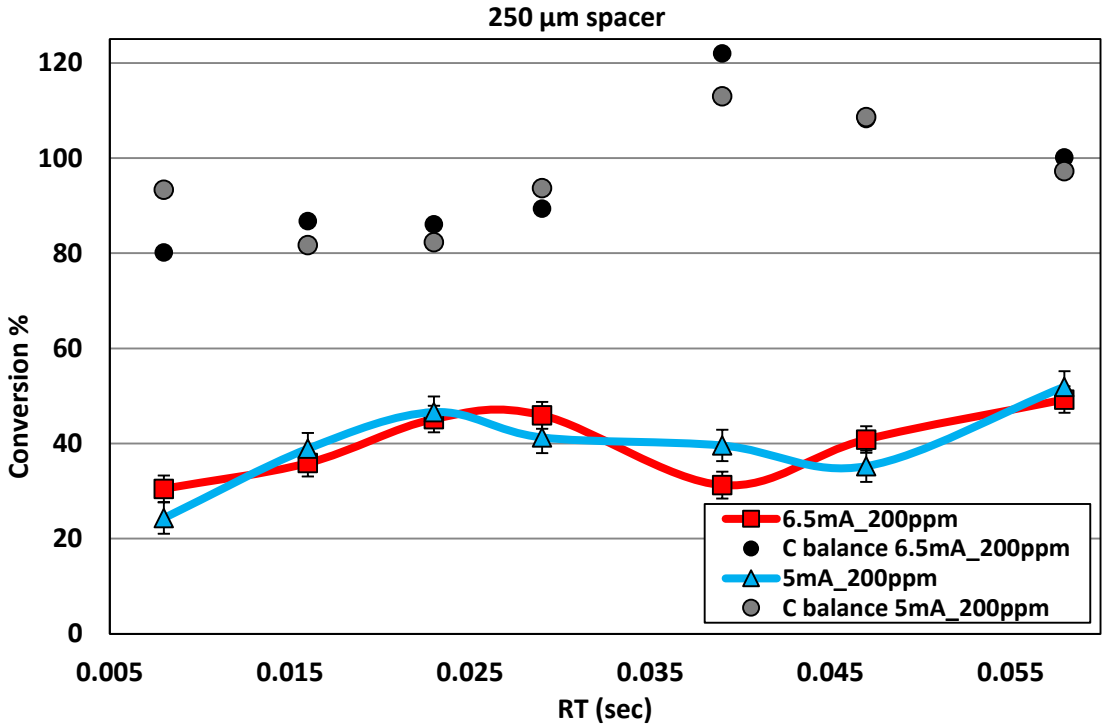

Figure 31.Plot of conversion of ethylene (%) vs. residence time (sec) in small spacer (250 µm) to identify the effects of different current values on conversion when the concentration of ethylene is low.

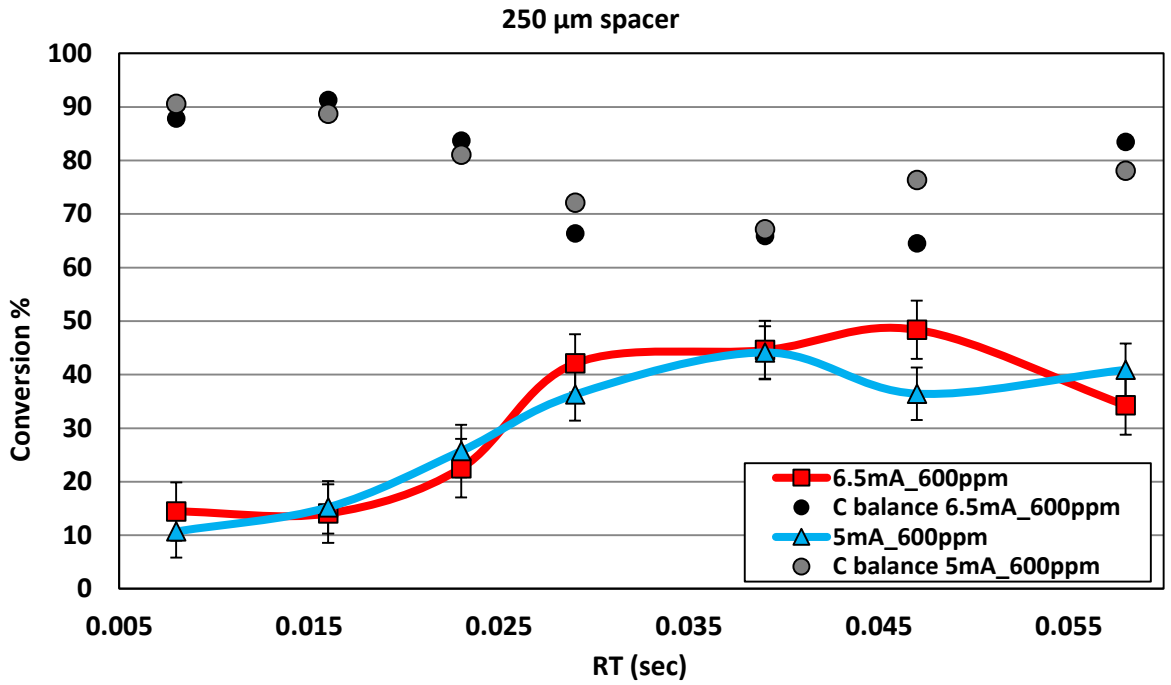

Figure 32. Plot of conversion of ethylene (%) vs. residence time (sec) in small spacer (250 µm) to see effects of different current value on conversion when the concentration of ethylene is high

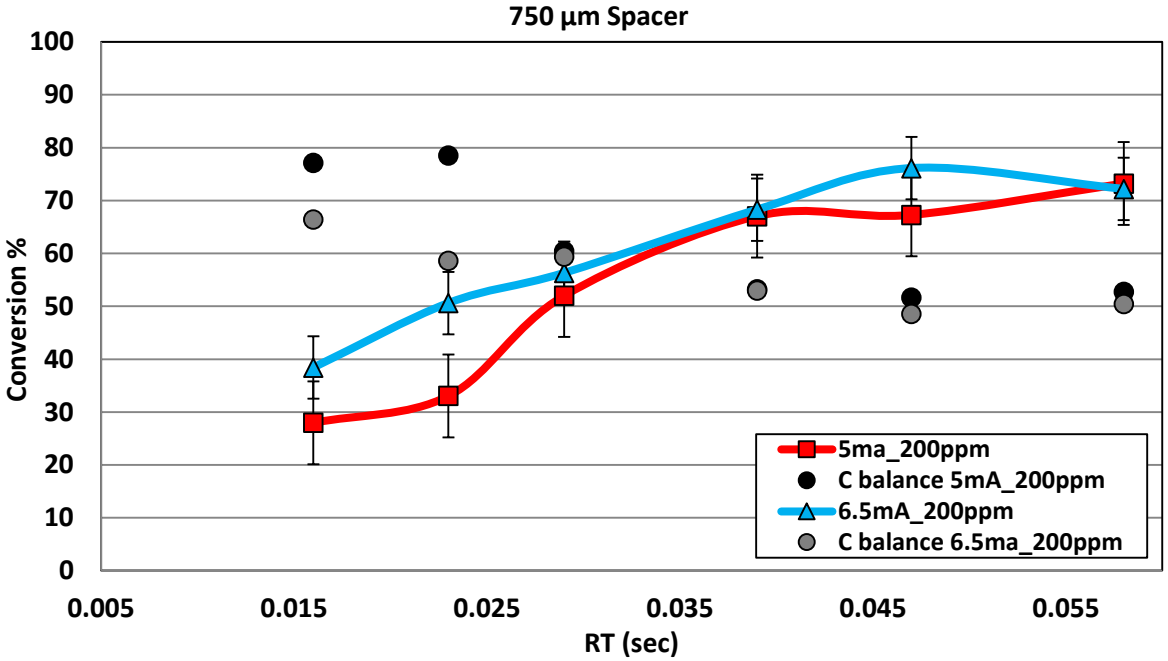

Figure 33. Plot of conversion of ethylene (%) vs. residence time (sec) in big spacer (750 µm) to see effects of different current value on conversion when the concentration of ethylene is low

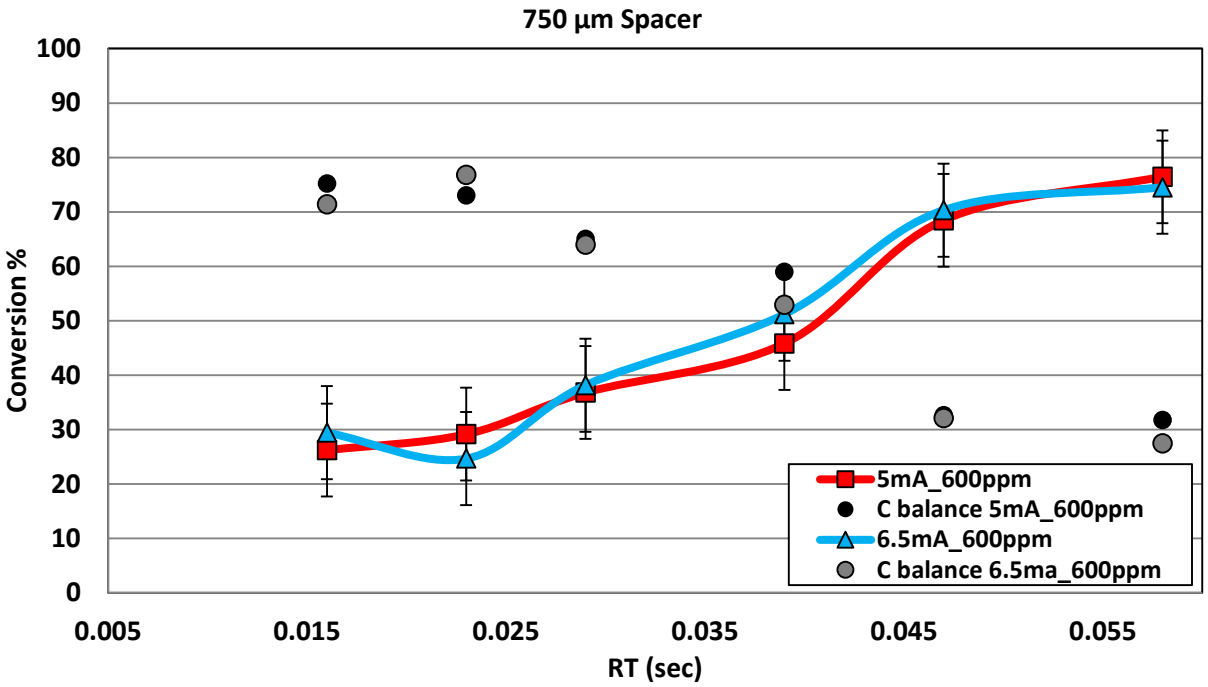

Figure 34. Plot of conversion of ethylene (%) vs. residence time (sec) in big spacer (750 µm) to see effects of different current value on conversion when the concentration of ethylene is high

5.3. Effects of Concentration on Conversion of Ethylene

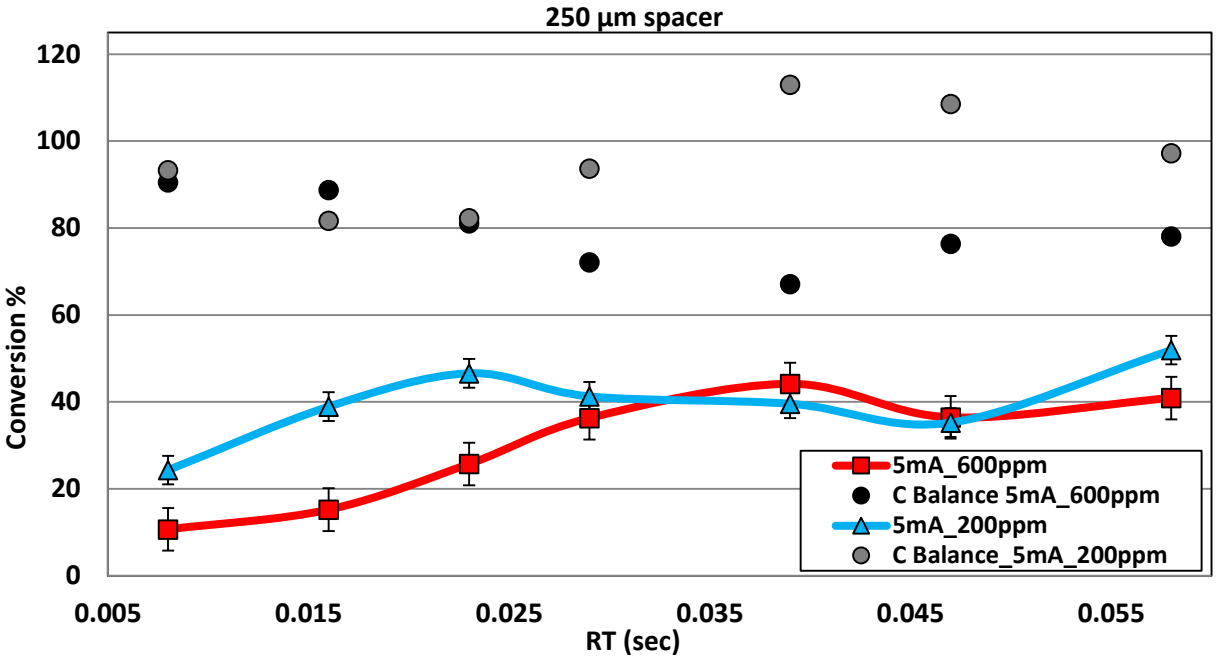

Figure 35. Plot of conversion of ethylene (%) vs. residence time (sec) in big spacer (250 µm) to see effects of different concentration of ethylene on conversion when the current value is low

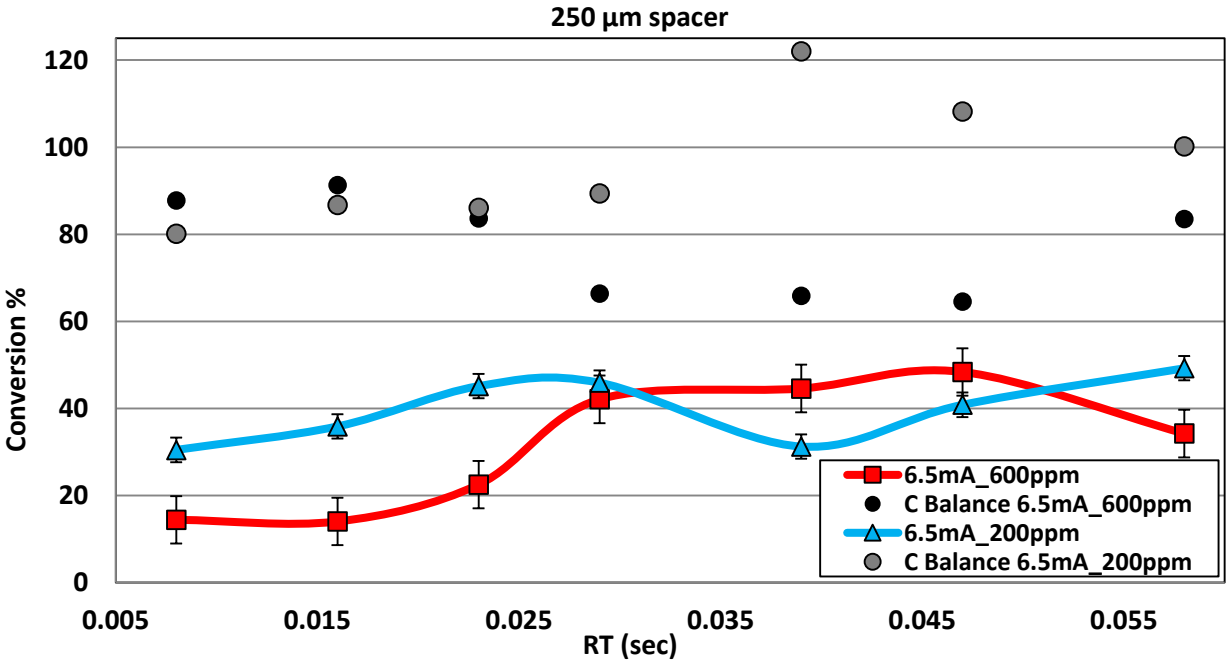

Figure 36. Plot of conversion of ethylene (%) vs. residence time (sec) in big spacer (250 µm) to see effects of different concentration of ethylene on conversion when the current value is high

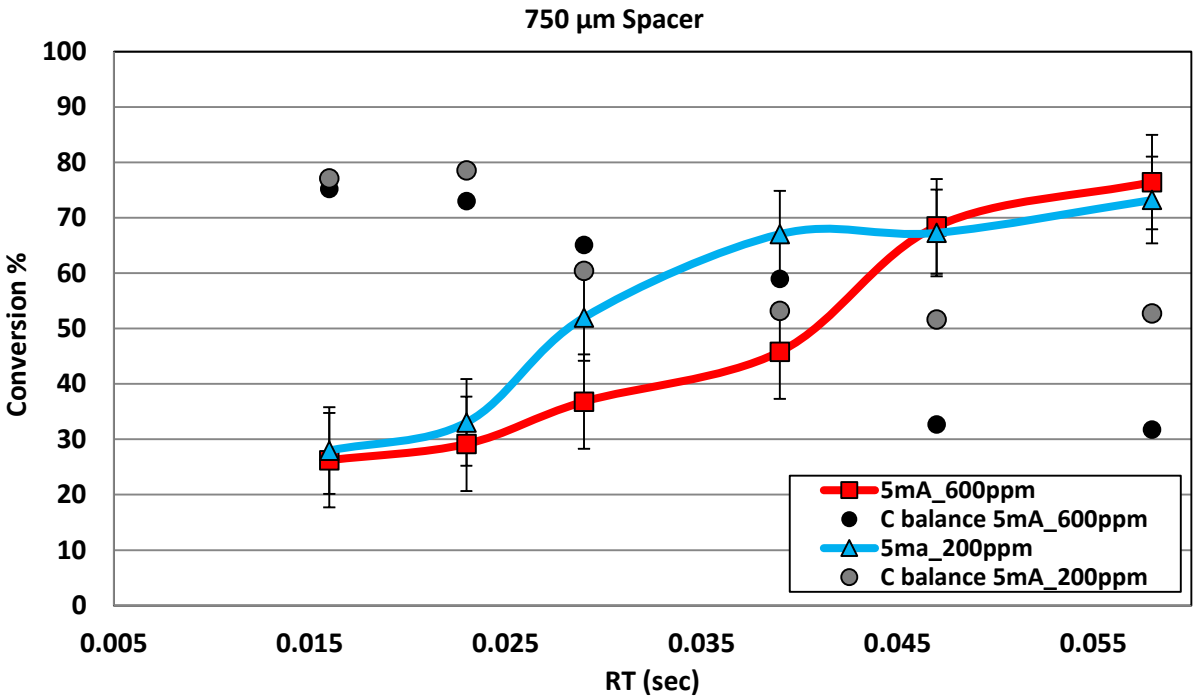

Figure 37. Plot of conversion of ethylene (%) vs. residence time (1/s) in big spacer (750 µm) to see effects of different concentration of ethylene on conversion when the current value is low

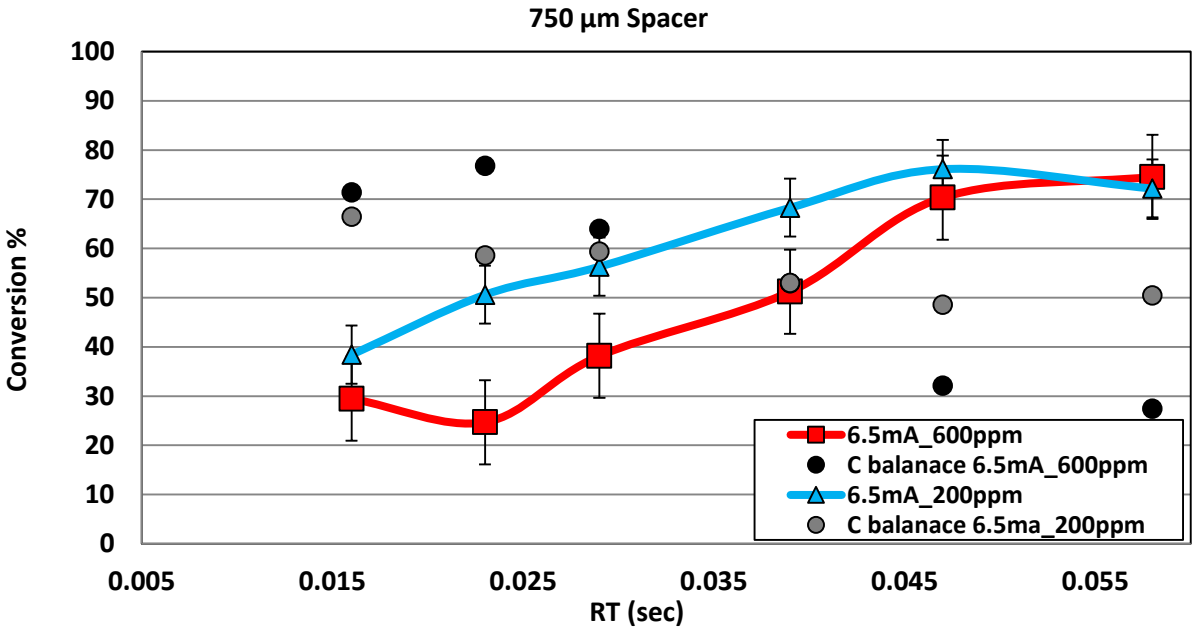

Figure 38. Plot of conversion of ethylene (%) vs. residence time (sec) in big spacer (750 µm) to see effects of different concentration of ethylene on conversion when the current value is high

5.4. Effects of Spacer on Conversion of Ethylene

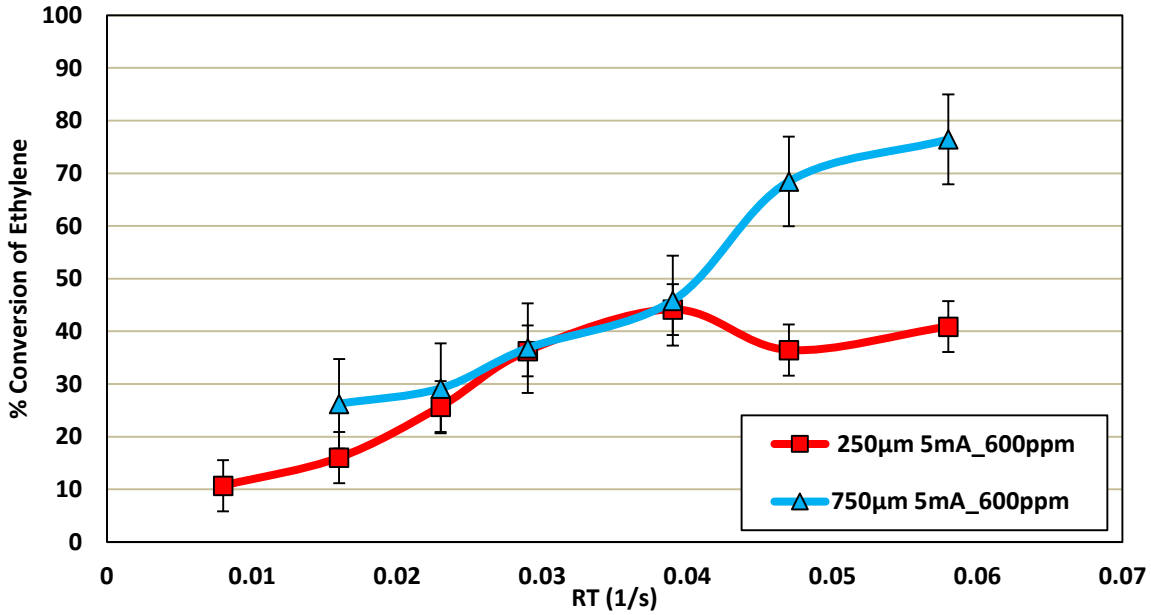

Figure 39.Plot of conversion of ethylene (%) vs. residence time (1/s) in low current when the higher concentration of ethylene to see effects of different spacer.

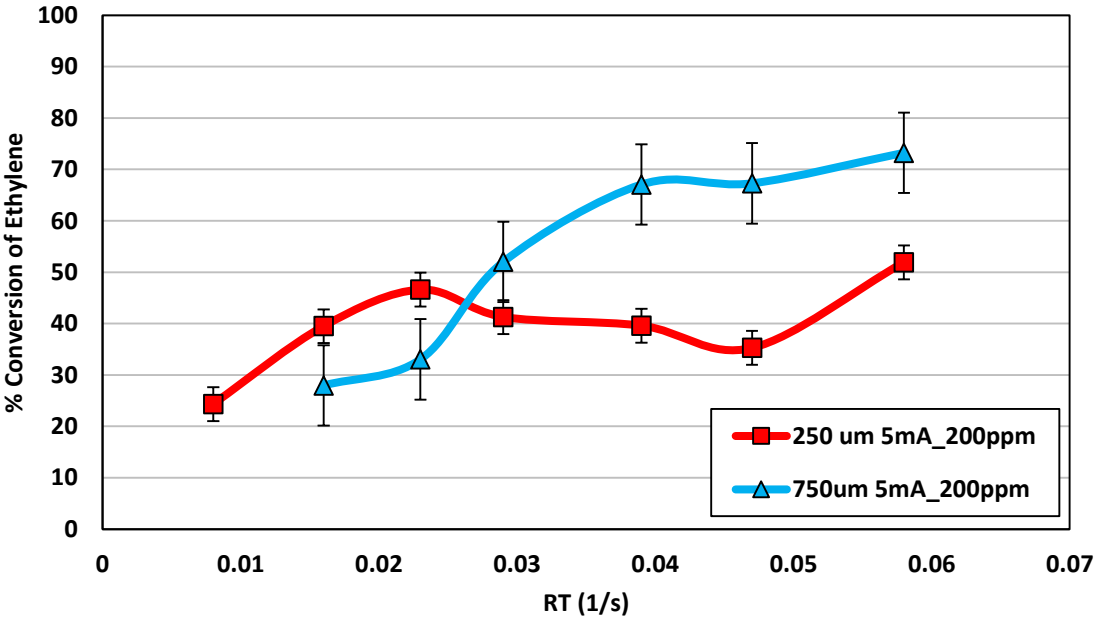

Figure 40.Plot of conversion of ethylene (%) vs. residence time (1/s) in low current when the lower concentration of ethylene to see effects of different spacer.

Chapter 6: Experimental results and discussion

6.1. Counter and Emitter Electrode

The results, shown in *Figure 41, 42.* demonstrate that carbon nanotubes on the emitter electrode are destroyed progressively during experimentation. This is due to the collision of electrons with the carbon nanotube surface as corona discharge is occurring. However, the behavior of the corona discharge is not affected significantly except during the initiation of the corona discharge. It delays the ignition of corona discharge (and it requires more supply voltage to initiate). The grounded electrode shows a deposition of a brown layer which appears to be carbon or an oxide layer. Also, a random location of darker dotes indicate localized sparking. The smaller channel appears less brightness.

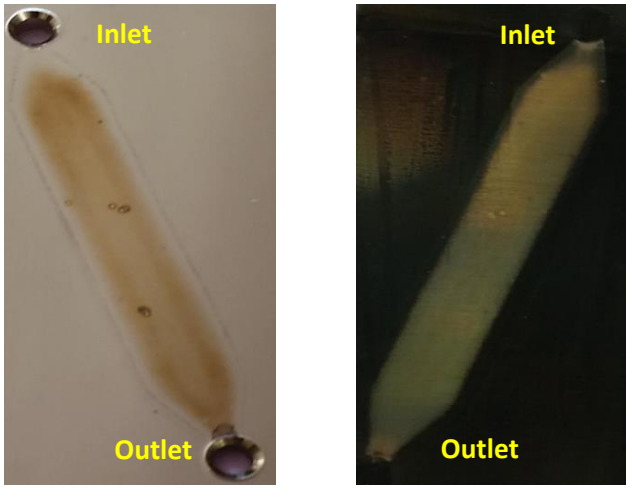

Figure 41. The conditions result of the counter and emitter electrodes in the small reaction channel (250 µm) after experiments completed.

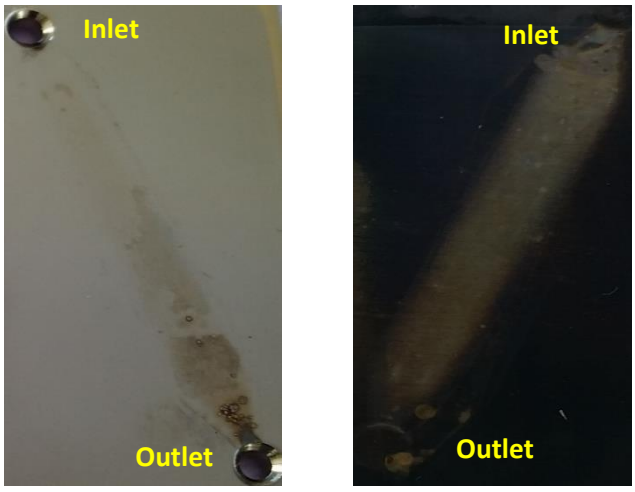

Figure 42. The conditions result of the counter and emitter electrodes in the big reaction channel (750 µm) after experiments completed.

Assuming that the operating phenomena is a localize spark, *Figure 43*, illustrate a behavior of localize spark (dark purple) and ionization area (light purple). The localized spark moves randomly and will generate more or less ionization area depending upon its location. This will have a tremendous effect on the oxidation process of ethylene and any other chemical reactions. The ionization area *(a)* has a big ionization area and that will produce more radicals to oxidize ethylene molecules to carbon dioxide and water. The lesser ionization areas shown as *(b)* and *(c)* will have lesser reactivity.

The stable localized spark, may be forced by flow rate to act random. When the flow rate is fast that will push the localized spark to the end of the channel *(c)* and when the flow rate is moving slowly that will allow it to happen nearer to the start of the channel *(a).*

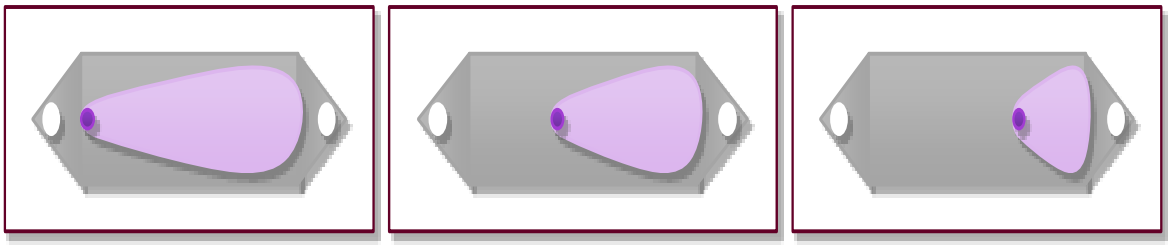

(a) (b) (c)

Figure 43. (a), (b), (c) Illustration of localize spark (dark purple) and the ionization area (light purple) going toward the outlet of the micro-channel.

It has been observed that the smaller channel appears less brightness, *Figure 44 (a)* And the bigger channel has a more brightness *(b).* This may be caused by the fact that it is a volume reaction and it occupies the entire height space. Thus, the bigger the channel is; the more volume and the more brightness is emitted.

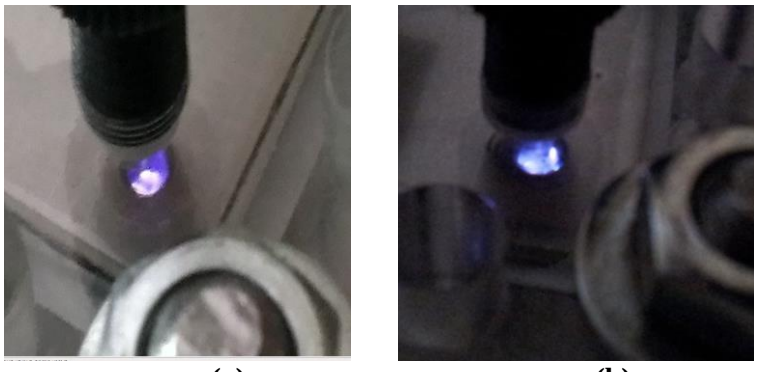

(a) (b)

Figure 44. (a) Photograph of the outlet of the micro reactor with a small spacer implemented (b) with a bigger spacer implemented.

6.2. Screening Design

From the experimental results of the screening design study that is shown in the standardized Pareto chart, *Figure 45*, and the main effects plot, *Figure 46*, all the results of all factors affect the process. These factors and the effects of interactions between those factors show that:

- *Spacer thickness:* considered to be the most significant factor, which means varying the space thickness from a small such as 250 µm to a bigger height such as 750 µm, will result in more oxidation toward the conversion of ethylene.

- *Concentration of the inlet ethylene:* considered to be a significant factor, due to the role that ethylene plays which quenching the reactions. Oxygen radicals in the reaction channel contribute to the essential dissociation of molecules such as ethylene but the more ethylene in the inlet mixture; the more the quenching reaction will lower the ethylene conversion. So with 200 ppm of ethylene in the inlet mixture the conversion of ethylene to a complete combustion producing carbon dioxide and water will be higher than at concentrations of 600 ppm of ethylene.

- *Flow rate:* considered to be a significant factor, due to the length of the discharge. The length will decreased dramatically as you go up in flow rate for example (120 mL/min to 425 mL/min). That maybe because of the transition from laminar to turbulent flow because viscosity of gas depends on temperature and in the channel will be a various kind of collision in the discharge so it is hard to reflect an accurate gas condition.

- *Power supply voltage:* considered to be a less significant factor, when the discharge happen and the operation in corona regime allowing more power supply voltage to the reactor will not have any benefit toward more conversion of ethylene, the only thing will occur with more voltage a transition will happen to a spark regime. This explanation can be apply if you allow current to flow or applied voltage to the reactor or power. Instead of power supply voltage.

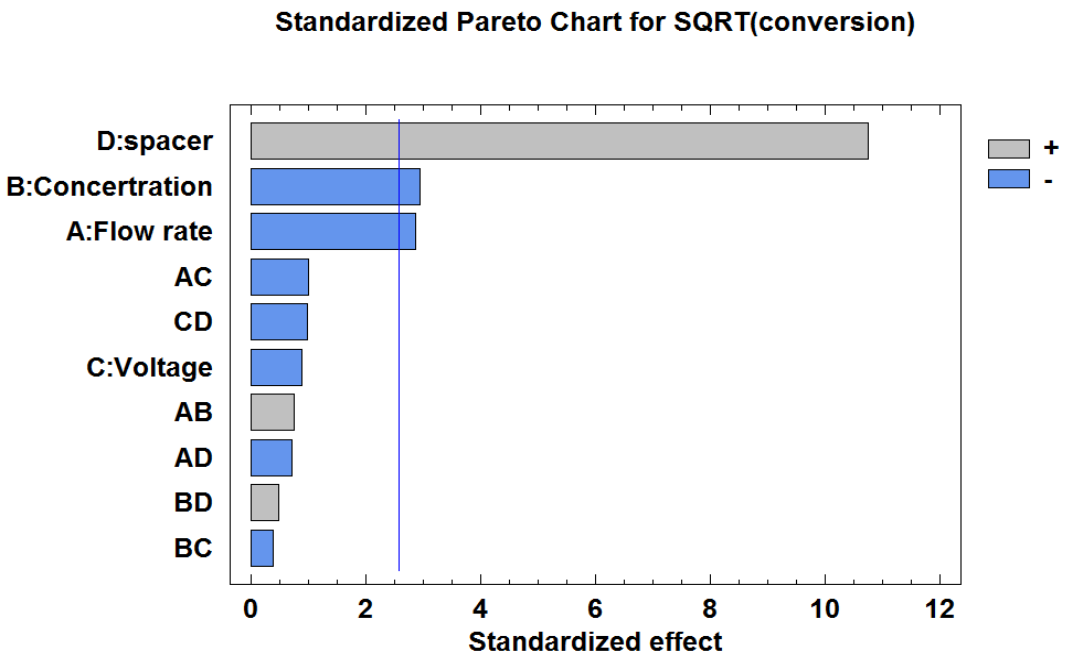

Figure 45. Standardized Pareto chart of the factors that effects the conversion of ethylene in atmospheric oxygen.

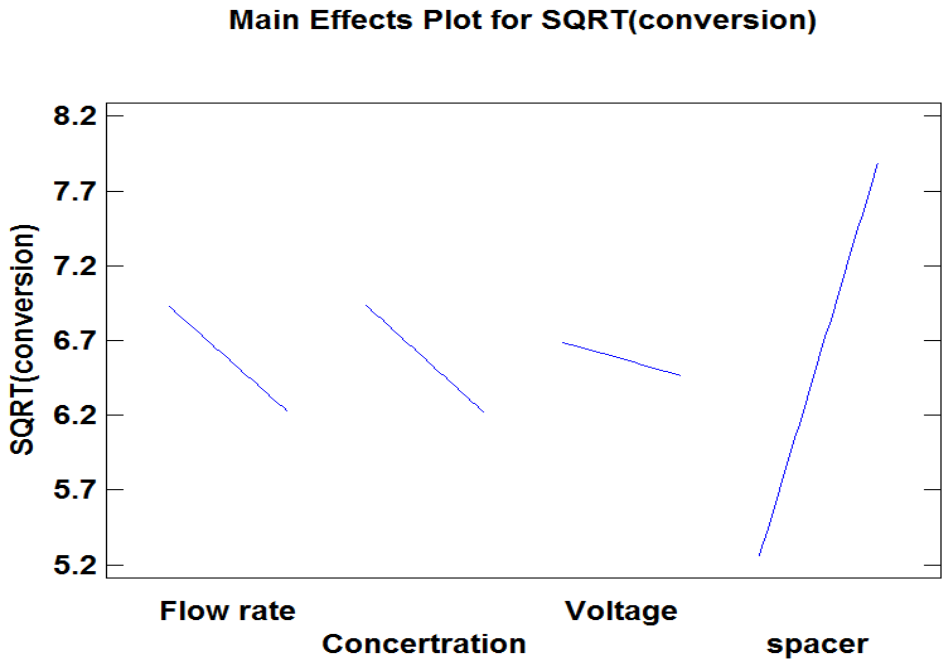

Figure 46. The main effects plot of the factors that effects the conversion of ethylene in atmospheric oxygen

6.3. Effect of Current on Conversion of Ethylene

From the experimental results in *Figure 47*, it indicates that with a 250 µm spacer the conversion of 200 ppm ethylene at low residence time is around 25% and it increases gradually by triple the residence time, so reactants will stay longer in the reactor, to achieve reaction equilibrium at 42% conversion after this is achieved the conversion will stay around this percentage due to the reversible reaction. For 600 ppm ethylene, the conversion diminishes. It starts at 10% at low residence times and increases as reactant stays longer in the reactor to achieve reaction equilibrium at 40% conversion. There is no significant effect of varying the current from 5mA to 6.5mA, in both of the results shown in the top and bottom Figure 47.

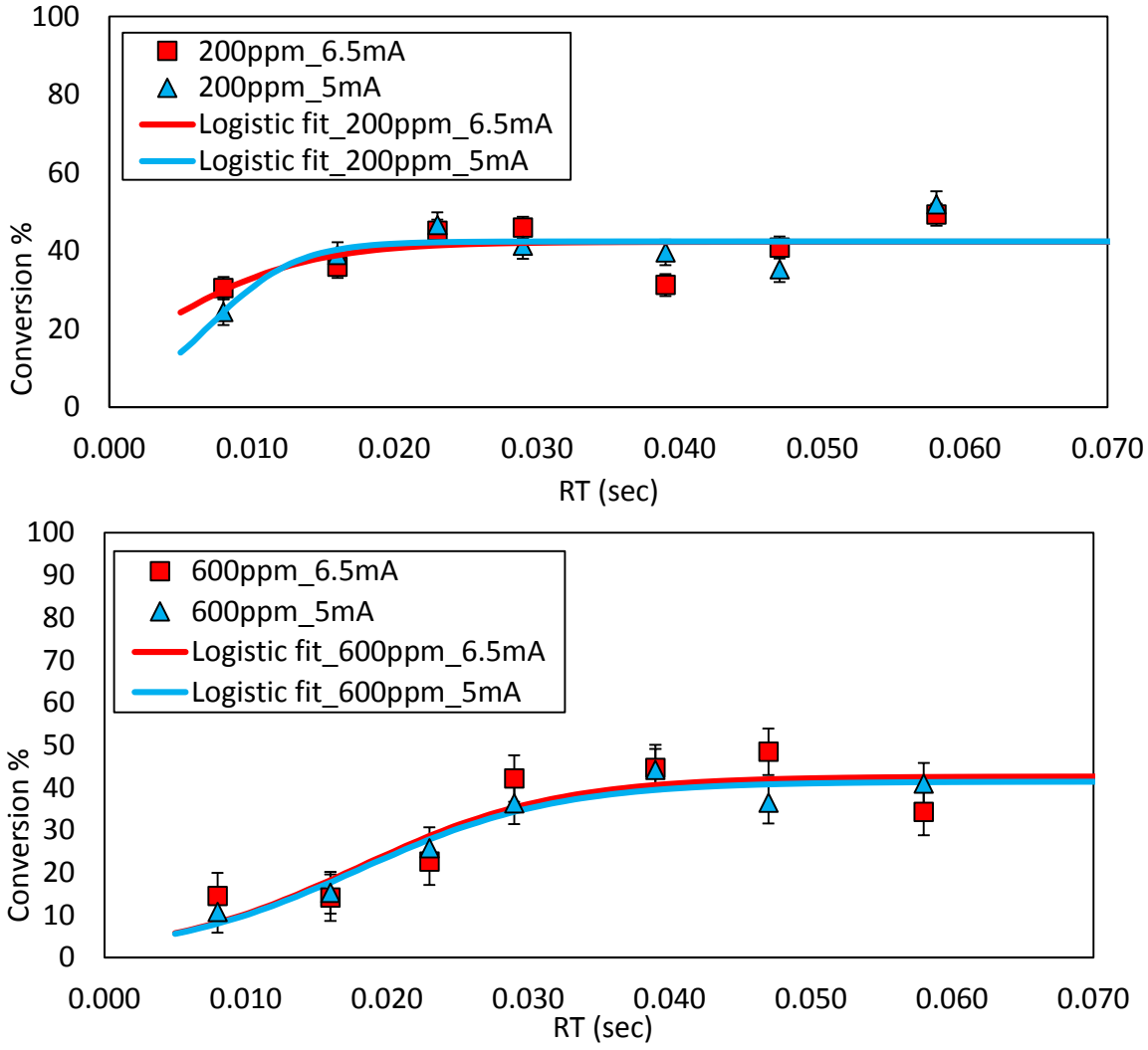

Figure 47. Logistic Plot fitting to the conversion of ethylene (%) vs. residence time (sec) in 250 µm spacer with ethylene concentration of 200 ppm (top plot) and 600 ppm (bottom plot)

The experimental results in *Figure 48*, it indicates with a 750 µm spacer, the conversion of 200 ppm of ethylene at low residence time is around 30% and it increases gradually until reaching the equilibrium conversion of 77% and no higher conversion is possible. For the 600 ppm of ethylene the conversion start at 25% than goes up to 73% before reaching equilibrium. There is no significant effect of varying the current from 5 mA to 6.5mA, in both of the results shown in the top and bottom Figure 48.

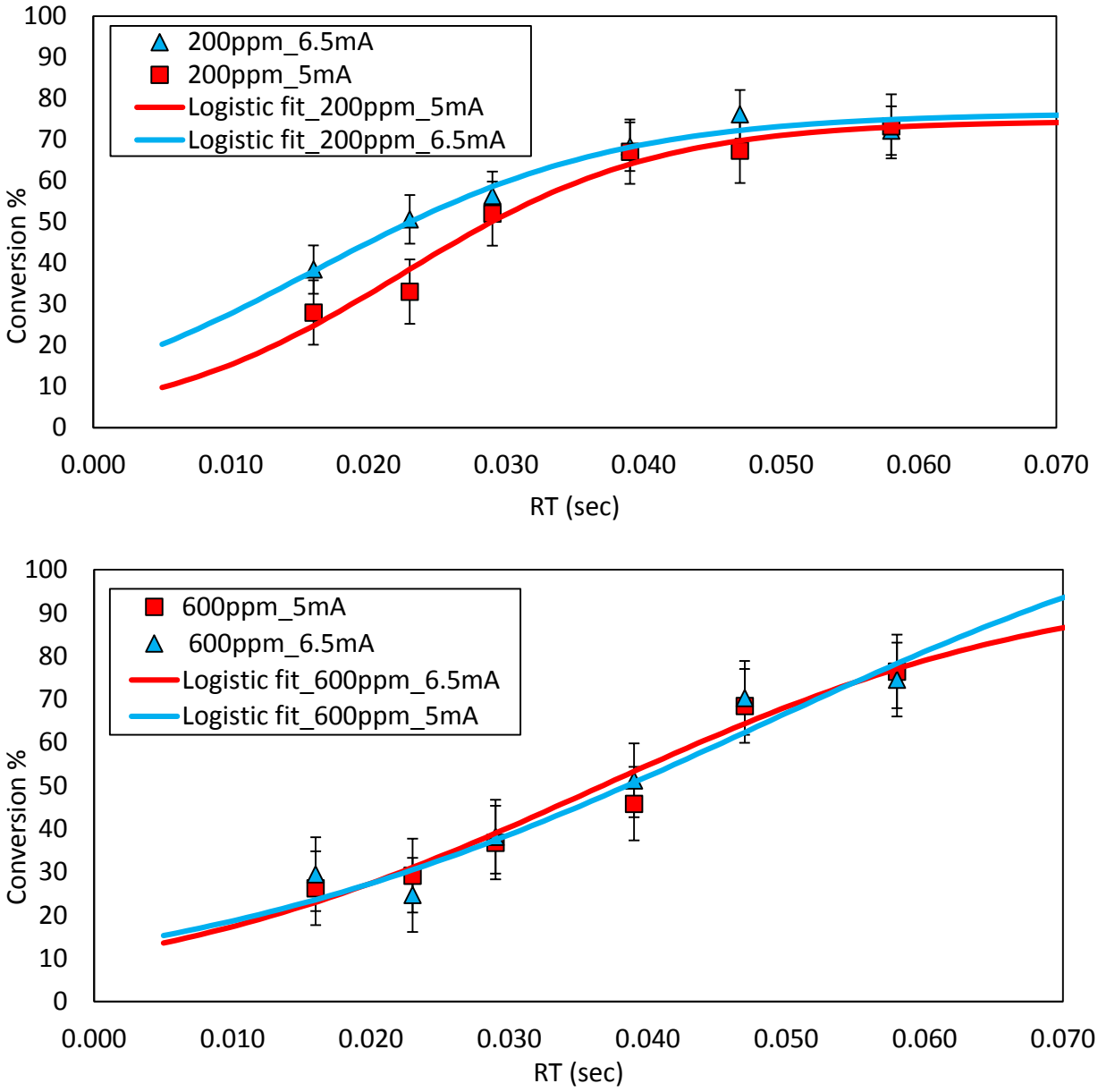

Figure 48. Logistic plot fitting to the conversion of ethylene (%) vs. residence time (sec) in 750 µm spacer with Ethylene concentration of 200 ppm (top plot) and 600 ppm (bottom plot)

6.4. Effect of Concentration on Conversion of Ethylene

From the experimental results in *Figure 49*, it indicates that with a 250 µm spacer, the conversion of 200 ppm ethylene at low residence around 25% and it increases gradually by triple the residence time to achieve reaction equilibrium at 42% and for 600 ppm the ethylene conversion will start at 10% and increase to 40% then level out. There is significant effect by verifying the concentration of ethylene from 200ppm to 600 ppm in both results in *Figure 49* top and bottom due to ethylene quenching the reaction when the concentration is high.

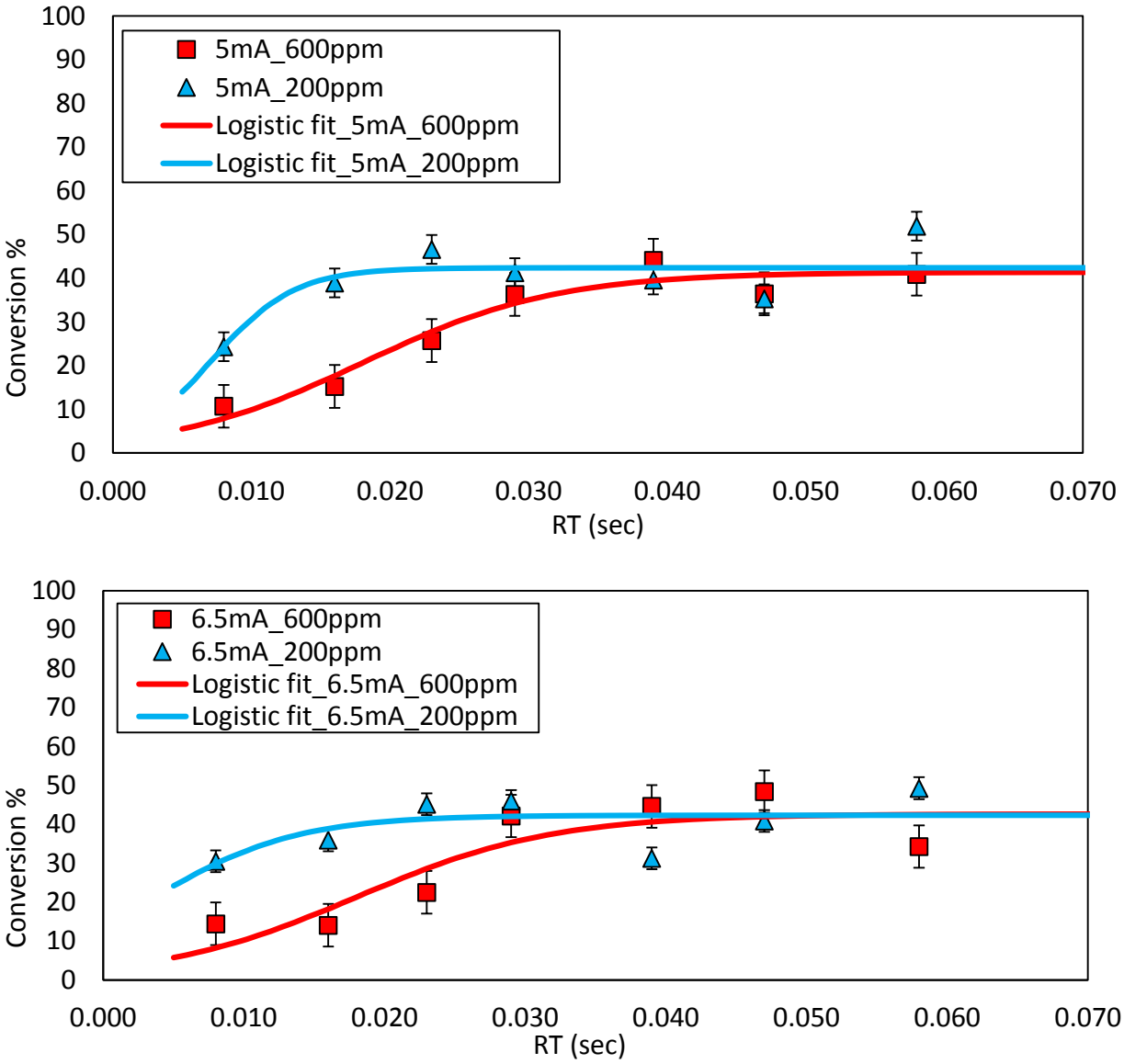

Figure 49. Logistic Plot fitting to the conversion of ethylene (%) vs. residence time (sec) in 250 µm spacer with current of 5 mA (top plot) and 6.5 mA (bottom plot)

From the experimental results in *Figure 50*, it indicates that with a 750 µm spacer, the conversion of 200 ppm ethylene at low residence is around 40% and it increases gradually by triple the residence time to achieve 75% after which the reaction reaches equilibrium and for 600 ppm the ethylene conversion is shifted down it will start at 30% and increase to 70% then level out. There is significant effect by varying the concentration of ethylene from 200 ppm to 600 ppm in both results in Figure top and bottom due to ethylene quenching the reaction when the concentration is high.

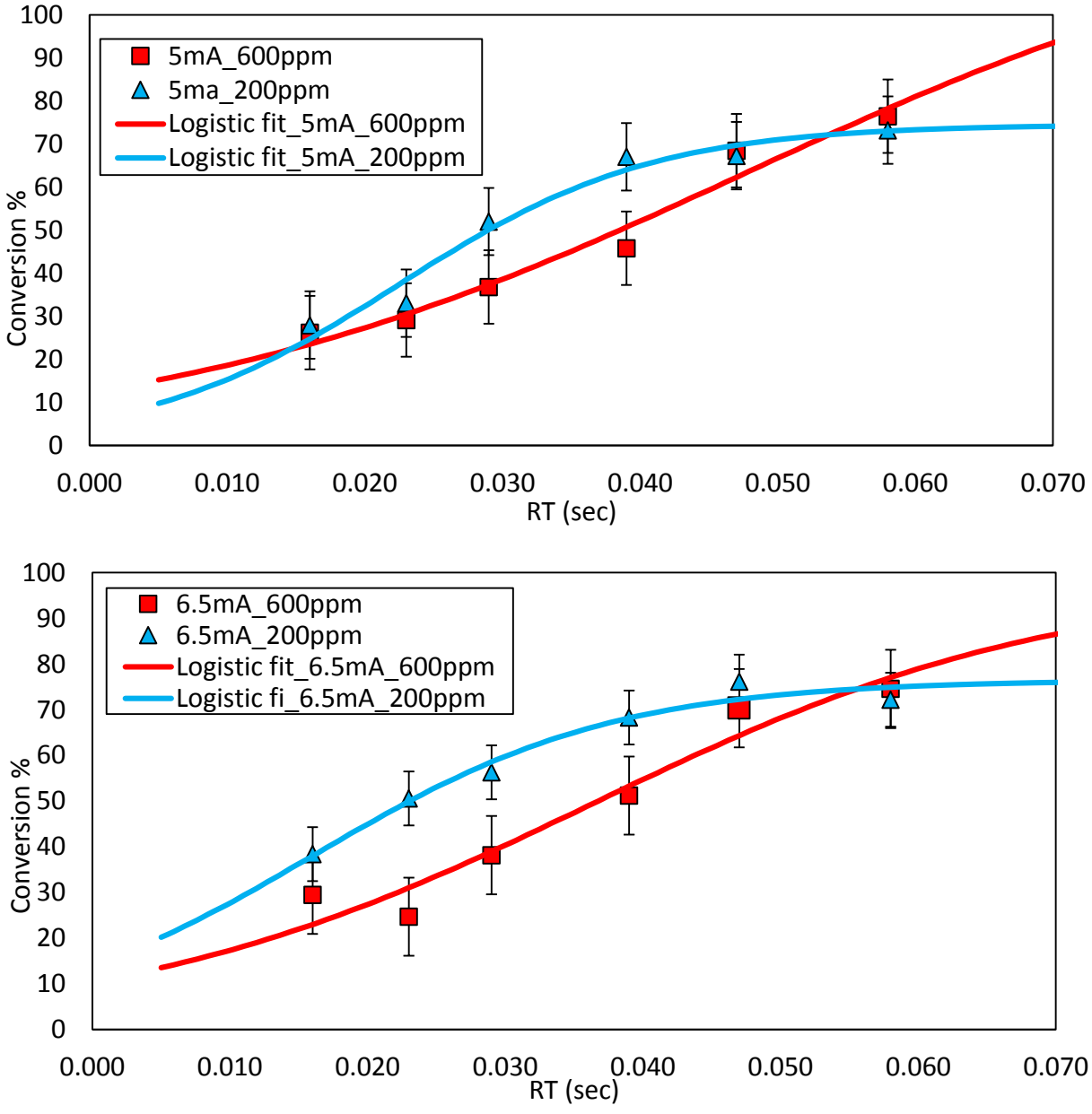

Figure 50. Logistic plot fitting to the conversion of ethylene (%) vs. residence time (sec) in 750 µm spacer with current of 5 mA (top plot) and 6.5 mA (bottom plot)

6.5. Effect of Spacer on Conversion of Ethylene

From the experimental results in *Figure 51*, it indicates that with a 250 µm spacer, the conversion of ethylene at low residence is around 10% and it increases gradually by triple the residence time to achieve 41% after that the reaction reaches equilibrium and with a 750 µm spacer, the ethylene conversion will go up at low residence times to about 30% and increase to 77% then level out. There is enormously significant effect of varying the spacer thickness from 250 µm to 750 µm in both results in Figure top and bottom.

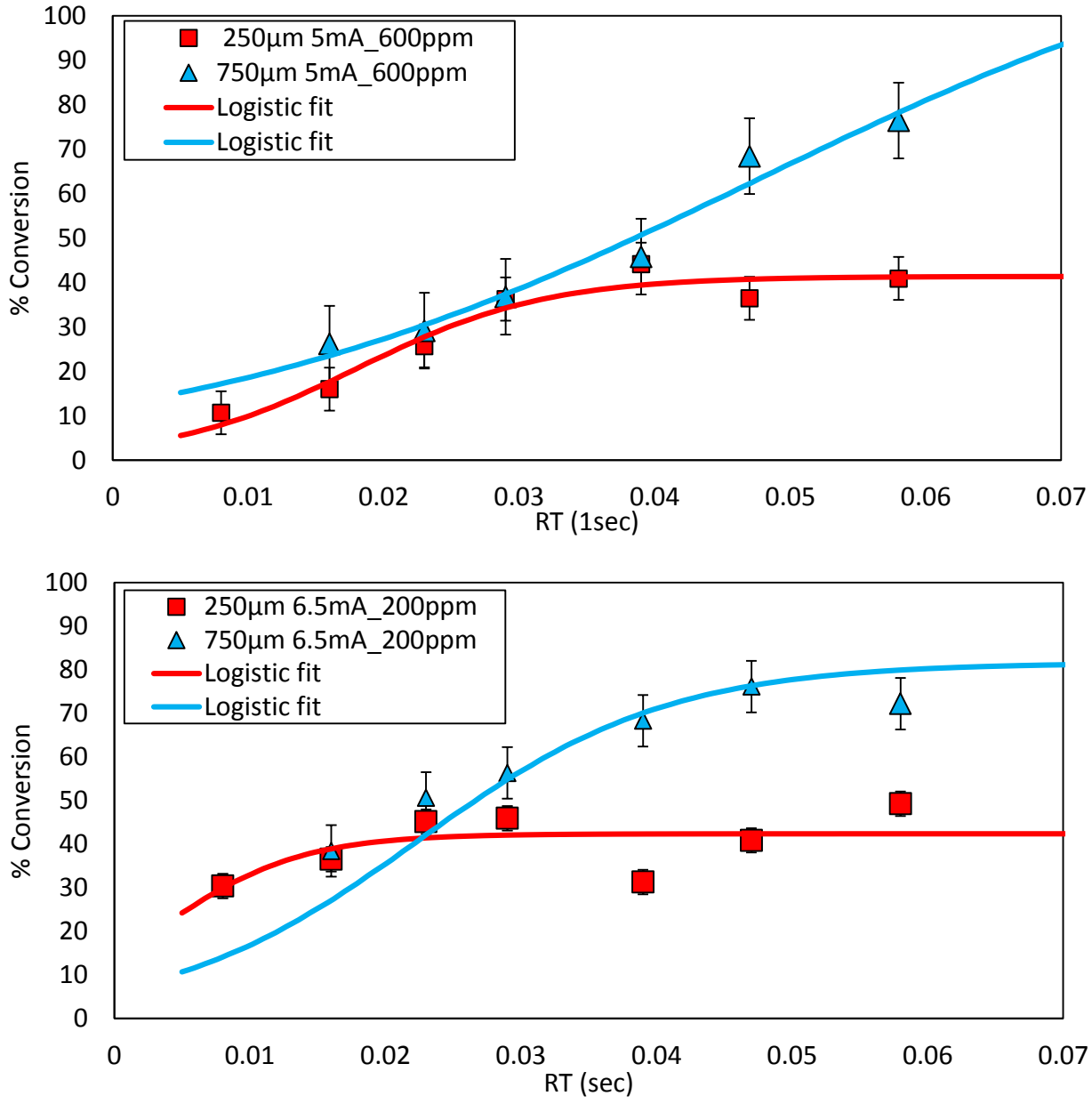

Figure 51. Logistic plot fitting to the conversion of ethylene (%) vs. residence time (sec) in 250 µm and 750 µm spacer with fixed concentration and current

The logistic function fitting parameters results are summarize in table 4. for the small spacer (250 µm) also, table 5. for the small spacer (750 µm)

- For the 250 µm

Parameters	200ppm_5.0mA	200ppm_6.5mA	600ppm_5.0mA	600ppm_6.5mA
r	0.0071	0.0035	0.018	0.018
K	42.3	42.3	41.3	42.6
C	10.77	1.98	13.20	13.10

Table 4. Logistic function parameters at small spacer (250 µm)

- For the 750 µm

Parameters	200ppm_5.0mA	200ppm_6.5mA	600ppm_5.0mA	600ppm_6.5mA
r	0.022	0.016	0.047	0.036
K	74.6	81.5	126.5	98.4
C	11.45	11.45	9.2	8.38

Table 5. Logistic function parameters at bigger spacer (750 µm)

6.6. Effect of Residence time on Conversion of Ethylene

In our system, the reaction rate is initially very slow, but after a while, when enough oxygen radicals are created in the system by the corona discharge, the rate increases rapidly and after a while the rate starts slow down to reach a saturation level caused by several factors: (see *Figure 52.*)

First, oxygen radicals will produce more radicals and species during propagation events at a certain concentration of radical species they will eventually favor a shifting of the oxygen radical priority to more dissociation of ethylene molecules.

Second, oxygen radicals will produce other radicals and species that have lower activation energies and that will cause will cause reversible reactions which will slow the destruction of ethylene.

Third, ethylene is responsible for deactivation of oxygen radicals by quenching the reactions when the ethylene concentration is high enough in the reaction volume.

Fourth, ethylene concentration is decreasing with time and there are not enough ethylene molecules to carry out further reactions.

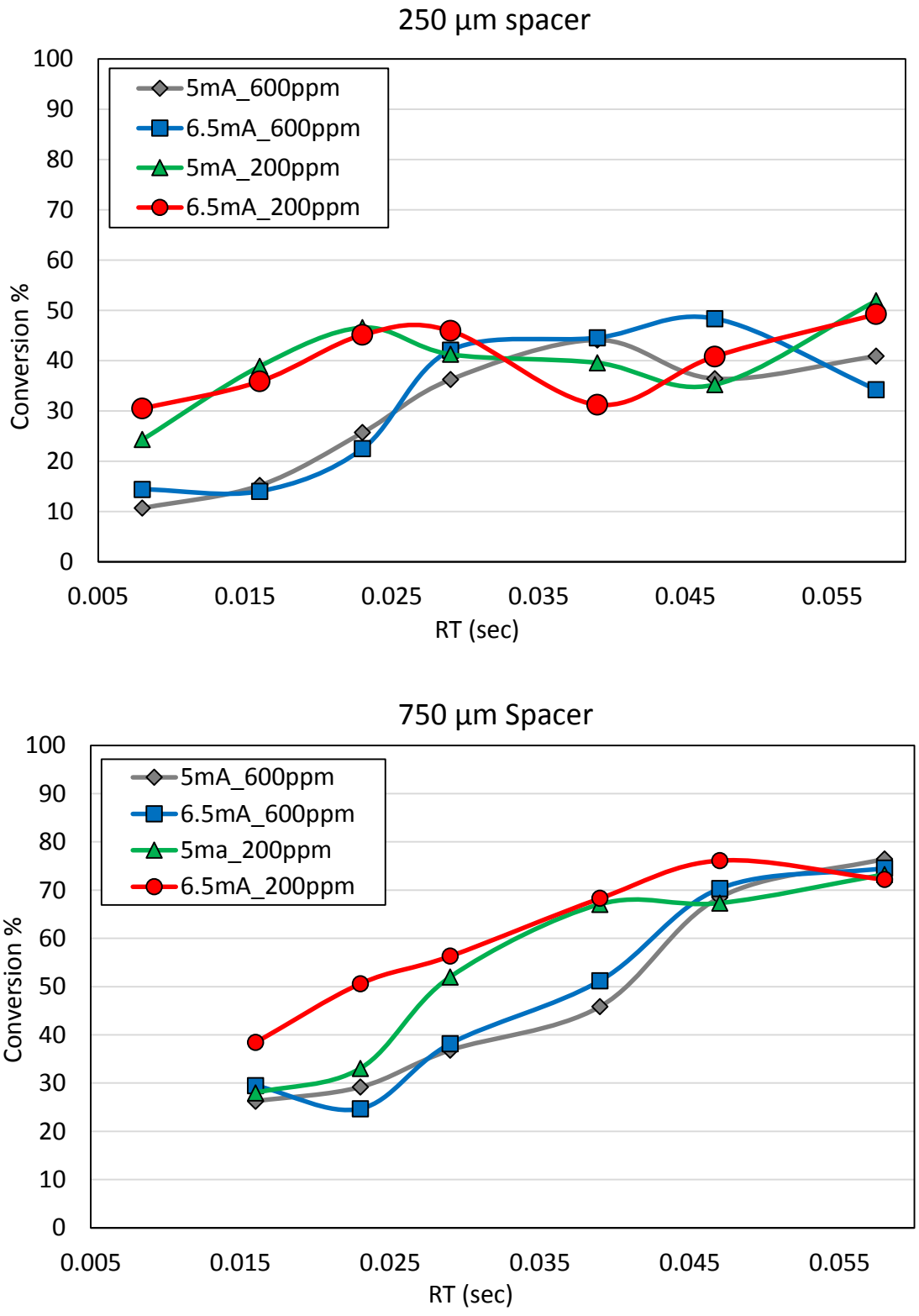

Figure 52. Plot of the conversion of ethylene (%) vs. residence time (sec) in 750 µm spacer with ethylene concentration of 200 ppm (top plot) and 600 ppm (bottom plot)

Assuming that the operating phenomena is a localized spark, *Figure 53*, illustrate a possible behavior of the localize spark (dark purple) and its ionization area (light purple). The ionization width area will vary with residence time. With small residence time, the ionization width will be small due to fast flow and the reactant will not stay longer in the reactor, *(a)*, and when the reactant is allowed to stay longer in the channel, *(b)*, the width of the ionization area will increase and for the even longer residence times, the bigger the width of the reaction volume, *(c)*.

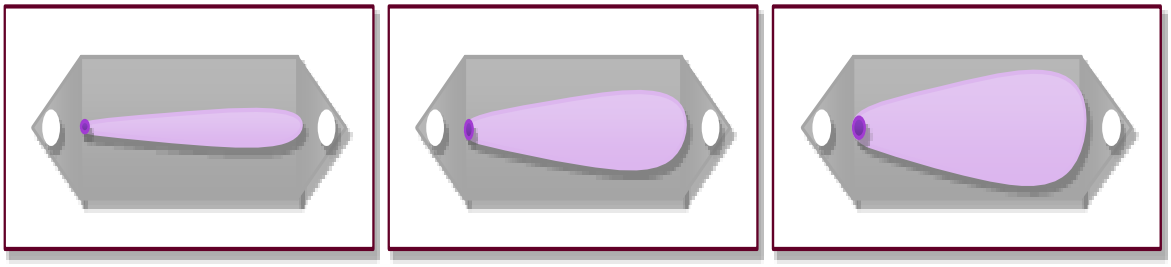

(a) **(b)** **(c)**

Figure 53. (a), (b), (c) Illustration of residence time for the localize spark (dark purple) and the ionization area (light purple) going toward the outlet of the micro-channel.

A. The results comparison in term of mole of ethylene destroyed per unit of power showing in *Figure 54.* for the lower spacer and *Figure 55.* for the bigger spacer. It is clearly that with higher inlet ethylene concentration the number of ethylene molecules destroyed per one unit energy is higher than the lower inlet ethylene concentration. *Appendix N* shows the calculation of number of Ethylene molecules destroyed per unit of power, charge and electron.

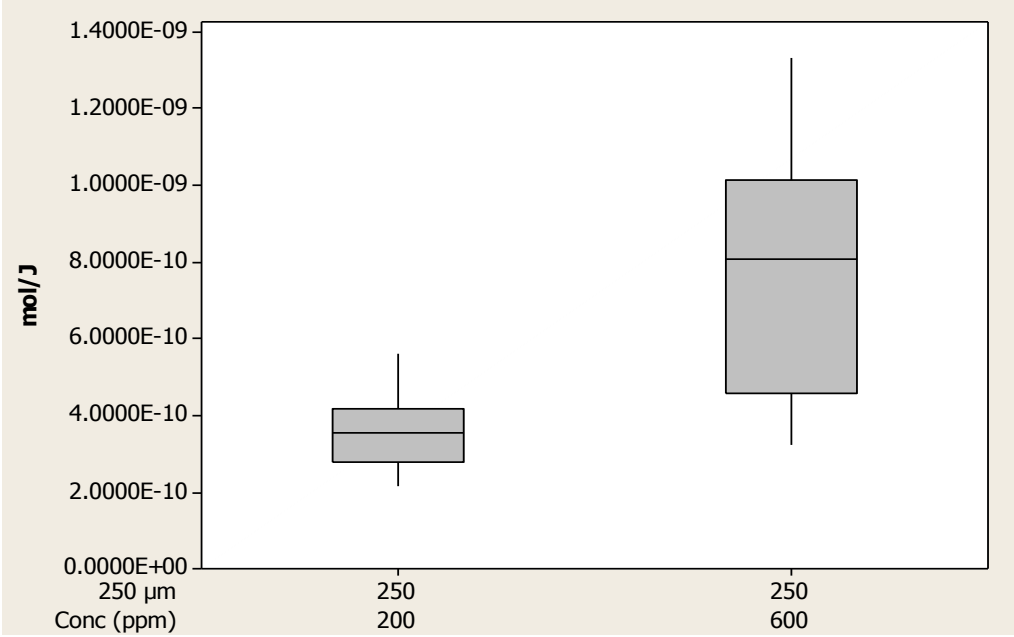

Figure 54. Number of ethylene molecules destroyed per one unit energy in smaller spacer

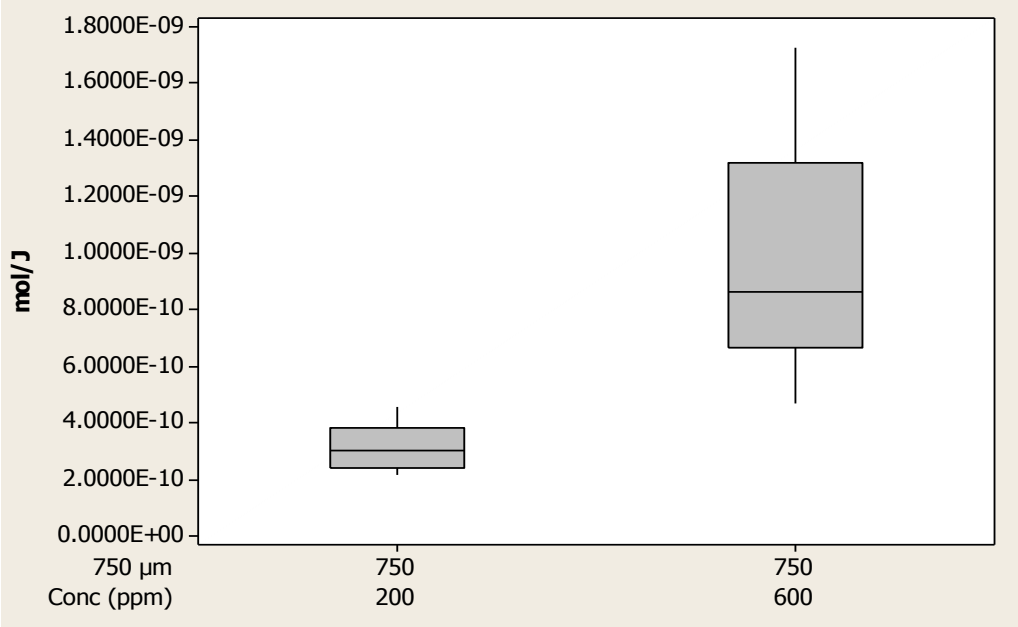

Figure 55. Number of ethylene molecules destroyed per one unit energy in bigger spacer

Chapter 7: Conclusion and Recommendations

7.1. Conclusions

A microreactor device was constructed and equipped with a carbon nanotube based emitter electrode. The carbon nanotube grow at atmospheric pressure with as catalyst support to produce low voltage corona discharge for the complete destruction of VOCs, such as ethylene, by converting them to carbon dioxide and water.
The microreactor device investigates the influence of current and the inlet concentration and the thickness spacer on the conversion of ethylene as the residence time is increased.

The current was varied from 5 mA to 6.5 mA. The results shows that there is no significant effect in varying the current and that also, the same behavioral result can be achieved by analyzing power supply voltage, applied voltage to the reactor or power instead of current.

The inlet concentration was varying from 200 ppm and 600 ppm. The results show there is a significant effect in varying the inlet concentration and it shows when the concentration is less the conversion of ethylene will be higher and when the concentration if high the conversion will be less and that due to the reactions of oxygen radical has been quenching by ethylene molecules and that lowering the ethylene conversion to a third.

The thickness spacer was varying from 250 µm and 750 µm. The results show there is a big significant effects in varying the thickness spacer and it shows that when thickness of the micro-channel is small, the conversion of ethylene is low and when it is bigger, the conversion is high. It is due to the reaction volume, the reaction happing in the bulk of the channel and the bigger the bulk the more reaction will occur. The conversion could increase or decrease by 50% when the thickness of the micro-channel is varying.

The results of the emitter electrode equipped with an atmospheric carbon nanotube emitter show, that current- voltage curve for the pulse corona, streamer corona, glow corona and spark has been accomplished using a low voltage corona.

Also, the result shows carbon nanotubes on the emitting electrode will be demolished gradually with time. This is due to the destructive environment of electrons and radicals that collide with the carbon nanotube surface.

7.2. Recommendation

- In this project the emitter electrode equipped with a carbon nanotube electrode was studied and approved as an emitter electrode, however other carbon nanotube geometries could enhanced the process if they were to be straight vertically aligned tubes. Also placing them at the beginning of the emitter electrode to prevent some random behaviors such as localized sparks forming later in the channel length would improve the process.
- Replacing the emitter electrodes with a different nanotube such as metallic nickel nanowires or semiconducting nanowires such as silicon nanowires may improve long term durability.
- For collecting data, the sample injection to the gas chromatography should be lowered from 1.0 mL per sample to 0.04 mL per sample, this will gives clear separation of air and carbon monoxide.
- This device could be implemented in wide applications such as in hospital air conditioners to kill bacteria and viruses, in refrigerated trucks and home refrigerators to prevent food from over-ripping and in the home air conditioner.

I enthusiastically recommend the continuation of this project

Bibliography

[1] Gardner, Brian. Global Food Futures Feeding the World in 2050.. London: Bloomsbury Publishing, 2013. Print.

[2] "FAO's Director-General On How To Feed The World In 2050." Population and Development Review 35.4 (2009): 837-839. Print.

[3] Chefurka, Paul. "What Drives Population - Food or Energy?," http://www.paulchefurka.com/PopulationFoodEnergy.html Accessed February 12, 2014

[4] Kontos, A.G., A. Katsanaki T. Maggos , V. Likodimos , A. Ghicovc, D. Kimc, J. Kunzec, C. Vasilakos P. Schmuki P. Falaras. "Photocatalytic degradation of gas pollutants on self-assembled titania nanotubes." Chemical Physics Letters 490 (2010): 58–62. Print.

[5] Mo, Jinhan, Yinping Zhanga, Qiujian Xu, Jennifer Joaquin Lamson, and Rongyi Zhao. "Photocatalytic purification of volatile organic compounds in indoor air: A literature review." Atmospheric Environment, 43 (2009): 2229–2246. Print.

[6] Jobling, Jenny. "Postharvest Ethylene: A critical factor in quality management." Sydney Postharvest Laboratory Information Sheet (2003): 1-4. Print.

[7] Barry, Cornelius S., and James Giovannoni J. "Ethylene and Fruit Ripening." Journal of Plant Growth Regulation 26 (2007): 143–159. Print.

[8] Saltveit, Mikal E.. "Effect of ethylene on quality of fresh fruits and vegetables." Postharvest Biology and Technology 15.3 (1999): 279-292. Print.

[9] Oglesby, Sabert, and Grady B. Nichols. Electrostatic precipitation. New York: M. Dekker, 1978. Print.

[10] Tendero, Claire, Christelle Tixier, Pascal Tristant, Jean Desmaison and Philippe Leprince, "Atmospheric pressure plasmas: A review." *Spectrochimica Acta Part B* 61 .1(2006): 2-30. Print.

[11] Raĭzer, I͡U. P. Gas discharge physics. Berlin: Springer-Verlag, 1991. Print.

[12] Fridman, Alexander A., and Lawrence A. Kennedy. Plasma physics and engineering. New York: Taylor & Francis, 2004. Print.

[13] Antao, Dion S. "A Study of Direct Current Corona Discharges in Gases and Liquids for Thin Film Deposition." Diss. Drexel U, 2009. Print.

[14] Meichsner, Jürgen, Martin Schmit, Ralf Schneider, and Hans-Erich Wagner. Nonthermal plasma chemistry and physics. Boca Raton, Fla.: CRC Press, 2012. Print.

[15] Mclean, Kenneth J., Phil A. Lawless, Leslie E. Sparks, and Geddes H. Ramsey. "Negative corona in wire-plate electrostatic precipitators. Part II: Calculation of electrical characteristics of contaminated discharge electrodes." Journal of Electrostatics 18.2 (1986): 219-231. Print.

[16] Chan, Jen-Shih, and I Maezono. "The electrode surface temperature profile in a corona discharge." Journal of Physics D: Applied Physics 21.6 (1988): 1023-1024. Print.

[17] Carroll, D. I., I. Dzidic, R. N. Stillwell, K. D. Haegele, and E. C. Horning. "Atmospheric pressure ionization mass spectrometry. Corona discharge ion source for use in a liquid chromatograph-mass spectrometer-computer analytical system." Analytical Chemistry 47.14 (1975): 2369-2373. Print.

[18] Yamamoto, T., P.a. Lawless, and L.a. Sparks. "Narrow-gap point-to-plane corona with high velocity flows." IEEE Transactions on Industry Applications 24.5 (1988): 934-939. Print.

[19] Peek, F. W.. Dielectric phenomena in high-voltage engineering,. 3d ed. New York [etc.: McGraw-Hill Book Company, inc., 1929. Print.

[20] Chang, J.-S., P.a. Lawless, and T. Yamamoto. "Corona discharge processes." IEEE Transactions on Plasma Science 19.6 (1991): 1152-1166. Print.

[21] Cooray, Vernon. The lightning flash. London: Institution of Electrical Engineers, 2003. Print

[22] Bartnikas, R., and Eugene Joseph McMahon. Engineering dielectrics. Philadelphia (PA.): American Society for Testing and Materials, 1979. Print.

[23] The Plasma Universe Wikipedia-like Encyclopedia. http://www.plasma-universe.com/Electric_glow_discharge#_note-1 Web. Accessed. November 28. 2013

[24] Gallo, C. F.. "Corona-A Brief Status Report." IEEE Transactions on Industry Applications IA-13.6 (1977): 550-557. Print.

[25] Snyder, Donald. Nickel Electroplating. *Products Finishing.* February 21, 2011. Web. Accessed. April 1, 2013. http://www.pfonline.com/articles/electrocoating

[26] Mallory, Glenn O.. Electroless plating fundamentals and applications. Repr. ed. Orlando, Fla.: AESF ;, 19902000. Print.

[27] Gunderson, E., Effect of Cosputtered Catalyst on Growth and Alignment of Carbon Nanotubes by Plasma Enhanced Chemical Vapor Deposition (Dissertation, Oregon State University, 2010).

[28] Wang, Yun and John Yeow. A Review of Carbon Nanotubes-Based Gas Sensors.*Journal of Sensors.*1.1 (2009): 1 – 24. Print.

[29] Jung-Tang Huang; Fu-Sheng Huang; Der-Chi Tien; Chih-Shan Li; Sheng-Xiong Shi, "Carbon nanotubes based corona discharger and its application," Nanotechnology, 2005. 5th IEEE Conference on , vol., no., pp.657,660 vol. 2, 11-15 July 2005

[30] Chen, Junhong. Nanoscale Corona Discharge Electrode. United States Patent, assignee. Patent US 7,504,628 B2. 17 Mar. 2009. Print.

[31] "Chemistry of Petroleum 2: What Happens to Hydrocarbons When They Burn?." - Science NetLinks. Web. Accessed. April 1, 2014. http://sciencenetlinks.com/lessons/chemistry-of-petroleum-2/

[32] Talapatra, Amrita. "Ambient Air Non-Methane Volatile Organic Compound (NMVOC) Study Initiatives in India–A Review." Journal of Environmental Protection 02.01 (2011): 21-36. Print.

[33] Mishra, T., P. Mohapatra, and K.m. Parida. "Synthesis, characterisation and catalytic evaluation of iron–manganese mixed oxide pillared clay for VOC decomposition reaction." Applied Catalysis B: Environmental 79.3 (2008): 279-285. Print.

[34] "VOC Controls - Institute of Clean Air Companies." VOC Controls - Institute of Clean Air Companies. Web. Accessed. April 1, 2014. http://www.icac.com/?VOC_Controls

[35] Cramer, J. S., Logit models from economics and other fields. Cambridge, UK: Cambridge University Press, 2003. Print

[36] Cavallini, Fabio. "Fitting a Logistic Curve to Data." The College Mathematics Journal 14.3 (1993): 247. Print.

[37] Arnold, David. "Fitting a Logistic Curve to Data." February 24, 2002

[38] Reed, L. J., and Joseph Berkson. "The Application of the Logistic Function to Experimental Data.." The Journal of Physical Chemistry 33.5 (1928): 760-779. Print.

[39] Aerts, R., X. Tu, W. Van Gaens, J. C. Whitehead, and A. Bogaerts. "Gas Purification by Nonthermal Plasma: A Case Study of Ethylene." Environmental Science & Technology 47 (2013): 130606123303005. Print.

[40] Uddi, Mruthunjaya, Naibo Jiang, Evgeny Mintusov, Igor V. Adamovich, and Walter R. Lempert. "Atomic oxygen measurements in air and air/fuel nanosecond pulse discharges by two photon laser induced fluorescence."*Proceedings of the Combustion Institute*32.1 (2009): 929-936. Print.

[41] Seo, Young Sik, Abdel-Aleam H. Mohamed, Kyung Chul Woo, Hyun Wook Lee, Jae Koo Lee, and Kyong Tai Kim. "Comparative Studies of Atmospheric Pressure Plasma Characteristics Between He and Ar Working Gases for Sterilization." *IEEE Transactions on Plasma Science* 38.10 (2010): 2954-2962. Print.

Appendix

Appendix

B. Flow rate calculation.

- The calculation of flow rate of Air and Ethylene that will provide the system with a mixture of specific concentration in ppm using the small spacer (250 μm)

Ethylene	**Ethylene**		**Air**		**Total**	**residence time**	
Concentration	flow rate		Flow Rate		Flow Rate		
ppm	μL/min	ml/min	μL/min	ml/min	ml/min	min	sec
600	165	0.1650	275000.0	275.00	275.17	0.00014	0.008
600	90	0.0900	150000.0	150.00	150.09	0.00026	0.016
600	60	0.0600	100000.0	100.00	100.06	0.00039	0.023
600	48	0.0480	80000.0	80.00	80.05	0.00048	0.029
600	36	0.0360	60000.0	60.00	60.04	0.00065	0.039
600	30	0.0300	50000.0	50.00	50.03	0.00078	0.047
600	24	0.0240	40000.0	40.00	40.02	0.00097	0.058
200	55	0.0550	275000.0	275.00	275.06	0.00014	0.008
200	30	0.0300	150000.0	150.00	150.03	0.00026	0.016
200	20	0.0200	100000.0	100.00	100.02	0.00039	0.023
200	16	0.0160	80000.0	80.00	80.02	0.00048	0.029
200	12	0.0120	60000.0	60.00	60.01	0.00065	0.039
200	10	0.0100	50000.0	50.00	50.01	0.00078	0.047
200	8	0.0080	40000.0	40.00	40.01	0.00097	0.058

Table A-1. Calculation of flow rate of Air and Ethylene in small spacer (250 μm)

- The calculation of flow rate of Air and Ethylene that will provide the system with a mixture of specific concentration in ppm using the big spacer (750 μm)

Ethylene	**Ethylene**		**Air**		**Total**	**residence time**	
Concentration	Flow Rate		Flow Rate		Flow Rate		
ppm	μL/min	ml/min	μL/min	ml/min	ml/min	min	sec
600	255	0.2550	425000.0	425.00	425.26	0.0003	0.016
600	180	0.1800	300000.0	300.00	300.18	0.0004	0.023
600	144	0.1440	240000.0	240.00	240.14	0.0005	0.029
600	108	0.1080	180000.0	180.00	180.11	0.0006	0.039
600	90	0.0900	150000.0	150.00	150.09	0.0008	0.047
600	72	0.0720	120000.0	120.00	120.07	0.0010	0.058
200	85	0.0850	425000.0	425.00	425.09	0.0003	0.016
200	60	0.0600	300000.0	300.00	300.06	0.0004	0.023
200	48	0.0480	240000.0	240.00	240.05	0.0005	0.029

200	36	0.0360	180000.0	180.00	180.04	0.0006	0.039
200	30	0.0300	150000.0	150.00	150.03	0.0008	0.047
200	24	0.0240	120000.0	120.00	120.02	0.0010	0.058

Table A-2. Calculation of flow rate of Air and Ethylene in big spacer (750 μm)

Unit Conversion used in this work:

1 ml	1000 μL
1 L	1000 ml
1 L	1000000 μL
1 μm	0.000001 m
1 mL	$1cm^3$

Table A-3. Unit Conversion

Example1:

The calculation of Mixing Air with Ethylene to get 600 ppm of Ethylene?

$$1ppm \quad Ethylene = \frac{1\mu L \quad Ethylene}{1L \quad Air}$$

$$Ethylene = \; 600\,ppm = \boxed{\frac{600\mu L}{\min}} = \frac{0.6mL}{\min}$$

$$Air = \; \frac{600\mu L/\min \quad Ethylene}{600\,ppm * 10^6} = \boxed{\frac{10^6\,\mu L}{\min}} = \frac{1000mL}{\min}$$

Example2:

The calculation of Mixing Air with Ethylene to get 600 ppm of Ethylene and what is the total flow rate going through the channel?

$$Ethylene = \; 600\,ppm = \boxed{\frac{90\mu L}{\min}}$$

$$Air = \; \frac{90\mu L/\min \quad Ethylene}{600\,ppm * 10^6} = \boxed{\frac{1.5 * 10^4\,\mu L}{\min}} = \frac{150mL}{\min}$$

Total flow rate= $\left(\frac{90\mu L}{\min} + \frac{15 * 10^4\,\mu L}{\min}\right)/10^3 = \frac{150.09mL}{\min}$

C. Residence time calculation

Spacer specification

Spacer (µm)	**750**	**250**
Length (cm)	3	3
width (cm)	0.517	0.517
Thickness (cm)	0.075	0.025
Volume (cm^3)	0.116	0.039

Table B-1. Spacer specification

Example3:
The calculation of Residence time of 250 µm spacer Using total flow rate of from Example 2

$$Residence\ time = \frac{Volume}{flow\ \ Rate}$$

$$Residence\ time = \left(\frac{0.039 cm^3}{150.09 mL/\min} \right) * \frac{60\sec}{1\min} = 0.016\sec$$

D. Calibration Curves:

- **Ethylene Calibration curve**
  Each point represent an average of four run

Sample injection (mL)					Average Area	St .dev	St error	%error
	1	2	3	4				
0.1	27020	25376	26979	27194	26642.3	735.51	0.028	2.761
0.05	19953	19885	19972	19381	19797.8	242.77	0.012	1.226
0.025	11132	10908	11053	11039	11033	80.41	0.007	0.729
0.005	4240	4233	4299	4510	1812.5	106.13	0.059	5.855
0.01	1642	1895	1805	1908	4320.5	112.37	0.026	2.601

Table C-1. Relative Uncertainty of Peak Areas of Ethylene

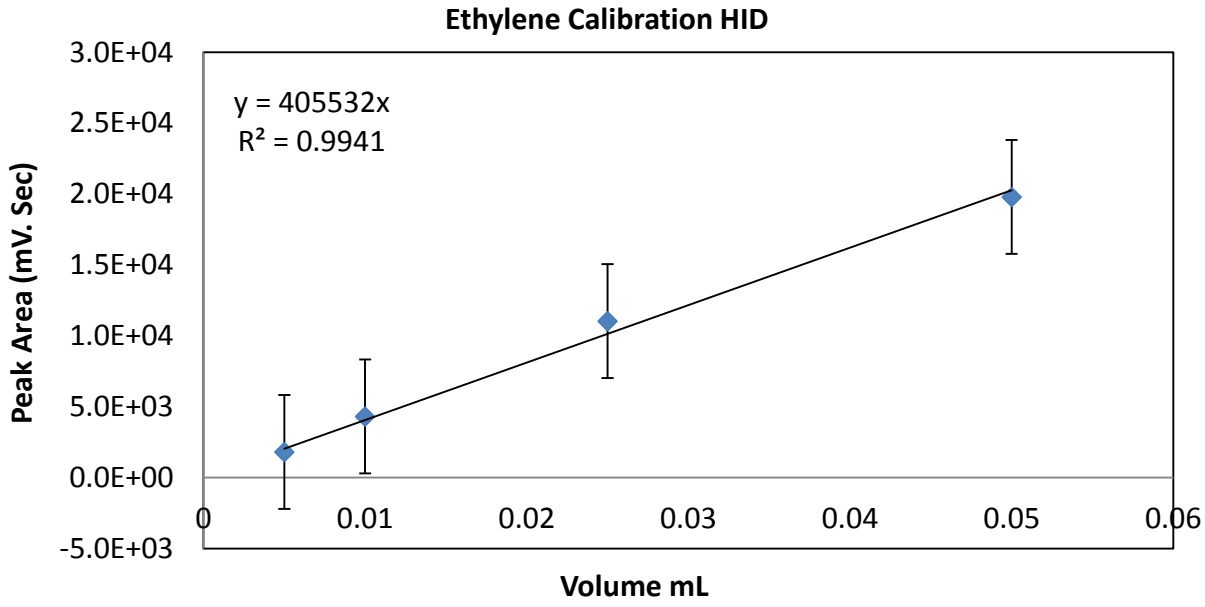

Figure C-1. Calibration curve for Ethylene with Trend line and Error Bars

- **Carbon dioxide Calibration curve**
  Each point represent an average of four run

Sample injection (mL)					Average Area	St .dev	St error	%error
	1	2	3	4				
0.1	12504	12247	12474	12681	12476.5	154.32	0.012	1.237
0.05	8153	7630	7930	8133	7961.5	210.34	0.026	2.642
0.025	4613	4580	4425	4599	4554.3	75.54	0.017	1.659
0.01	1902	1843	1881	1772	1849.5	49.49	0.027	2.676
0.005	870	886	817	836	852.3	27.21	0.032	3.192

Table C-2. Relative Uncertainty of Peak Areas of Carbon Dioxide

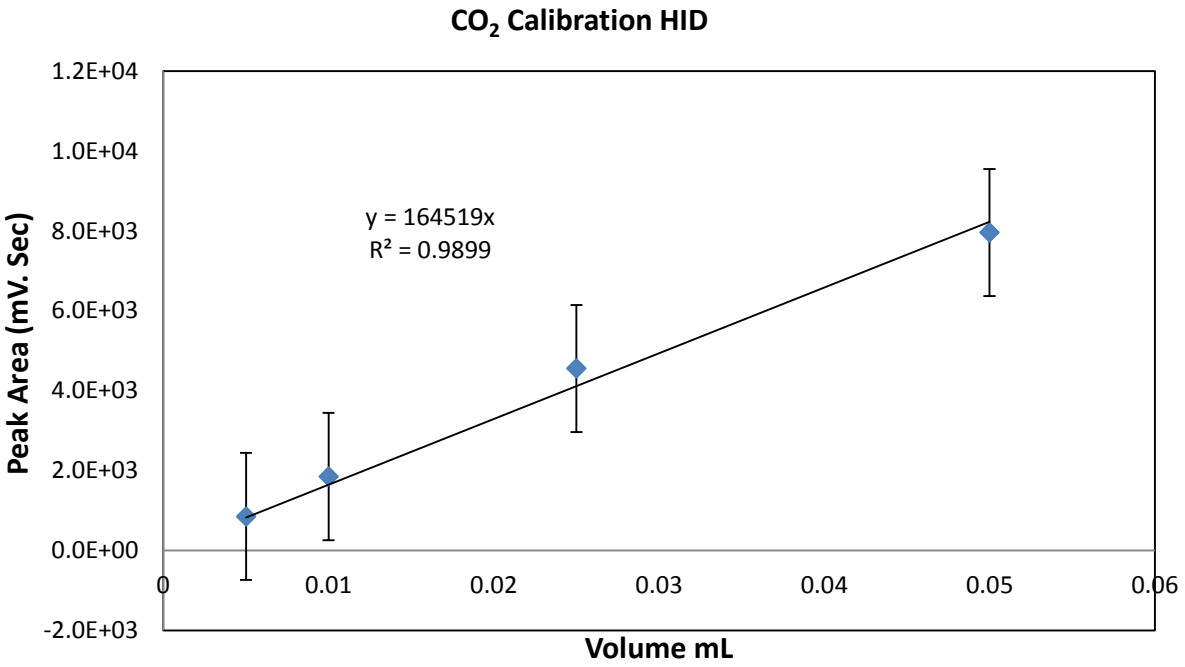

Figure C-2. Calibration curve for CO_2 with Trend line and Error Bars

- **Mass flow controller Calibration curve**

voltage (v)	flow rate cal. (mL/min)	time (sec)	volume (mL)
0.5	41.33	90	62
1	98.67	90	148
2.5	248.00	45	186
3.5	357.00	40	238
5	486.00	20	162

Table C-3. Mass flow controller 2 Calibration curve of Air

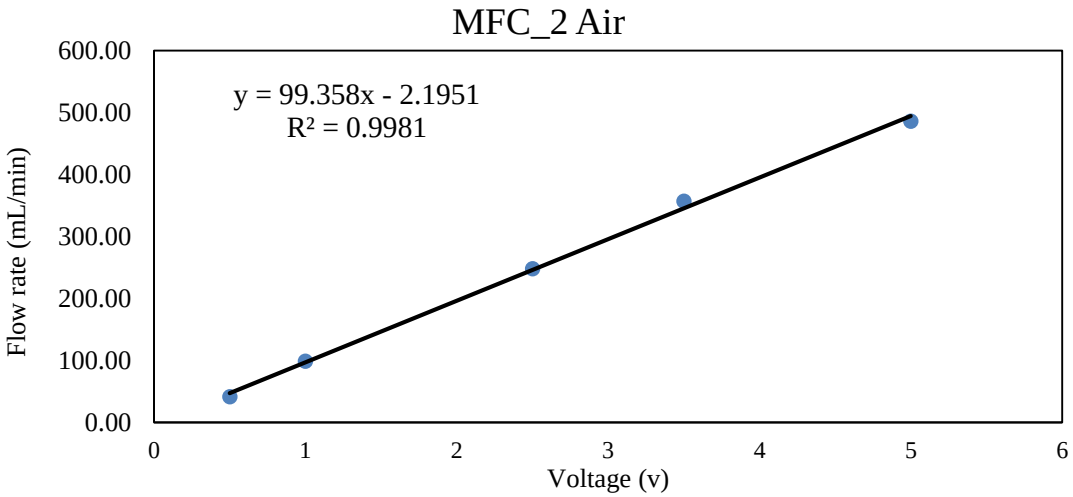

Figure C-3. Calibration curve for Mass flow controller 2 of Air with Trend line

- MFC programed in LabView

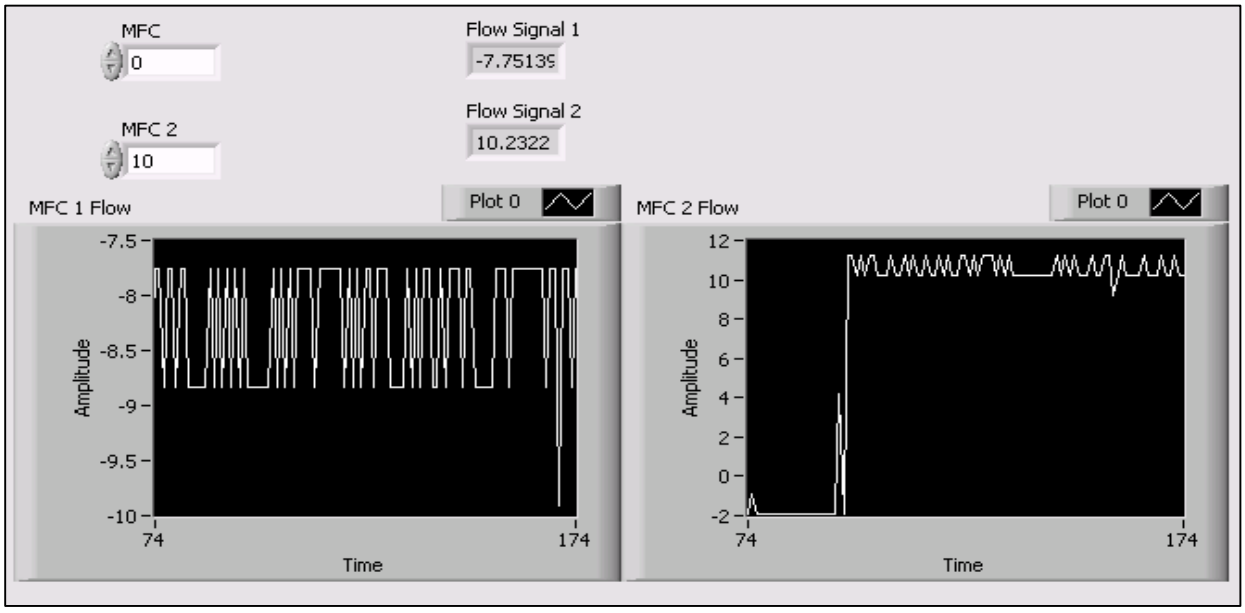

Figure C-4. Photograph of Front panel window of the Mass flow controller in Lab View

MFC Block diagram

Fir the Air only consider the route of MFC 2.

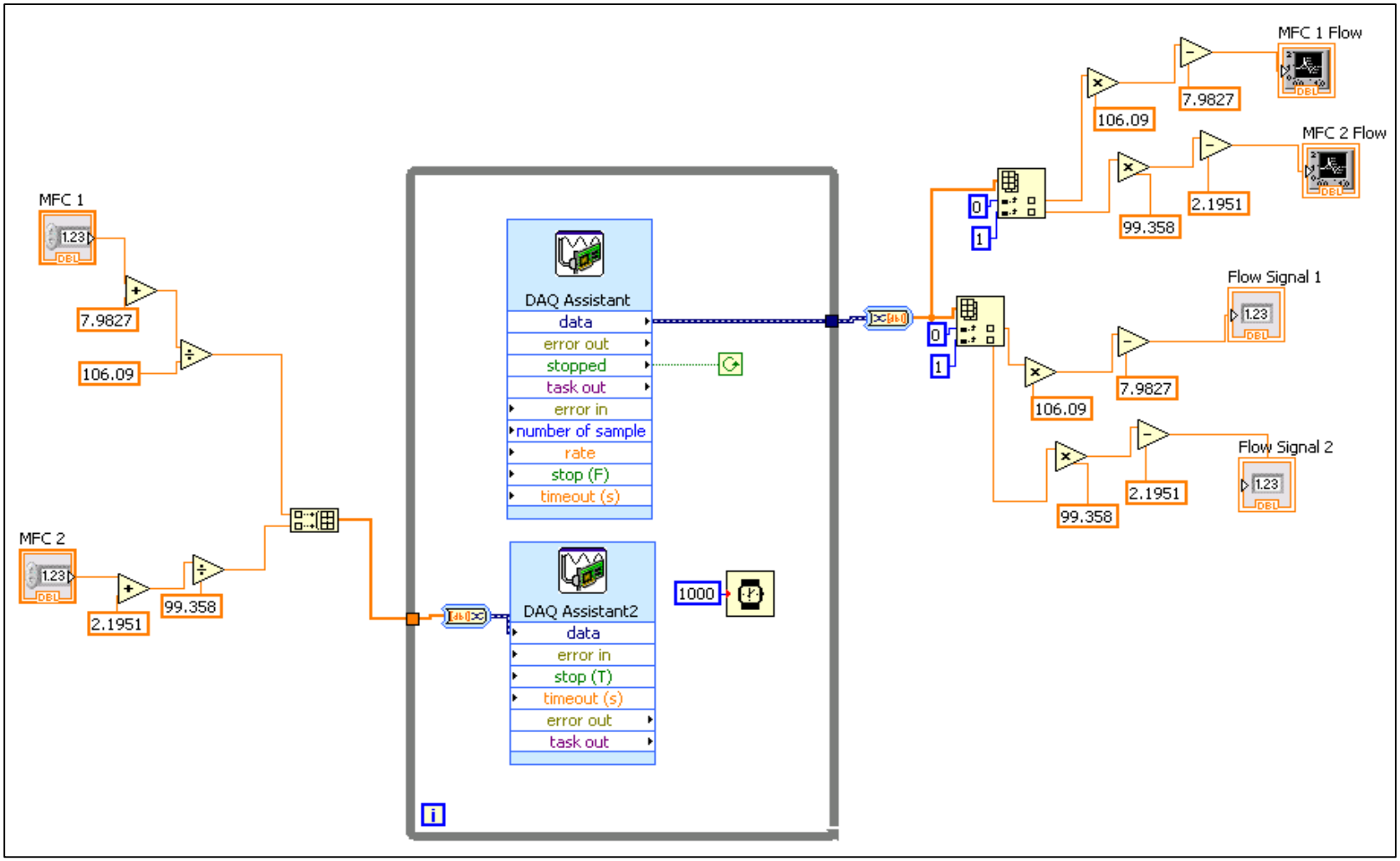

Figure C-5. Photograph of Black diagram window of the Mass flow controller in Lab View

E. Reactor Voltage and Power calculation

Example: calculate the Voltage applied to the reactor and the power applied to Reactor?

Power Supply Current (PSC) (mA) = 6.5 mA

Power Supply Voltage (PSV) (kV) = 1.93 kV

Resister (R) = 210 kΩ = 0.210 Ω

Voltage applied to the reactor =

$$\left[\left(PSV\right)-\left(R*\ PSC\right)\right]*1000\ =\left[\left(1.93\right)-\left(0.210*6.5\right)\right]*1000=\ 565\ V$$

Power applied to Reactor =

$$\left[\left(\frac{Applied\,V}{1000}\right)*\left(PSC\right)\right]\ =\left[\left(\frac{565\ V}{1000}\right)*\left(6.5\right)\right]=\ 3.67\text{W}$$

F. Nickel Electroplating Calculation :

Example: How much time required deposit a thickness of 50 nanometer of nickel into the cathode plate if we pass a current of 0.0013 ampere?

T = Desired thickness in nanometer. T=50
n = valence of the dissolved metal in solution in equivalents per mole. n = 2
F = Faraday's constant in coulombs per equivalent. F = 9.65*10^4
ρ= density in grams per cubic centimeter. ρ= 8.907
S = surface area of the plated part in square centimeters. S =12.90
I = current in coulombs per second (ampere). I=0.0013
A = atomic weight of the metal in grams per mole. A=58.7
t = time in seconds.

$$t = \frac{T\,n\,F\,\rho\,S}{I\,A*10^{7}*60} = \frac{50*2*9.65*10^{4}*8.907*12.9}{0.0013*58.7*10^{7}*60} = 24.21\text{sec}$$

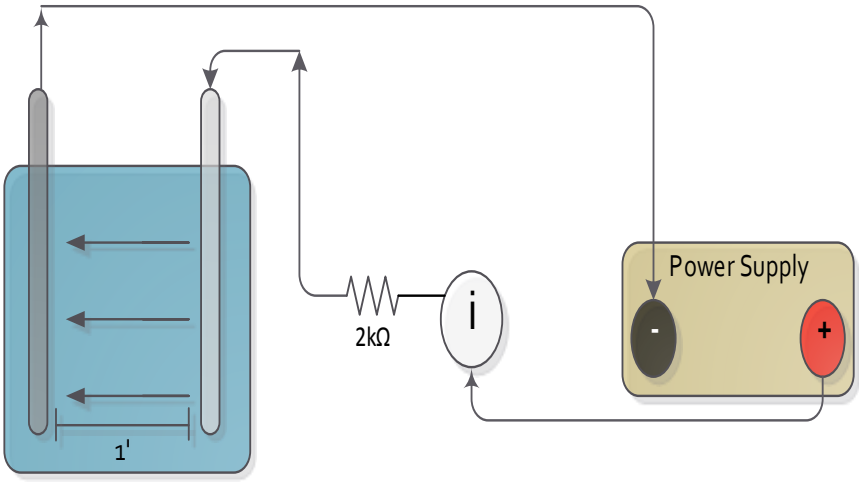

Figure E-1. Photograph of Nickel electroplating process set-up

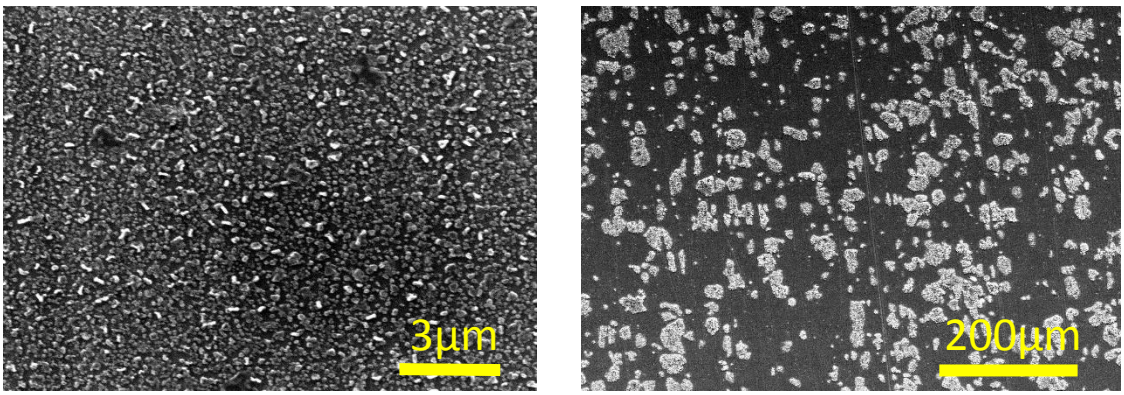

Figure E-2. Photograph of Nickel electroplating SEM imaging at different zoom-in

G. Carbon Nanotube Growth specification

Stage	Gases	Flow rate ratio (SCCM)	Temperature (°C)	Time (min)
1	N_2 / H_2	200/20	0 - 775	70
2	C_2H_4 / H_2	250/20	775	5
3	N_2	200	775 - 0	70

Table F-1. Carbon Nanotube Stages Growth specification

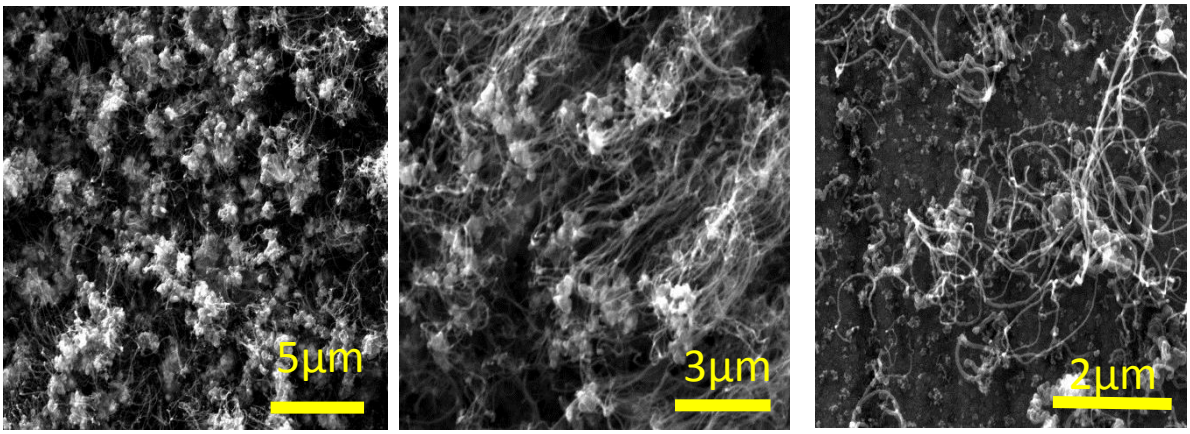

Figure F-1. Photograph of Carbon Nanotube by SEM imaging at different zoom-in

H. Convert the (GC) Peak area to ppm for Ethylene and the ethylene conversion

- **convert the area to ppm**

Example: giving the fallowing data, convert the area to ppm unit?
Peak Area = 235.53
Ethylene Calibration slope = 409363

$$\left[\left(\frac{Peak\ Area}{\text{calibration slop}}\right)/(60)\right]*10^6 = \left[\left(\frac{235.53}{409363}\right)/(60)\right]*10^6 = 9.59\,ppm$$

- **Ethylene % Conversion**

$$\left[\left(\frac{Inlet\ \text{Ethylene ppm} - Outlet\ \text{Ethylene ppm}}{Inlet\ \text{Ethylene ppm}}\right)\right]*100\% = \left[\left(\frac{9.59-2.18}{9.59}\right)\right]*100 = 77.29\%$$

I. Carbon balance calculation

$$C_2H_4 + 3O_2 \rightarrow 2CO_2 + 2H_2O$$

Inlet carbon

$$C = 12.011 \qquad H = 1.008 \qquad O = 15.99$$

$$\left(\frac{2C}{2C+4H}\right) * C_2H_4 inlet = \left(\frac{2*12.011}{2*12.011+4*1.008}\right) * 9.59 = 8.21 ppm$$

Outlet carbon

$$\left(\frac{2C}{2C+4H}\right) * C_2H_4 outlet + \left(\frac{C}{C+2O}\right) * CO_2 outlet$$

$$\left(\frac{2*12.011}{2*12.011+4*1.008}\right) * 2.18 + \left(\frac{12.011}{12.011+2*15.99}\right) * 0.86 = 2.10 ppm$$

Carbon balance

$$\left(\frac{C\ outlet}{C\ intlet}\right) * 100\% = \left(\frac{2.10}{8.21}\right) * 100\% = 25.55\%$$

J. Screening Design Calculation :

Flow rate	Spacer	Conc.	Syringe flow	Voltage	Current	Applied Reactor	Power	C2H4	C2H4 inlet	C2H4	C2H4 outlet	C2H4 Conversion	F/V
mL/min	μm	ppm	μL./min	kV	mA	V	W	Area before	[ ] ppm	Area after	[ ] ppm	%	1/s
50	750	200	10	2	6.8	572	3.89	78.53	3.23	18.39	0.76	76.58	0.112
50	750	200	10	1.4	3.9	581	2.27	73.84	3.03	17.07	0.70	76.88	0.112
50	750	600	30	1.4	3.9	581	2.27	178.57	7.34	58.35	2.40	67.32	0.112
50	750	600	30	2	6.8	572	3.89	182.53	7.50	77.34	3.18	57.63	0.112
100	750	200	20	1.4	3.8	602	2.29	54.94	2.26	24.05	0.99	56.22	0.056
100	750	200	20	2	6.8	572	3.89	49.10	2.02	19.63	0.81	60.02	0.056
100	750	600	60	1.4	3.9	581	2.27	262.00	10.77	94.27	3.87	64.02	0.056
100	750	600	60	2	6.8	572	3.89	207.04	8.51	118.09	4.85	42.96	0.056
50	250	200	10	1.4	4.4	476	2.09	95.67	3.93	62.22	2.56	34.96	0.037
50	250	200	10	2	7.4	446	3.30	82.72	3.40	52.11	2.14	37.00	0.037
50	250	600	30	1.4	4.6	434	2.00	217.82	8.95	168.28	6.92	22.74	0.037
50	250	600	30	2	7.4	446	3.30	220.42	9.06	157.75	6.48	28.43	0.037
100	250	200	20	1.4	4.6	434	2.00	87.24	3.59	57.82	2.38	33.72	0.019
100	250	200	20	2	7.3	467	3.41	74.94	3.08	56.82	2.34	24.18	0.019
100	250	600	60	1.4	4.6	434	2.00	234.04	9.62	186.34	7.66	20.38	0.019
100	250	600	60	2	7.3	467	3.41	231.25	9.50	178.85	7.35	22.66	0.019

Table I-1. Calculation of Screening Design Experiment

K. Comprehensive Experiment calculation at lower spacer (250 µm)

flow rate	RT	[conc]_ Syringe flow	I	V	Applied Reactor	Power	C2H4 A	[C2H4 inlet]	C2H4 A	[C2H4 outlet]	C2H4 Conversion	CO2 A	[CO2 inlet]	CO2 A	[CO2 outlet]	C before	C after	carbon balance
mL/min	1/s	Ppm_ µL./min	mA	kv	V	W	before	ppm	after	ppm	%	before	ppm	after	ppm	ppm	ppm	ppm %
100	b1						220.40	9.06				0.00	0.00			7.76		
	0.023	600_60	6.5	1.81	445	2.89			169.73	6.98	22.99			22.59	2.07		6.54	84.29
			5	1.50	450	2.25			168.52	6.93	23.54			21.04	1.93		6.46	83.24
			6.5	1.81	445	2.89			176.27	7.24	20.02			10.78	0.99		6.47	83.45
			5	1.50	450	2.25			162.26	6.67	26.38			20.36	1.86		6.22	80.18
			6.5	1.81	445	2.89			166.34	6.84	24.53			24.35	2.23		6.46	83.31
			5	1.50	450	2.25			160.36	6.59	27.24			21.87	2.00		6.19	79.80
	b2						257.10	10.57				0.00	0.00					
	b1						81.70	3.36				0.00	0.00			2.88		
	0.023	200_20	6.5	1.81	445	2.89			47.64	1.96	41.69			32.87	3.01		2.50	86.87
			5	1.50	450	2.25			39.10	1.61	52.14			31.64	2.90		2.17	75.35
			6.5	1.81	445	2.89			43.38	1.78	46.90			34.39	3.15		2.39	82.98
			5	1.50	450	2.25			46.04	1.89	43.65			35.00	3.20		2.49	86.76
			6.5	1.81	445	2.89			43.43	1.78	46.84			40.49	3.70		2.54	88.34
			5	1.50	450	2.25			45.76	1.88	43.99			33.16	3.03		2.44	84.82
	b2						75.28	3.09				0.00	0.00					
80	b1						245.04	10.07				0.00	0.00			8.62		
	0.029	600_48	6.5	1.81	445	2.89			153.86	6.32	37.21			28.87	2.64		6.14	71.15
			5	1.50	450	2.25			154.75	6.36	36.85			30.50	2.79		6.21	71.99
			6.5	1.81	445	2.89			135.50	5.57	44.70			28.21	2.58		5.47	63.47
			5	1.50	450	2.25			150.81	6.20	38.45			27.30	2.50		5.99	69.45
			6.5	1.81	445	2.89			136.27	5.60	44.39			30.63	2.80		5.56	64.49
			5	1.50	450	2.25			162.86	6.69	33.54			29.15	2.67		6.46	74.91

	b2						266.32	10.95				0.00	0.00					
	b1						83.71	3.44				0.00	0.00			2.95		
	0.029	200_16	6.5	1.81	445	2.89			44.93	1.85	46.33			44.26	4.05		2.69	91.21
			5	1.50	450	2.25			52.49	2.16	37.30			43.54	3.98		2.93	99.63
			6.5	1.81	445	2.89			44.72	1.84	46.58			39.32	3.60		2.56	86.77
			5	1.50	450	2.25			50.13	2.06	40.11			40.93	3.75		2.79	94.60
			6.5	1.81	445	2.89			46.13	1.90	44.89			41.39	3.79		2.66	90.21
			5	1.5	450	2.25			44.84	1.84	46.43			39.18	3.58		2.56	86.79
	b2						79.80	3.28				0.00	0.00					
60	b1						242.37	9.96				0.00	0.00			8.53		
	0.039	600_36	6.5	1.81	445	2.89			135.15	5.55	44.24			34.50	3.16		5.62	65.87
			5	1.50	450	2.25			125.82	5.17	48.09			41.48	3.80		5.46	64.06
			6.5	1.81	445	2.89			140.65	5.78	41.97			35.99	3.29		5.85	68.57
			5	1.50	450	2.25			138.10	5.68	43.02			39.68	3.63		5.85	68.60
			6.5	1.81	445	2.89			127.11	5.22	47.56			36.69	3.36		5.39	63.19
			5	1.50	450	2.25			142.24	5.85	41.31			34.54	3.16		5.87	68.80
	b2						250.88	10.31				0.00	0.00					
	b1						71.69	2.95				0.00	0.00			2.52		
	0.039	200_12	6.5	1.81	445	2.89			53.42	2.20	25.48			52.30	4.79		3.19	126.30
			5	1.5	450	2.25			40.79	1.68	43.10			45.09	4.13		2.56	101.55
			6.5	1.81	445	2.89			49.24	2.02	31.32			50.38	4.61		2.99	118.57
			5	1.5	450	2.25			45.64	1.88	36.34			56.87	5.20		3.03	119.98
			6.5	1.81	445	2.89			45.19	1.86	36.96			58.65	5.37		3.06	121.11
			5	1.5	450	2.25			43.49	1.79	39.34			57.30	5.24		2.96	117.40
	b2						82.30	3.38				0.00	0.00					
50	b1						214.79	8.83				0.00	0.00			7.56		
	0.047	600_30	6.5	1.81	445	2.89			107.06	4.40	50.16			43.94	4.02		4.87	64.37
			5	1.50	450	2.25			125.80	5.17	41.43			37.75	3.45		5.37	71.05
			6.5	1.81	445	2.89			115.94	4.76	46.02			35.91	3.29		4.98	65.85
			5	1.50	450	2.25			155.85	6.41	27.44			35.87	3.28		6.38	84.41
			6.5	1.81	445	2.89			109.62	4.51	48.96			37.29	3.41		4.79	63.36

			5	1.50	450	2.25		127.87	5.26	40.47		42.67	3.90		5.57	73.64
	b2						220.95	9.08			0.00	0.00					
	b1						77.97	3.20			0.00	0.00			2.74		
	0.047	200_10	6.5	1.81	445	2.89		32.64	1.34	58.14		62.16	5.69		2.70	98.46
			5	1.5	450	2.25		56.93	2.34	26.98		47.96	4.39		3.20	116.68
			6.5	1.81	445	2.89		60.36	2.48	22.59		42.37	3.88		3.18	115.99
			5	1.5	450	2.25		54.42	2.24	30.20		49.61	4.54		3.15	114.96
			6.5	1.81	445	2.89		45.37	1.86	41.81		57.18	5.23		3.03	110.25
			5	1.5	450	2.25		40.08	1.65	48.60		46.91	4.29		2.58	94.11
	b2						91.40	3.76			0.00	0.00					
40	b1						178.35	7.33			0.00	0.00			6.28		
	0.058	600_24	6.5	1.81	445	2.89		93.26	3.83	47.71		54.97	5.03		4.66	74.17
			5	1.50	450	2.25		104.55	4.30	41.38		49.56	4.53		4.92	78.35
			6.5	1.81	445	2.89		154.10	6.33	13.60		29.23	2.67		6.15	98.04
			5	1.50	450	2.25		104.17	4.28	41.59		47.39	4.34		4.85	77.27
			6.5	1.81	445	2.89		104.44	4.29	41.44		49.34	4.51		4.91	78.20
			5	1.50	450	2.25		107.47	4.42	39.74		46.32	4.24		4.94	78.70
	b2						165.88	6.82			0.00	0.00					
	b1						86.75	3.57			0.00	0.00			3.05		
	0.058	200_8	6.5	1.81	445	2.89		46.65	1.92	46.22		60.08	5.50		3.14	102.94
			5	1.5	450	2.25		40.58	1.67	53.22		65.92	6.03		3.07	100.72
			6.5	1.81	445	2.89		47.33	1.95	45.44		60.52	5.54		3.18	104.08
			5	1.5	450	2.25		44.87	1.84	48.28		59.25	5.42		3.06	100.21
			6.5	1.81	445	2.89		38.11	1.57	56.07		60.54	5.54		2.85	93.47
			5	1.5	450	2.25		39.66	1.63	54.28		55.00	5.03		2.77	90.73
	b2						93.82	3.86			0.00	0.00					
150	b1						240.83	9.81			0.00	0.00			8.40		
	0.016	600_90	6.5	1.81	445	2.89		211.51	8.61	12.17		17.05	1.56		7.80	92.90
			5	1.50	450	2.25		207.98	8.47	13.64		12.86	1.18		7.57	90.19
			6.5	1.81	445	2.89		200.24	8.15	16.85		23.20	2.12		7.56	90.05
			5	1.50	450	2.25		205.05	8.35	14.86		14.40	1.32		7.51	89.43

			6.5	1.81	445	2.89		209.26	8.52	13.11		13.49	1.23		7.63	90.91
			5	1.50	450	2.25		195.93	7.98	18.64		17.51	1.60		7.27	86.57
	b2						243.00	9.99			0.00	0.00				
	b1						83.18	3.39			0.00	0.00		2.90		
	0.016	200_30	6.5	1.81	445	2.89		53.63	2.18	35.53		25.00	2.29		2.49	86.01
			5	1.5	450	2.25		51.14	2.08	38.52		25.64	2.35		2.42	83.57
			6.5	1.81	445	2.89		57.10	2.32	31.35		27.47	2.51		2.68	92.31
			5	1.5	450	2.25		51.74	2.11	37.80		22.57	2.07		2.37	81.65
			6.5	1.81	445	2.89		49.26	2.01	40.78		26.27	2.40		2.37	81.85
			5	1.5	450	2.25		49.54	2.02	40.44		23.56	2.16		2.32	79.85
	b2						80.56	3.31			0.00	0.00				
275	b1						320.60	13.05			0.00	0.00		11.18		
	0.008	600_165	6.5	1.83	465	3.02		266.11	10.83	17.00		7.83	0.72		9.47	84.75
			5	1.52	470	2.35		290.94	11.85	9.25		5.50	0.50		10.28	91.98
			6.5	1.83	465	3.02		284.78	11.59	11.17		8.65	0.79		10.14	90.76
			5	1.52	470	2.35		283.70	11.55	11.51		4.45	0.41		10.00	89.48
			6.5	1.82	455	2.96		272.12	11.08	15.12		13.44	1.23		9.82	87.88
			5	1.51	460	2.30		284.28	11.57	11.33		6.75	0.62		10.08	90.18
	b2						316.72	13.02			0.00	0.00				
	b1						88.72	3.61			0.00	0.00		3.09		
	0.008	200_55	6.5	1.83	465	3.02		61.58	2.51	30.59		13.35	1.22		2.48	80.19
			5	1.52	470	2.35		69.90	2.85	21.21		44.88	4.11		3.56	115.04
			6.5	1.82	455	2.96		59.89	2.44	32.50		14.67	1.34		2.45	79.35
			5	1.49	440	2.20		60.24	2.45	32.10		11.24	1.03		2.38	76.98
			6.5	1.81	445	2.89		63.56	2.59	28.36		11.50	1.05		2.50	80.93
			5	1.5	450	2.25		71.26	2.90	19.68		9.58	0.88		2.72	88.06
	b2						77.21	3.17			0.00	0.00				

Table J-1. Comprehensive Experiment calculation at lower spacer (250 µm)

L. Comprehensive Experiment calculation at bigger spacer (750 µm)

flow rate	RT	[conc]	I	V	Applied Reactor	Power	C2H4 A	[C2H4 inlet]	C2H4 A	[C2H4 outlet]	C2H4 Conversion	CO2 A	[CO2 inlet]	CO2 A	[CO2 outlet]	C before	C after	carbon balance
mL/min	1/s	ppm	mA	kv	V	W	before	ppm	after	ppm	%	before	ppm	after	ppm	ppm	ppm	ppm %
120	B1						235.53	9.59				0.00	0.00			8.21		
	0.058	600/72	6.5	1.93	565	3.67			53.48	2.18	77.29			9.35	0.86		2.10	25.55
			5	1.63	580	2.90			64.77	2.64	72.50			30.73	2.81		3.03	36.85
			6.5	1.93	565	3.67			55.45	2.26	76.46			6.36	0.58		2.09	25.48
			5	1.63	580	2.90			50.72	2.06	78.47			1.75	0.16		1.81	22.07
			6.5	1.93	565	3.67			70.97	2.89	69.87			4.08	0.37		2.58	31.37
			5	1.63	580	2.90			50.88	2.07	78.40			48.59	4.45		2.99	36.39
	b2						262.54	10.69				0.00	0.00					
	b1						53.77	2.19				0.00	0.00			1.87		
	0.058	200/24	6.5	1.93	565	3.67			15.85	0.65	70.52			8.18	0.75		0.76	40.38
			5	1.63	580	2.90			14.97	0.61	72.16			13.23	1.21		0.85	45.47
			6.5	1.93	565	3.67			15.21	0.62	71.71			20.41	1.87		1.04	55.49
			5	1.63	580	2.90			15.76	0.64	70.69			20.17	1.85		1.05	56.19
			6.5	1.93	565	3.67			13.80	0.56	74.34			22.41	2.05		1.04	55.53
			5	1.63	580	2.90			12.46	0.51	76.83			25.01	2.29		1.06	56.50
	b2						54.20	2.21				0.00	0.00					
150	b1						244.76	9.97				0.00	0.00			8.53		
	0.047	600/90	6.5	1.93	565	3.67			53.51	2.18	78.14			14.85	1.36		2.24	26.21
			5	1.63	580	2.90			71.33	2.90	70.86			4.23	0.39		2.59	30.38
			6.5	1.93	565	3.67			73.55	2.99	69.95			4.32	0.40		2.67	31.31
			5	1.63	580	2.90			67.57	2.75	72.39			4.95	0.45		2.48	29.06
			6.5	1.93	565	3.67			90.83	3.70	62.89			5.67	0.52		3.31	38.77
			5	1.63	580	2.90			92.71	3.77	62.12			2.30	0.21		3.29	38.55
	b2						243.15	9.90				0.00	0.00					
	b1						70.94	2.89				0.00	0.00			2.47		

	0.047	200/30	6.5	1.93	565	3.67		14.52	0.59	79.53		23.40	2.14		1.09	44.11
			5	1.63	580	2.90		23.74	0.97	66.54		17.82	1.63		1.27	51.47
			6.5	1.93	565	3.67		15.58	0.63	78.04		28.40	2.60		1.25	50.65
			5	1.63	580	2.90		21.53	0.88	69.65		15.46	1.41		1.14	45.97
			6.5	1.93	565	3.67		20.70	0.84	70.82		21.46	1.96		1.26	50.86
			5	1.63	580	2.90		24.35	0.99	65.68		22.97	2.10		1.42	57.53
	b2						65.78	2.68			0.00	0.00					
180	b1						200.90	8.18			0.00	0.00			7.00		
	0.039	600/108	6.5	1.93	565	3.67		95.87	3.90	52.28		11.64	1.07		3.63	51.87
			5	1.63	580	2.90		89.41	3.64	55.50		20.02	1.83		3.62	51.65
			6.5	1.93	565	3.67		110.85	4.51	44.82		13.43	1.23		4.20	59.97
			5	1.63	580	2.90		117.93	4.80	41.30		12.60	1.15		4.43	63.20
			6.5	1.93	565	3.67		87.34	3.56	56.53		9.80	0.90		3.29	46.97
			5	1.63	580	2.90		119.16	4.85	40.69		7.93	0.73		4.35	62.14
	b2						219.16	8.92			0.00	0.00					
	b1						60.21	2.45			0.00	0.00			2.10		
	0.039	200/36	6.5	1.93	565	3.67			19.92	0.81	66.92		22.57	2.07		1.26	59.95
			5	1.63	580	2.90			21.56	0.88	64.19		21.02	1.92		1.28	60.83
			6.5	1.93	565	3.67			18.64	0.76	69.04		14.19	1.30		1.00	47.85
			5	1.63	580	2.90			15.50	0.63	74.26		12.31	1.13		0.85	40.39
			6.5	1.93	565	3.67			18.72	0.76	68.91		16.90	1.55		1.07	51.21
			5	1.63	580	2.90			22.45	0.91	62.71		17.72	1.62		1.23	58.38
	b2						62.44	2.54			0.00	0.00					
240	b1						286.86	11.68			0.00	0.00			10.00		
	0.029	600/144	6.5	1.93	565	3.67		162.70	6.62	43.28		10.43	0.95		5.93	59.32
			5	1.63	580	2.90		175.25	7.14	38.91		7.74	0.71		6.30	63.03
			6.5	1.93	565	3.67		189.45	7.71	33.96		9.66	0.88		6.85	68.46
			5	1.63	580	2.90		196.84	8.01	31.38		7.31	0.67		7.04	70.44
			6.5	1.93	565	3.67		172.54	7.02	39.85		8.15	0.75		6.22	62.18
			5	1.63	580	2.90		171.71	6.99	40.14		7.56	0.69		6.18	61.75
	b2						260.48	10.61			0.00	0.00					

	b1						65.10	2.65				0.00	0.00			2.27		
	0.029	200/48	6.5	1.93	565	3.67			41.94	1.71	35.58			14.86	1.36		1.83	80.78
			5	1.63	580	2.90			51.06	2.08	21.57			13.90	1.27		2.13	93.73
			6.5	1.93	565	3.67			21.35	0.87	67.20			13.60	1.24		1.08	47.77
			5	1.63	580	2.90			19.08	0.78	70.69			6.29	0.58		0.82	36.23
			6.5	1.93	565	3.67			22.03	0.90	66.16			14.28	1.31		1.12	49.56
			5	1.63	580	2.90			23.60	0.96	63.75			13.70	1.25		1.17	51.33
	b2						86.94	3.54				0.00	0.00					
300	b1						250.23	10.19				0.00	0.00			8.72		
	0.023	600/180	6.5	1.93	565	3.67			179.60	7.31	28.23			2.05	0.19		6.31	72.36
			5	1.63	580	2.90			181.01	7.37	27.66			8.05	0.74		6.51	74.64
			6.5	1.93	565	3.67			186.39	7.59	25.51			6.20	0.57		6.65	76.26
			5	1.63	580	2.90			176.32	7.18	29.54			6.90	0.63		6.32	72.44
			6.5	1.93	565	3.67			199.33	8.12	20.34			7.48	0.68		7.14	81.80
			5	1.63	580	2.90			174.41	7.10	30.30			8.18	0.75		6.28	72.04
	b2						248.06	10.10				0.00	0.00					
	b1						73.07	2.97				0.00	0.00			2.55		
	0.023	200/60	6.5	1.93	565	3.67			33.09	1.35	54.71			5.59	0.51		1.29	50.77
			5	1.63	580	2.90			53.40	2.17	26.92			12.06	1.10		2.16	84.91
			6.5	1.93	565	3.67			34.47	1.40	52.83			11.96	1.09		1.50	58.90
			5	1.63	580	2.90			49.77	2.03	31.89			12.28	1.12		2.04	80.16
			6.5	1.93	565	3.67			40.71	1.66	44.29			10.64	0.97		1.69	66.15
			5	1.63	580	2.90			43.60	1.78	40.33			11.11	1.02		1.80	70.56
	b2						64.11	2.61				0.00	0.00					
425	b1						260.00	10.59				0.00	0.00			9.06		
	0.016	600/255	6.5	1.93	565	3.67			218.54	8.90	15.95			3.13	0.29		7.70	84.92
			5	1.63	580	2.90			187.16	7.62	28.02			5.38	0.49		6.66	73.47
			6.5	1.93	565	3.67			175.55	7.15	32.48			3.11	0.28		6.20	68.38
			5	1.63	580	2.90			149.25	6.08	42.60			5.96	0.55		5.35	59.05
			6.5	1.93	565	3.67			156.00	6.35	40.00			3.04	0.28		5.51	60.84
			5	1.63	580	2.90			238.93	9.73	8.10			4.25	0.39		8.44	93.07

	b2						210.44	8.57				0.00	0.00				
	b1						80.69	3.29				0.00	0.00		2.81		
	0.016	200/85	6.5	1.95	585	3.80			41.02	1.67	49.16			7.85	0.72		1.63	57.81
			5	1.63	580	2.90			48.43	1.97	39.98			7.02	0.64		1.86	66.25
			6.5	1.95	585	3.80			60.50	2.46	25.02			2.63	0.24		2.17	77.31
			5	1.63	580	2.90			65.23	2.66	19.16			5.04	0.46		2.40	85.32
			6.5	1.95	585	3.80			47.57	1.94	41.05			5.93	0.54		1.81	64.22
			5	1.63	580	2.90			60.72	2.47	24.75			5.18	0.47		2.25	79.85
	b2						86.82	3.53				0.00	0.00				

Table K-1. Comprehensive Experiment calculation at bigger spacer (750 µm)

M. Analytic solution of the logistic differential equation

The logistic differential equation can be solve using separation of variables function:

$$\frac{dX}{dt} = rX\left(1-\frac{X}{K}\right)$$

$$\int \frac{dX}{\mathrm{X}\left(1-\frac{X}{K}\right)} = \int r\,dt \quad \rightarrow \quad \int \frac{dX}{\mathrm{X}\left(K-X\right)} = \int r\,dt$$

$$\int \frac{dX}{\mathrm{X}} + \int \frac{dX}{K-X} = \int r\,dt$$

$$\ln|X| - \ln|K-X| = r\,t + C$$

$$\ln\left|\frac{K-X}{X}\right| = -r\,t - C$$

$$\frac{K-X}{X} = e^{-r\,t-C} \quad \rightarrow \quad \frac{K-X}{X} = Ce^{-r\,t}$$

$$\boxed{X(t) = \frac{K}{1+Ce^{-r\,t}}} \qquad (2)$$

$$t \rightarrow \infty, \quad X\left(t\right) \rightarrow K$$
$$t \rightarrow 0, \quad X\left(t\right) \rightarrow K/\left(1+C\right)$$

N. Matlab code of fitting a logistic curve to data.

Logistic_fit 1:

```
%250um__600ppm_5mA
%250um__600ppm_6.5mA
T=[0.008,0.016,0.023,0.029,0.039,0.047,0.058];
M=[10.69,16.01,25.72,36.28,44.14,36.44,40.90];
T=T';
M=M';
T1=[0.008,0.016,0.023,0.029,0.039,0.047,0.058];
M1=[14.54,14.85,22.51,42.10,44.58,44.99,34.24];
T1=T1';
M1=M1';

r=linspace(0,1,50);
t0=linspace(0,50,50);
[r,t0]=meshgrid(r,t0);
[m,n]=size(r);

e=zeros(size(r));


for i=1:m
for j=1:n
e(i,j)=myerror1([r(i,j);t0(i,j)],T,M);
e(i,j)=myerror2([r(i,j);t0(i,j)],T1,M1);
end
end

min=fminsearch(@myerror1,[1;40],[],T,M)
r=min(1);
t0=min(2);
min1=fminsearch(@myerror1,[1;42.5],[],T1,M1)
r1=min1(1);
t01=min1(2);

H=1./(1+exp(-r*(T-t0)));
K=(H'*M)/(H'*H)
s_sq_e = sum_sq_e1([r; t0; K;],T,M)
t=linspace(0.005,0.09);
y=K./(1+exp(-r*(t-t0)));
H1=1./(1+exp(-r1*(T1-t01)));
K1=(H1'*M1)/(H1'*H1)
s_sq_e = sum_sq_e1([r1; t01; K1;],T1,M1)
t1=linspace(0.005,0.09);
y1=K1./(1+exp(-r*(t1-t01)));

figure(1)
plot(T,M,'r^',t,y,'r-.',T1,M1,'bo',t1,y1,'linewidth', 2)
xlabel('RT (sec)')
ylabel('Ethylene Conversion (%)')
legend('600ppm-5mA','logistic fit','600ppm-6.5mA','logistic fit')
axis([0,0.07,0,100])
```

Logistic_fit 2:

```
%250um__600ppm_6.5mA
%250um__200ppm_6.5mA

T=[0.008,0.016,0.023,0.029,0.039,0.047,0.058];
M=[14.54,14.85,22.51,42.10,44.58,44.99,34.24];
T=T';
M=M';
T1=[0.008,0.016,0.023,0.029,0.039,0.047,0.058];
M1=[30.25,36.48,45.14,45.93,31.25,40.84,49.24];
T1=T1';
M1=M1';

r=linspace(0,1,50);
t0=linspace(0,50,50);
[r,t0]=meshgrid(r,t0);
[m,n]=size(r);

e=zeros(size(r));

for i=1:m
for j=1:n
e(i,j)=myerror2([r(i,j);t0(i,j)],T,M);
e(i,j)=myerror4([r(i,j);t0(i,j)],T1,M1);
end
end

min=fminsearch(@myerror2,[1;42.5],[],T,M)
r=min(1);
t0=min(2);
min1=fminsearch(@myerror4,[1;29],[],T1,M1)
r1=min1(1);
t01=min1(2);

H=1./(1+exp(-r*(T-t0)));
K=(H'*M)/(H'*H)
s_sq_e = sum_sq_e2([r; t0; K;],T,M)
t=linspace(0.005,0.09);
y=K./(1+exp(-r*(t-t0)));
H1=1./(1+exp(-r1*(T1-t01)));
K1=(H1'*M1)/(H1'*H1)
s_sq_e = sum_sq_e2([r1; t01; K1;],T1,M1)
t1=linspace(0.005,0.09);
y1=K1./(1+exp(-r1*(t1-t01)));

figure(2)
plot(T,M,'r^',t,y,'r-.',T1,M1,'bo',t1,y1,'linewidth', 2)
xlabel('RT (sec)')
ylabel('Ethylene Conversion (%)')
legend('600ppm-6.5mA','logistic fit','200ppm-6.5mA','logistic fit')
axis([0,0.07,0,100])
```

Logistic_fit 3:

```
%250um__200ppm_5mA
%250um__600ppm_5mA
T=[0.008,0.016,0.023,0.029,0.039,0.047,0.058];
M=[24.34,39.49,46.59,41.28,37.47,35.26,51.92];
T=T';
M=M';
T1=[0.008,0.016,0.023,0.029,0.039,0.047,0.058];
M1=[10.69,16.01,25.72,36.28,44.14,36.44,40.90];
T1=T1';
M1=M1';

r=linspace(0,1,50);
t0=linspace(0,40,50);
[r,t0]=meshgrid(r,t0);
[m,n]=size(r);

e=zeros(size(r));

for i=1:m
for j=1:n
e(i,j)=myerror3([r(i,j);t0(i,j)],T,M);
e(i,j)=myerror1([r(i,j);t0(i,j)],T1,M1);
end
end

min=fminsearch(@myerror3,[1;41],[],T,M)
r=min(1);
t0=min(2);
min=fminsearch(@myerror1,[1;40],[],T1,M1)
r1=min(1);
t01=min(2);

H=1./(1+exp(-r*(T-t0)));
K=(H'*M)/(H'*H)
s_sq_e = sum_sq_e3([r; t0; K;],T,M)
t=linspace(0.005,0.09);
y=K./(1+exp(-r*(t-t0)));
H1=1./(1+exp(-r1*(T1-t01)));
K1=(H1'*M1)/(H1'*H1)
s_sq_e = sum_sq_e1([r1; t01; K1;],T1,M1)
t1=linspace(0.005,0.09);
y1=K1./(1+exp(-r1*(t1-t01)));

figure(3)
plot(T,M,'r^',t,y,'r-.',T1,M1,'bo',t1,y1,'linewidth', 2)
xlabel('RT (sec)')
ylabel('Ethylene Conversion (%)')
legend('200ppm-5mA','logistic fit','600ppm-5mA','logistic fit')
axis([0,0.07,0,100])
```

Logistic_fit 4:

```
%250um__200ppm_6.5mA
%250um__200ppm_5mA

T=[0.008,0.016,0.023,0.029,0.039,0.047,0.058];
M=[30.25,36.48,45.14,45.93,31.25,40.84,49.24];
T=T';
M=M';
T1=[0.008,0.016,0.023,0.029,0.039,0.047,0.058];
M1=[24.34,39.49,46.59,41.28,37.47,35.26,51.92];
T1=T1';
M1=M1';

r=linspace(0,1,50);
t0=linspace(0,45,50);
[r,t0]=meshgrid(r,t0);
[m,n]=size(r);

e=zeros(size(r));

for i=1:m
for j=1:n
e(i,j)=myerror4([r(i,j);t0(i,j)],T,M);
e(i,j)=myerror3([r(i,j);t0(i,j)],T1,M1);
end
end

min=fminsearch(@myerror4,[1;29],[],T,M)
r=min(1);
t0=min(2);
min=fminsearch(@myerror3,[1;41],[],T1,M1)
r1=min(1);
t01=min(2);

H=1./(1+exp(-r*(T-t0)));
K=(H'*M)/(H'*H)
s_sq_e = sum_sq_e4([r; t0; K;],T,M)
t=linspace(0.005,0.09);
y=K./(1+exp(-r*(t-t0)));
H1=1./(1+exp(-r1*(T1-t01)));
K1=(H1'*M1)/(H1'*H1)
s_sq_e = sum_sq_e3([r1; t01; K1;],T1,M1)
t1=linspace(0.005,0.09);
y1=K1./(1+exp(-r1*(t1-t01)));

figure(4)
plot(T,M,'r^',t,y,'r-.',T1,M1,'bo',t1,y1,'linewidth', 2)
xlabel('RT (sec)')
ylabel('Ethylene Conversion (%)')
legend('200ppm-6.5mA','logistic fit','200ppm-5mA','logistic fit')
axis([0,0.07,0,100])
```

Logistic_fit 5:

```
%750um__600ppm_5mA
%750um__600ppm_6.5mA
T=[0.016,0.023,0.029,0.039,0.047,0.058];
M=[26.23,29.16,36.81,45.82,68.45,76.45];
T=T';
M=M';
T1=[0.016,0.023,0.029,0.039,0.047,0.058];
M1=[29.47,24.69,38.17,51.21,70.32,74.54] ;
T1=T1';
M1=M1';

r=linspace(0,1,50);
t0=linspace(0,300,50);
[r,t0]=meshgrid(r,t0);
[m,n]=size(r);

e=zeros(size(r));

for i=1:m
for j=1:n
e(i,j)=myerror5([r(i,j);t0(i,j)],T,M);
e(i,j)=myerror6([r(i,j);t0(i,j)],T1,M1);
end
end

min=fminsearch(@myerror5,[2;34.5],[],T,M)
r=min(1);
t0=min(2);
min1=fminsearch(@myerror6,[0.2;73.5],[],T,M)
r1=min1(1);
t01=min1(2);

H=1./(1+exp(-r*(T-t0)));
K=(H'*M)/(H'*H)
s_sq_e = sum_sq_e5([r; t0; K;],T,M)
t=linspace(0.005,0.09);
y=K./(1+exp(-r*(t-t0)));
H1=1./(1+exp(-r1*(T1-t01)));
K1=(H1'*M1)/(H1'*H1)
s_sq_e = sum_sq_e6([r1; t01; K1;],T1,M1)
t1=linspace(0.005,0.09);
y1=K1./(1+exp(-r1*(t1-t01)));

figure(5)
plot(T,M,'r^',t,y,'r-.',T1,M1,'bo',t1,y1,'linewidth', 2)
xlabel('RT (sec)')
ylabel('Ethylene Conversion (%)')
legend('600ppm-5mA','logistic fit','600ppm-6.5mA','logistic fit')
axis([0,0.07,0,100])
```

Logistic_fit 6:

```
%750um__600ppm_6.5mA
%750um__200ppm_6.5mA

T=[0.016,0.023,0.029,0.039,0.047,0.058];
M=[29.47,24.69,38.17,51.21,70.32,74.54] ;
T=T';
M=M';
T1=[0.016,0.023,0.029,0.039,0.047,0.058];
M1=[38.41,50.60,56.31,68.28,76.13,72.19];
T1=T1';
M1=M1';

r=linspace(0,1,50);
t0=linspace(0,300,50);
[r,t0]=meshgrid(r,t0);
[m,n]=size(r);

e=zeros(size(r));

for i=1:m
for j=1:n
e(i,j)=myerror6([r(i,j);t0(i,j)],T,M);
e(i,j)=myerror8([r(i,j);t0(i,j)],T1,M1);
end
end

min=fminsearch(@myerror6,[0.2;73.5],[],T,M)
r=min(1);
t0=min(2);
min1=fminsearch(@myerror8,[1;27.5],[],T1,M1)
r1=min1(1);
t01=min1(2);

H=1./(1+exp(-r*(T-t0)));
K=(H'*M)/(H'*H)
s_sq_e = sum_sq_e6([r; t0; K;],T,M)
t=linspace(0.005,0.09);
y=K./(1+exp(-r*(t-t0)));
H1=1./(1+exp(-r1*(T1-t01)));
K1=(H1'*M1)/(H1'*H1)
s_sq_e = sum_sq_e8([r1; t01; K1;],T1,M1)
t1=linspace(0.005,0.09);
y1=K1./(1+exp(-r1*(t1-t01)));

figure(6)
plot(T,M,'r^',t,y,'r-.',T1,M1,'bo',t1,y1,'linewidth', 2)
xlabel('RT (sec)')
ylabel('Ethylene Conversion (%)')
legend('600ppm-6.5mA','logistic fit','200ppm-6.5mA','logistic fit')
axis([0,0.07,0,100])
```

Logistic_fit 7:

```
%750um__200ppm_5mA
%750um__200ppm_6.5mA

T=[0.016,0.023,0.029,0.039,0.047,0.058];
M=[27.96,33.04,52.00,67.05,67.28,73.22];
T=T';
M=M';
T1=[0.016,0.023,0.029,0.039,0.047,0.058];
M1=[38.41,50.60,56.31,68.28,76.13,72.19];
T1=T1';
M1=M1';

r=linspace(0,1,50);
t0=linspace(0,45,50);
[r,t0]=meshgrid(r,t0);
[m,n]=size(r);

e=zeros(size(r));

for i=1:m
for j=1:n
e(i,j)=myerror7([r(i,j);t0(i,j)],T,M);
e(i,j)=myerror8([r(i,j);t0(i,j)],T1,M1);
end
end

min=fminsearch(@myerror7,[1;20.5],[],T,M)
r=min(1);
t0=min(2);
min1=fminsearch(@myerror8,[1;27.5],[],T1,M1)
r1=min(1);
t01=min(2);

H=1./(1+exp(-r*(T-t0)));
K=(H'*M)/(H'*H)
s_sq_e = sum_sq_e7([r; t0; K;],T,M)
t=linspace(0.005,0.09);
y=K./(1+exp(-r*(t-t0)));

H1=1./(1+exp(-r1*(T1-t01)));
K1=(H1'*M1)/(H1'*H1)
s_sq_e = sum_sq_e8([r1; t01; K1;],T1,M1)
t1=linspace(0.005,0.09);
y1=K1./(1+exp(-r1*(t1-t01)));

figure(7)
plot(T,M,'r^',t,y,'r-.',T1,M1,'bo',t1,y1,'linewidth', 2)
xlabel('RT (sec)')
ylabel('Ethylene Conversion (%)')
legend('200ppm-5mA','logistic fit','200ppm-6.5mA','logistic fit')
axis([0,0.07,0,100])
```

Logistic_fit 8:

```
%750um__200ppm_6.5mA
%750um__600ppm_5mA

T=[0.016,0.023,0.029,0.039,0.047,0.058];
M=[38.41,50.60,56.31,68.28,76.13,72.19];
T=T';
M=M';
T1=[0.016,0.023,0.029,0.039,0.047,0.058];
M1=[26.23,29.16,36.81,45.82,68.45,76.45];
T1=T1';
M1=M1';

r=linspace(0,1,50);
t0=linspace(0,45,50);
[r,t0]=meshgrid(r,t0);
[m,n]=size(r);

e=zeros(size(r));

for i=1:m
for j=1:n
e(i,j)=myerror8([r(i,j);t0(i,j)],T,M);
e(i,j)=myerror5([r(i,j);t0(i,j)],T1,M1);
end
end

min=fminsearch(@myerror8,[1;27.5],[],T,M)
r=min(1);
t0=min(2);
min1=fminsearch(@myerror5,[2;34.5],[],T1,M1)
r1=min1(1);
t01=min1(2);

H=1./(1+exp(-r*(T-t0)));
K=(H'*M)/(H'*H)
s_sq_e = sum_sq_e8([r; t0; K;],T,M)
t=linspace(0.005,0.09);
y=K./(1+exp(-r*(t-t0)));
H1=1./(1+exp(-r1*(T1-t01)));
K1=(H1'*M1)/(H1'*H1)
s_sq_e = sum_sq_e5([r1; t01; K1;],T1,M1)
t1=linspace(0.005,0.09);
y1=K1./(1+exp(-r1*(t1-t01)));

figure(8)
plot(T,M,'r^',t,y,'r-.',T1,M1,'bo',t1,y1,'linewidth', 2)
xlabel('RT (sec)')
ylabel('Ethylene Conversion (%)')
legend('600ppm-5mA','logistic fit','600ppm-6.5mA','logistic fit')
axis([0,0.07,0,100])
```

Logistic_fit 9:

```
%250um__600ppm_5mA
%750um__600ppm_5mA

T=[0.008,0.016,0.023,0.029,0.039,0.047,0.058];
M=[10.69,16.01,25.72,36.28,44.14,36.44,40.90];
T=T';
M=M';
T1=[0.016,0.023,0.029,0.039,0.047,0.058];
M1=[26.23,29.16,36.81,45.82,68.45,76.45];
T1=T1';
M1=M1';

r=linspace(0,1,50);
t0=linspace(0,45,50);
[r,t0]=meshgrid(r,t0);
[m,n]=size(r);

e=zeros(size(r));

for i=1:m
for j=1:n
e(i,j)=myerror1([r(i,j);t0(i,j)],T,M);
e(i,j)=myerror5([r(i,j);t0(i,j)],T1,M1);
end
end

min=fminsearch(@myerror1,[1;40],[],T,M)
r=min(1);
t0=min(2);
min1=fminsearch(@myerror5,[2;34.5],[],T1,M1)
r1=min1(1);
t01=min1(2);

H=1./(1+exp(-r*(T-t0)));
K=(H'*M)/(H'*H)
s_sq_e = sum_sq_e1([r; t0; K;],T,M)
t=linspace(0.005,0.09);
y=K./(1+exp(-r*(t-t0)));
H1=1./(1+exp(-r1*(T1-t01)));
K1=(H1'*M1)/(H1'*H1)
s_sq_e = sum_sq_e5([r1; t01; K1;],T1,M1)
t1=linspace(0.005,0.09);
y1=K1./(1+exp(-r1*(t1-t01)));

figure(9)
plot(T,M,'r^',t,y,'r-.',T1,M1,'bo',t1,y1,'linewidth', 2)
xlabel('RT (sec)')
ylabel('Ethylene Conversion (%)')
legend('250um-600ppm-5mA','logistic fit','750um-600ppm-5mA','logistic fit')
axis([0,0.07,0,100])
```

Logistic_fit 10:

```
%250um__200ppm_5mA
%750um__200ppm_5mA

T=[0.008,0.016,0.023,0.029,0.039,0.047,0.058];
M=[24.34,39.49,46.59,41.28,37.47,35.26,51.92];
T=T';
M=M';
T1=[0.016,0.023,0.029,0.039,0.047,0.058];
M1=[27.96,33.04,52.00,67.05,67.28,73.22];

T1=T1';
M1=M1';

r=linspace(0,1,50);
t0=linspace(0,45,50);
[r,t0]=meshgrid(r,t0);
[m,n]=size(r);

e=zeros(size(r));

for i=1:m
for j=1:n
e(i,j)=myerror3([r(i,j);t0(i,j)],T,M);
e(i,j)=myerror7([r(i,j);t0(i,j)],T1,M1);
end
end

min=fminsearch(@myerror3,[1;41],[],T,M)
r=min(1);
t0=min(2);
min1=fminsearch(@myerror7,[1;20.5],[],T1,M1)
r1=min1(1);
t01=min1(2);

H=1./(1+exp(-r*(T-t0)));
K=(H'*M)/(H'*H)
s_sq_e = sum_sq_e3([r; t0; K;],T,M)
t=linspace(0.005,0.09);
y=K./(1+exp(-r*(t-t0)));


H1=1./(1+exp(-r1*(T1-t01)));
K1=(H1'*M1)/(H1'*H1)
s_sq_e = sum_sq_e7([r1; t01; K1;],T1,M1)
t1=linspace(0.005,0.09);
y1=K1./(1+exp(-r1*(t1-t01)));

figure(10)
plot(T,M,'r^',t,y,'r-.',T1,M1,'bo',t1,y1,'linewidth', 2)
xlabel('RT (sec)')
ylabel('Ethylene Conversion (%)')
legend('250um-200ppm-5mA','logistic fit','750um-200ppm-5mA','logistic fit')
axis([0,0.07,0,100])
```

O. Calculation of number of Ethylene molecules destroyed per unit of power, charge and electron

- 250 µm spacer

Conc	RT	current	Δ [C2H4]	Δ [C2H4]	Ethylene destroyed per unit of energy	Ethylene destroyed per unit of charge	Ethylene destroyed per shooting electron
ppm	sec	C/sec	ppm	mol/sec	mol/J	mol/C	mol/mol e
600	0.008	0.005	1.40	9.51E-10	4.05E-10	1.90E-07	1.84E-02
600	0.016	0.005	1.54	1.05E-09	4.67E-10	2.10E-07	2.03E-02
600	0.023	0.005	2.33	1.59E-09	7.05E-10	3.17E-07	3.06E-02
600	0.029	0.005	3.65	2.49E-09	1.11E-09	4.98E-07	4.80E-02
600	0.039	0.005	4.40	3.00E-09	1.33E-09	5.99E-07	5.78E-02
600	0.047	0.005	3.22	2.19E-09	9.74E-10	4.38E-07	4.23E-02
600	0.058	0.005	3.00	2.04E-09	9.08E-10	4.09E-07	3.94E-02
600	0.008	0.0065	1.88	1.28E-09	4.25E-10	1.97E-07	1.90E-02
600	0.016	0.0065	1.38	9.38E-10	3.24E-10	1.44E-07	1.39E-02
600	0.023	0.0065	2.04	1.39E-09	4.80E-10	2.14E-07	2.06E-02
600	0.029	0.0065	4.24	2.89E-09	9.99E-10	4.44E-07	4.29E-02
600	0.039	0.0065	4.44	3.03E-09	1.05E-09	4.66E-07	4.49E-02
600	0.047	0.0065	4.27	2.91E-09	1.01E-09	4.48E-07	4.32E-02
600	0.058	0.0065	2.51	1.71E-09	5.91E-10	2.63E-07	2.54E-02
200	0.008	0.005	0.88	5.99E-10	2.55E-10	1.20E-07	1.16E-02
200	0.016	0.005	1.32	8.98E-10	3.99E-10	1.80E-07	1.73E-02
200	0.023	0.005	1.56	1.07E-09	4.74E-10	2.13E-07	2.06E-02
200	0.029	0.005	1.42	9.68E-10	4.30E-10	1.94E-07	1.87E-02
200	0.039	0.005	1.17	7.95E-10	3.53E-10	1.59E-07	1.53E-02
200	0.047	0.005	1.13	7.70E-10	3.42E-10	1.54E-07	1.49E-02
200	0.058	0.005	1.85	1.26E-09	5.61E-10	2.52E-07	2.43E-02
200	0.008	0.0065	1.10	7.50E-10	2.48E-10	1.15E-07	1.11E-02
200	0.016	0.0065	1.22	8.28E-10	2.86E-10	1.27E-07	1.23E-02
200	0.023	0.0065	1.52	1.03E-09	3.57E-10	1.59E-07	1.53E-02
200	0.029	0.0065	1.58	1.08E-09	3.72E-10	1.66E-07	1.60E-02
200	0.039	0.0065	0.92	6.27E-10	2.17E-10	9.65E-08	9.31E-03
200	0.047	0.0065	1.31	8.92E-10	3.08E-10	1.37E-07	1.32E-02
200	0.058	0.0065	1.76	1.20E-09	4.14E-10	1.84E-07	1.78E-02

Table N-1. Calculation of number of Ethylene molecules destroyed per unit of power, charge and electron lower spacer (250 µm)

- 750 µm spacer

Cnce	RT	current	Δ [C2H4]	Δ [C2H4]	Ethylene destroyed per unit of energy	Ethylene destroyed per unit of charge	Ethylene destroyed per shooting electron
ppm	sec	C/sec	ppm	mol/sec	mol/J	mol/C	mol/mol e
600	0.016	0.005	2.78	1.90E-09	6.54E-10	3.79E-07	3.66E-02
600	0.023	0.005	2.97	2.03E-09	6.99E-10	4.05E-07	3.91E-02
600	0.029	0.005	4.30	2.93E-09	1.01E-09	5.86E-07	5.65E-02
600	0.039	0.005	3.75	2.55E-09	8.81E-10	5.11E-07	4.93E-02
600	0.047	0.005	6.83	4.65E-09	1.60E-09	9.30E-07	8.98E-02
600	0.058	0.005	7.33	5.00E-09	1.72E-09	9.99E-07	9.64E-02
600	0.016	0.0065	3.12	2.13E-09	5.80E-10	3.28E-07	3.16E-02
600	0.023	0.0065	2.52	1.72E-09	4.67E-10	2.64E-07	2.55E-02
600	0.029	0.0065	4.56	3.11E-09	8.46E-10	4.78E-07	4.61E-02
600	0.039	0.0065	4.19	2.85E-09	7.77E-10	4.39E-07	4.24E-02
600	0.047	0.0065	7.01	4.78E-09	1.30E-09	7.35E-07	7.09E-02
600	0.058	0.0065	7.15	4.87E-09	1.33E-09	7.49E-07	7.23E-02
200	0.016	0.005	0.92	6.29E-10	2.17E-10	1.26E-07	1.21E-02
200	0.023	0.005	0.98	6.66E-10	2.30E-10	1.33E-07	1.29E-02
200	0.029	0.005	1.38	9.39E-10	3.24E-10	1.88E-07	1.81E-02
200	0.039	0.005	1.64	1.12E-09	3.86E-10	2.24E-07	2.16E-02
200	0.047	0.005	1.95	1.33E-09	4.57E-10	2.65E-07	2.56E-02
200	0.058	0.005	1.60	1.09E-09	3.77E-10	2.19E-07	2.11E-02
200	0.016	0.0065	1.27	8.63E-10	2.27E-10	1.33E-07	1.28E-02
200	0.023	0.0065	1.50	1.02E-09	2.78E-10	1.57E-07	1.52E-02
200	0.029	0.0065	1.49	1.02E-09	2.77E-10	1.56E-07	1.51E-02
200	0.039	0.0065	1.67	1.14E-09	3.10E-10	1.75E-07	1.69E-02
200	0.047	0.0065	2.20	1.50E-09	4.08E-10	2.31E-07	2.23E-02
200	0.058	0.0065	1.58	1.08E-09	2.93E-10	1.66E-07	1.60E-02

Table N-2. Calculation of number of Ethylene molecules destroyed per unit of power, charge and electron lower spacer (750 µm)